8-31-2019

A Role of Ubiquitin Regulatory X-Domain Containing Proteins (UBXN6) in Antiviral Immunity

Harshada Ketkar

Harshada Ketkar
New York Medical College

A Role of Ubiquitin Regulatory X-Domain Containing Proteins (UBXN6) in Antiviral Immunity

Harshada Ketkar

A Thesis in the Program in Basic Medical Sciences

Submitted to the Faculty of the

Graduate School of Basic Medical Sciences

in Partial Fulfillment of the Requirements

for the Degree of Doctor of Philosophy

at New York Medical College

2019

A Role of Ubiquitin Regulatory X-Domain Containing Proteins (UBXN6) in Antiviral Immunity

Harshada Ketkar

Penghua Wang, Ph.D.

Chandra Shekhar Bakshi, DVM, Ph.D.

Doris Bucher, Ph.D.

Dazhong Xu, Ph.D.

Tonya Colpitts, Ph.D.

06|28|2019

Date of Approval

Acknowledgments

I want to thank my mentor Dr. Penghua Wang for all his help, encouragement and guidance. I thank him for his thoughtful suggestions in science and life. The completion of my Ph.D. would not have been possible without his support. Most importantly I thank him for having trust in me and building my confidence.

Thanks to my committee! I thank, Dr. Bakshi for his invaluable guidance and feedback that helped shape this thesis into its final form. I thank him for the encouragement and kindness. I thank Dr. Bucher for providing her expertise in Virology field. Thanks, Dr. Xu for providing insights into the mechanistic study. Thanks, Dr. Colpitas for providing valuable advice of completion of one figure at a time.

I sincerely thank Dr. Tiwari, Program Director for his guidance and support throughout the course. I also sincerely appreciate Dr. Belloni, former Dean of Graduate School for his involvement in my academic progress. I am thankful to Dr. Holz, Dean of graduate school for encouragement during the completion of my thesis.

I want to thank my parents, brothers, and friends for supporting me in my desire to pursue my dreams. Most deeply thank my husband, daughter, and son for sharing their time unconditional and for all the years of bestowing encouragement, patience, and love.

Table of Contents

List of Tables

List of Figures and illustrations

Abbreviations

activator protein 1 (AP-1)

adipose triglyceride lipase (ATGL)

alveolar soft part sarcoma (ASPS)

American Type Culture Collection (ATCC)

apolipoprotein B (ApoB)

ATPase associated with diverse cellular activities (AAA)-ATPase

atrophin-interacting protein 4 (AIP4)

beta-actin (ACTB)

BRCA1 Associated RING Domain 1 (BARD1)

breast cancer type 1 susceptibility protein (BRCA1)

caspase recruitment domain (CARD)

Caveolin-1 (CAV1)

cellular inhibitors of apoptosis proteins (cIAPs)

clustered regularly interspaced short palindromic repeats (CRISPR)

colon antigen-1 (COA-1)

comparative gene identification (CGI-58)

cullin 1 (CUL 1)

cystic fibrosis transmembrane conductance regulator (CFTR)

cytokine-inducible SH2 domain protein (CIS)

danger associated molecular pattern (DAMP)

death effector domain (DED)

death effector domains (DEDs)

deoxyribonucleic acid (DNA)

DExD/H-Box Helicase 58 (DDX58)

diacylglycerols (DAGs)

double-strand break (DSB)

enzyme-linked immunosorbent assay (ELISA)

Encephalomyocarditis virus (EMCV)

endoplasmic reticulum (ER)

endoplasmic-reticulum-associated protein degradation (ERAD)

epidermal growth factor receptor mutation vIII (EGFRvIII)

epithelial-to-mesenchymal transition (EMT)

ER-Golgi intermediate compartment 53 kDa protein (ERGIC-53)

extended UBX domain (eUBX)

extracellular signal-regulated protein kinase (ERK)

Fas-associated death domain protein (FADD)

FAS-associated factor 1 (FAF1)

Fas-death-inducing signaling complex (Fas-DISC)

fatty acids (FAs)

green fluorescence protein (GFP)

guanosine triphosphatases (GTPases)

guide RNA (gRNA)

hepatitis B virus (HBV)

hepatitis C virus (HCV)

herpes simplex virus 1 (HSV-1)

herpes simplex virus-2 (HSV-2)

histone deacetylase (HDAC)

HMG-CoA reductase (HMGCR)

homology-directed repair (HDR)

human embryonic kidney 293 cells transformed with T antigen of SV40 (HEK293T)

human immunodeficiency virus 1 (HIV-1)

hypoxia-induced factor 1-α (HF-1α)

IFN stimulated gene (ISG)

IFN-induced gene 15 (ISG15)

IFN-α/β receptor (IFNAR 1/2)

IFN-γ receptor complex (IFNGR)

I-kappa-B kinase (IKKs)

inhibitor of kappa B (IκBα)

inhibitor of κB (IκB)

inhibitor-3 (I3)

interferon (IFN)

interferon induced transmembrane protein-1 (IFITM1)

interferon induced with helicase C domain 1 (IFIH1)

interferon regulatory factor (IRF3)

interferon regulatory factor (IRF3)

interferon-stimulated response element (ISRE)

interleukin (IL)

interleukin -10 receptors 2 (IL-10R2)

interleukin1 receptor-associated kinase (IRAK)

intra-flagellar transport B (IFT-B)

Itchy ubiquitin E3 protein ligase (ITCH)

janus Kinase (JAK)

JUN N-terminal kinase (JNK)

lipid droplets (LD)

major histocompatibility complex (MHC)

melanoma differentiation-associated 5 (MDA5)

mitochondrial antiviral signaling protein (MAVS)

mortalin (mot2)

myeloid cell Leukemia sequence-1(MCL1)

myeloid differentiation primary response 88 (MyD88)

Myxovirus resistance proteins Myxovirus resistance (Mx)

neuronal nicotinic acetylcholine receptors (nAChRs)

NF-kappa B Essential Modulator (NEMO)

NLR family member X1 (NLRX1)

NOD-like receptors (NLR)

non-homologous end joining (NHEJ)

Npl4-Ufd1 heterodimer (NU)

nuclear factor kappa-light-chain-enhancer of activated B cells (NFκB)

nuclear mitotic apparatus protein (NuMA)

nuclear protein localization protein 4 (NPL4)

nucleotide-binding and oligomerization domain (NOD)

of triglyceride (TGs)

oligoadenylate synthetase (OAS)

open reading frame (ORF)

OTU Binding protein1(OTUB1)

ovarian tumor (OTU)

pathogen-associated molecular patterns (PAMPs)

pattern recognition receptors (PRR)

peptide N-glycosidase (PNGase)

phosphate-buffered saline (PBS)

phospholipase A-2-activating protein (PLAA)

Poly C binding protein2 (PCBP-2)

polymerase chain reaction (PCR)

Post-translation modifications (PTM)

protein arginine methyltransferase 5 (PRMT5)

Protein Inhibitors of Activated STATs (PIAS)

protein kinase Cδ (PKCδ)

protein kinase R (PKR)

protein phosphatase 1 (PP1)

Protein Tyrosine Phosphatases (PTPs)

Protospacer Adjacent Motif (PAM)

PUB (PNGase /ubiquitin-associated)

quantitative reverse transcriptase polymerase chain reaction (q-RT-PCR)

receptor-interacting serine/threonine protein kinase 1 (RIPK1)

retinoic acid-inducible gene-I (RIG-I)

ribonucleic acid (RNA)

RIG-I like receptors (RLR)

ring finger protein 5 (RNF5)

shp1, eyc, and p47 (SEP)

signal transducer and activator of transcription proteins (STAT)

Skp, Cullin, F-box protein (SCF)

small interfering RNA (siRNA)

small ubiquitin-related modifier (SUMO)lyation

SRC homology 2 (SH2)

stimulator-of-interferon Genes (STING)

suppressor of cytokine signaling 1 (SOCS)

T cell protein tyrosine phosphatase (TCPTP)

TANK-binding kinase 1 (TBK1)

TNF receptor 1 (TNFR1)

TNF receptor-associated factor 3 (TRAF)

Toll-like receptors (TLR)

TRAF family member-associated NF-B activator (TANK)

TRAF-interacting motif (TIM)

transforming growth factor β receptor II (TGF-βRII)

tripartite motif-containing (TRIM)

tumor necrosis factor receptor-associated factor (TRAF)

tumor protein 53 (TP53)

tyrosine kinase (TYK)

UBA domain containing 2 (UBAC2)

UBD (ubiquitin D)

ubiquitin-interacting motif (UIM)

Ubiquitin Recognition Factor in ER-Associated Degradation 1 (UFD1)

ubiquitin-associated (UBA)

ubiquitin-proteasome system (UPS)

ubiquitin-regulatory-X (UBX)

ubiquitin-specific peptidase 18 (USP18)

UBX domain-containing proteins (UBXN)

valosin-containing protein (VCP)

VCP-binding motif (VBM)

VCP-interacting motif (VIM)

very low-density lipoprotein (VLDL)

vesicular stomatitis virus (VSV)

wild type (WT)

Abstract

The roles of UBXNs in the regulation of antiviral immune responses have not been much explored. Previous work in our lab identified UBXN1 as a negative regulator of the retinoic acid-inducible gene-I (RIG-I) like receptors (RLR) pathway and UBXN3B as a positive regulator of stimulator-of-interferon Genes (STING) -mediated immune responses. In this study, I aimed to determine the member of UBXNs as a positive regulator of ribonucleic acid (RNA) virus infection-induced innate immune responses. By using an interferon stimulated response element (ISRE)-driven luciferase reporter assay that monitors the activity of type I/III interferon (IFN)-induced janus kinase (JAK) - signal transducer and activator of transcription proteins (STAT) signaling, I found that over expressed UBXN6 synergized with RIG-I, IFN-β or IFN-λ to enhance antiviral immune responses.

I further used small interfering RNA (siRNA) and clustered regularly interspaced short palindromic repeats (CRISPR)-Cas9 technology to abrogate UBXN6 function, aiming to establish the function of UBXN6 in viral infection and JAK-STAT signaling. By polymerase chain reaction (PCR) array I found that UBXN6-deficiency led to a reduction in type I/III IFN-induced gene expression, which was validated by quantitative reverse transcriptase polymerase chain reaction (q-RT-PCR). Also, RNA virus replication was increased in UBXN6-deficient when compared to UBXN6-sufficient cells, which was accompanied by a significant reduction in IFN-β and IFN-λ. Lastly, I decoded the mechanism by which UBXN6 regulates the JAK-STAT pathway. I observed that IFN-β-stimulated STAT1 phosphorylation was impaired in UBXN6-deficient cells. By co-immunoprecipitation techniques and mass spectrometry analysis, I identified that following IFN-β stimulation UBXN6 interacted with protein arginine methyltransferase 5 (PRMT5) that is known to

interact with JAK1/2. Our results demonstrate that UBXN6 positively regulates JAK1-STAT1/2 signaling to combat viral infections.

1 Introduction and Background:

The series of events generated by the host immune system against a virus determines the fate of viral infection. Both the innate and adaptive responses are induced after viral infection consecutively. The major component of innate immune responses includes an anatomical barrier, inflammation, complement cascade, and several types of white blood cells. The most critical innate antiviral mechanism is the production of Interferon, which is secreted and act in an autocrine and paracrine fashion. The recognition of interferon leads to the expression of hundreds of interferon-stimulated genes (ISGs). This primarily leads to either production of antiviral proteins like protein kinase R (PKR) that inhibit viral protein synthesis or the production of 2', 5'-oligoadenylate synthetase family that degrades viral RNA. The adaptive immune responses are characterized by two main components namely humoral immunity generating specific antibodies and cell-mediated effectors against a pathogen. The primary function of the acquired immune system is the specific recognition of non-self-antigens presented in context with Major histocompatibility complex (MHC) molecules, generation of tailored responses to eliminate pathogen or pathogen-infected cells, and the development of immunologic memory. Together, the innate and adaptive immune responses hinder viral replication and propagation.

1.1 Pathogen pattern recognition receptors

The host innate immune response sets within a few hours of viral infection. The degree and magnitude of such response decide the outcome of infection, containment or dissemination. Host cytoplasmic pattern recognition receptors (PRR) initiate the antiviral immune response that recognizes pathogen-associated molecular patterns (PAMPs) of viral nucleic acid. The primary PRRs families are Toll-like receptors (TLR), retinoic acid-inducible gene-I (RIG-I) like receptors (RLR) and Nucleotide-binding and oligomerization domain (NOD)-like receptors (NLR) (Figure 1). The binding of PAMPs to PRRs activates downstream signals to stimulate the transcription of a broad spectrum of genes to produce cytokines and chemokines (Wilkins and Gale, 2010) . Production and secretion of interferon including type-I interferon (IFN-I)/ IFN-αβ or type II interferon (IFN-II), or type III interferon (IFN-III)/ IFN-λ is a central event. The IFN pathway signaling is central to the generation of an antiviral state through ISGs in virus-infected and non-infected cells (S.-Y. Liu et al., 2011) . IFNs act as the first line of cell-intrinsic defense against viral infection and play a crucial role in initiating adaptive immune responses.

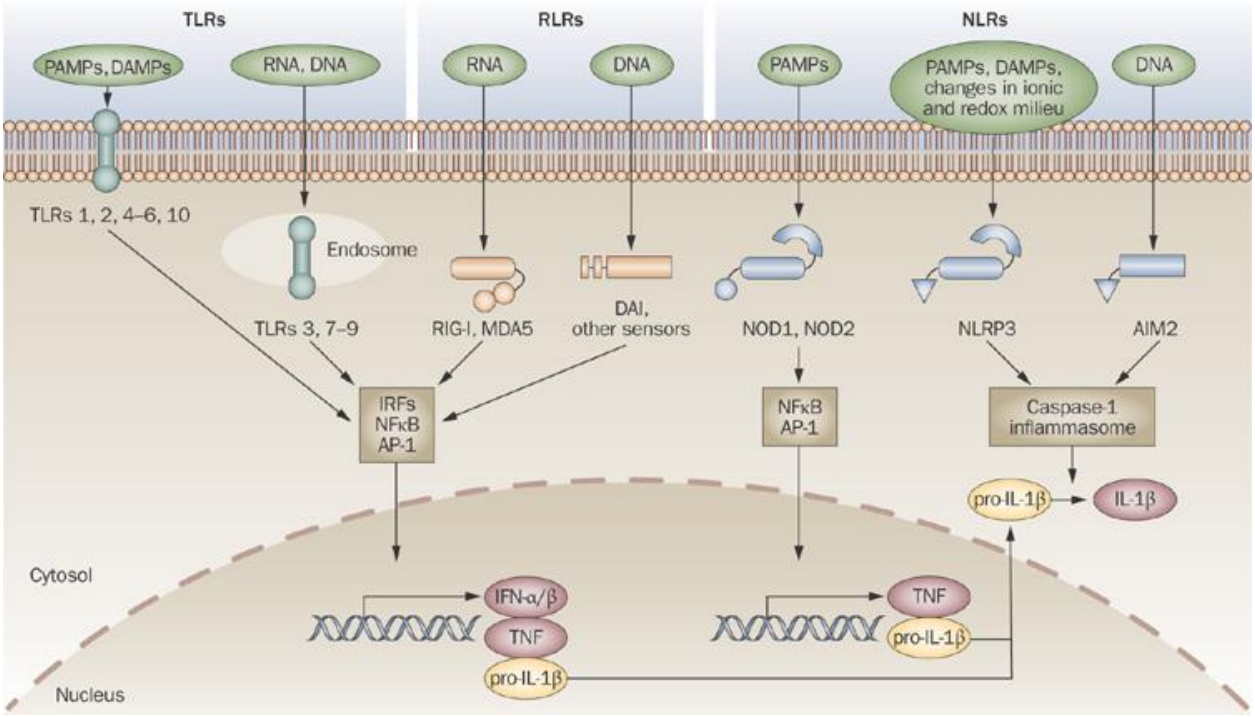

Figure 1: TLR, RLR, and NLR signaling pathways.

Three known innate immune sensors; TLRs, RLRs, and NLRs recognize harmful signals such as PAMPs, DAMPs, non-self nucleic acid, change in ionic or redox state at the cell surface, in the endosome or the cytoplasm. The recognition by TLRs and RLRs activate secondary messengers, which ultimately transduce the signal for activation and nuclear translocation of transcription factors such as IRFs, NFκB, and AP-1 that stimulate expression of cytokines like IFN-α/β, TNF and pro-IL-lβ. The NLRs further promotes the assembly of the caspase-1 inflammasome and subsequent maturation of IL-1β from pro-IL-1β (As adapted from Theofilopoulos et al. 2010).

Abbreviations: Danger-associated molecular pattern (DAMP), interleukin-1 (IL-1), interferon regulatory factor (IRF3), nuclear factor kappa-light-chain-enhancer of activated B cells (NFκB), Activator protein 1 (AP-1)

1.1.1 The RLR pathway

The two RLRs, RIG-I/ DExD/H-Box Helicase 58 (DDX58) and melanoma differentiation-associated 5 (MDA5) / interferon induced with helicase C domain 1 (IFIH1), sense double-stranded viral RNA (Onoguchi et al., 2011) . Engagement of viral RNA leads to a conformational change in RLR. In the open conformation, the amino-terminal caspase recruitment domain (CARD) is available to interact with mitochondrial antiviral signaling protein, mitochondrial antiviral signaling protein (MAVS) (Seth et al., 2005) . Activated MAVS undergoes topological change to expose its TNF receptor-associated factor 3 (TRAF) -interacting motif (TIM) domain for binding to TRAF3 and TRAF6 (Paz et al., 2011) . This leads to activation of canonical I-kappa-B kinase (IKKs) and related kinases like tumor necrosis factor receptor-associated factor (TRAF)-family member-associated NF-B activator (TANK)-binding kinase 1 (TBK1) (Pichlmair et al., 2006) . MAVS is also involved in assembling NF-kappa B Essential Modulator (NEMO) and TBK1 complex on the mitochondrial surface. MAVS is then degraded by proteasomal machinery to release this complex into the cytosol. Further, TBK1 phosphorylates interferon regulatory factor (IRF3) (Castanier et al., 2012) . The phosphorylated IRF3 dimerizes and translocates to the nucleus to bind to the ISRE promoter to trigger IFN production (Z. Wang et al., 2016) . Peroxisome also provides a platform for co-localization of activated MAVS. It induces IFN-independent antiviral response characterized by rapid and short-term protection (Dixit et al., 2010) .

1.1.1.1 Regulation of the RLR signaling:

Stimulation of both innate and adaptive immune pathways is crucial to host defense against infection. At the same time, these pathways are subjected to stringent regulation by cellular factors to maintain an appropriate degree of immune responses and to prevent cellular damage. All signaling pathways and activated proteins must be regulated, and the RLR pathway is no exception to this. Stringent regulatory mechanisms are needed to prevent any deleterious effect on the host.

1.1.1.2 Regulation of immune pathways by post-translation modifications

Post-translation modifications (PTM) is another mechanism by which various molecules involved in immune signaling are modified and regulated for its activation or destruction. PTMs increase the functional diversity of the proteome by the covalent addition of functional groups or proteins, proteolytic cleavage of regulatory subunits, or degradation of complete proteins. These modifications include phosphorylation, glycosylation, ubiquitination, nitrosylation, methylation, acetylation, lipidation and proteolysis, and influence almost all aspects of normal cell biology and pathogenesis.

1.1.1.2.1 Ubiquitination

Ubiquitination is one of the universal posttranslational protein modifications occurring in the cell. Ubiquitin, an evolutionarily highly conserved 76 amino acid polypeptide, is covalently attached to lysine residues of target proteins through a highly organized and hierarchical group of enzymes. As there are seven lysine residues on ubiquitin, it is possible that during ubiquitination, new ubiquitin molecules added to one of the seven lysine residues of the previously conjugated ubiquitin. This process, called polyubiquitination, is a standard cellular signal. Depending on the usage of the lysine residues on ubiquitin, various linkage-specific ubiquitinations could happen; which include K6, K11, K27, K29, K33, K48, K63, and M1. K48 and K63 linkage-specific ubiquitinations are the most effective forms of polyubiquitination; In contrast to the proteolytic role of the K48-specific linkage, the K63-specific linkage has been demonstrated to regulate a variety of nonproteolytic cellular functions, including deoxyribonucleic acid (DNA) damage repair, stress responses, and inflammatory pathways (Figure 2)

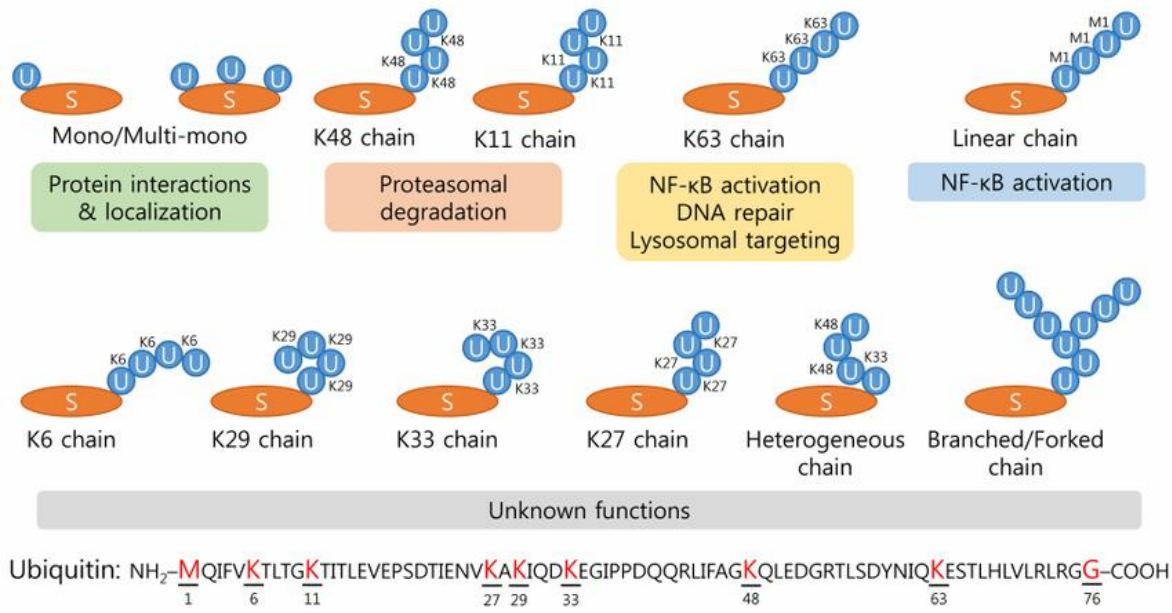

Figure 2: Types of ubiquitination and their role in cellular processes.

Mono-ubiquitination of the target protein is involved in protein interaction and localization. Poly-ubiquitination of K-48 and K-11 was found to be required for proteasomal degradation. Ubiquitination of K-63 chain plays a role in NF-κB activation, DNA repair, and lysosomal targeting. Linear chain M1 poly-ubiquitination was found to activate NF-κB signaling. The function of various other types ubiquitination including K-6, K-29, K-33, K-27, heterogenous chain, and branched chain is not known As adapted from(C. W. Park and Ryu, 2014) .

1.1.1.3 Regulation of RLR signaling by host cellular proteins

The levels of RIG-I are subjected to transcriptional and post-transcriptional regulations, which maintain its appropriate response. Post-translational modifications activate or deactivate the protein function, which ultimately decides the fate of the signaling pathway. An E3 ligase including tripartite motif-containing (TRIM)-25 binds to the CARD domain of RIG-I, resulting in the conjugation of K-63 ubiquitin chain to the lysine 172 of the CARD domain. Ubiquitination of RIG-I is critical for its activation and binding to MAVS that ultimately activate IFN production (Matsumiya and Stafforini, 2010) . TRIM25 B30.2 domain interacts with both CARD1 and CARD2 domains of RIG-I to open the N terminal α helix (D'Cruz et al., 2018) .

MAVS is a central mediator of the RLR pathway and subjected to the regulation by host factors and is also the target of viral proteins (F. Liu and Gu, 2011) . The host protein NLR family member X1 (NLRX1) co-exists with MAVS on the outer mitochondrial membrane. It was found to be a potent inhibitor of MAVS-mediated IFNβ promoter activity (Moore et al., 2008) . Another protein, Poly C binding protein2 (PCBP-2) is induced after viral infection. It recruits E3 ligase, atrophin-interacting protein 4 (AIP4), which polyubiquitinates MAVS leading to proteasomal degradation (You et al., 2009) . Thus, NLRX1 and PCBP2 are involved in the negative regulation of MAVS-mediated signaling.

Another host protein HSCARG was found to regulate IFNβ production negatively (Figure 3). Following the viral infection, HSCARG interacts with TRAF3 and cooperates with ovarian tumor (OTU) deubiquitinase Ubiquitin Aldehyde Binding (OTUB1) to remove

Lys63-linked polyubiquitin chain from TRAF3. This further decreases the recruitment of IKKε and results in decreased phosphorylation of IKKε and IRF3, and finally reduces the production of IFN-β (Peng et al., 2014) . Some host proteins like ring finger protein 5 (RNF5), Itchy ubiquitin E3 protein ligase (ITCH), myeloid differentiation primary response 88 (MyD88), and interleukin1 receptor-associated kinase (IRAK) participates in the regulation of RIG-I and TLR pathway (Heaton et al., 2016) .

1.1.1.4 Regulation by TRIM proteins

Upon recognition of RNA viruses, RIG-I induces the synthesis of inflammatory cytokines and type I IFNs. Briefly, RIG-I recruits the adapter MAVS and activates NF-κB (p50/RelA heterodimer) and IRF3 via IKKα/IKKβ/NEMO and TBK1/IKKi, respectively. The transcription factor is translocated to the nucleus and promote IFN transcription, translation, and secretion. The secreted IFNs activate the STAT1/STAT2/IRF9 complex via JAK or tyrosine kinase (TYK) to induce ISGs, including TRIM proteins.

More than 60 TRIM proteins are known in human and mice. IFN-I/ IFN-II induces several TRIM proteins that are involved in the tight regulation of antiviral immune pathways. Many TRIM proteins like TRIM 5, 8, 11, 21, 25, 32, 63 have E3 ubiquitin ligase activity (Keiko Ozato et al., 2008a) . Several cellular target proteins and their positive or negative regulation by TRIM have been identified (Figure 4). TRIM25 induces the ubiquitination of RIG-I to promote downstream signaling. TRIM23 enhances NEMO

function by promoting ubiquitination and TRIM27 interferes with IKKα/IKKβ and TBK1/IKKi activation. TRIM21 is involved in the inhibition of IKKβ and IRF7 and positive or negative regulation of IRF3 and IRF8. TRIM56 enhances STING function during DNA sensor signaling pathways for the induction of type I IFNs (Kawai and Akira, 2011) . Collectively, due to the diversity of TRIM proteins, they are capable of either stimulation or inhibition of a signaling pathway that is involved in recognition of PRRs.

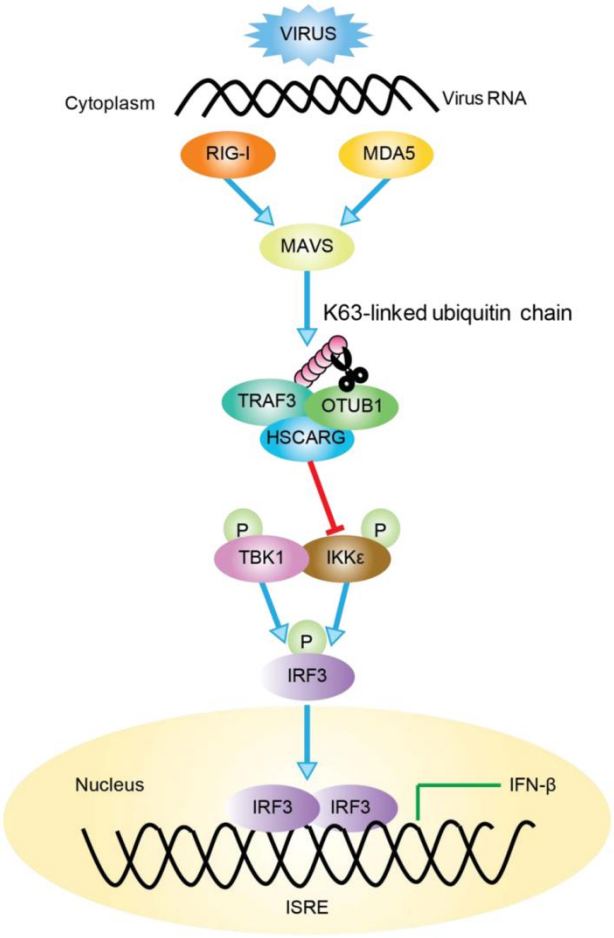

Figure 3: A model of TRAF3-dependent regulation of RLR signaling pathway by HSCARG.

Following the viral infection, HSCARG interacts with TRAF3 and OTUB1 to decreases the recruitment of IKKε and results in decreased phosphorylation of IKKε and IRF3, and finally reduces the production of IFN-β As adapted from (Peng et al., 2014) .

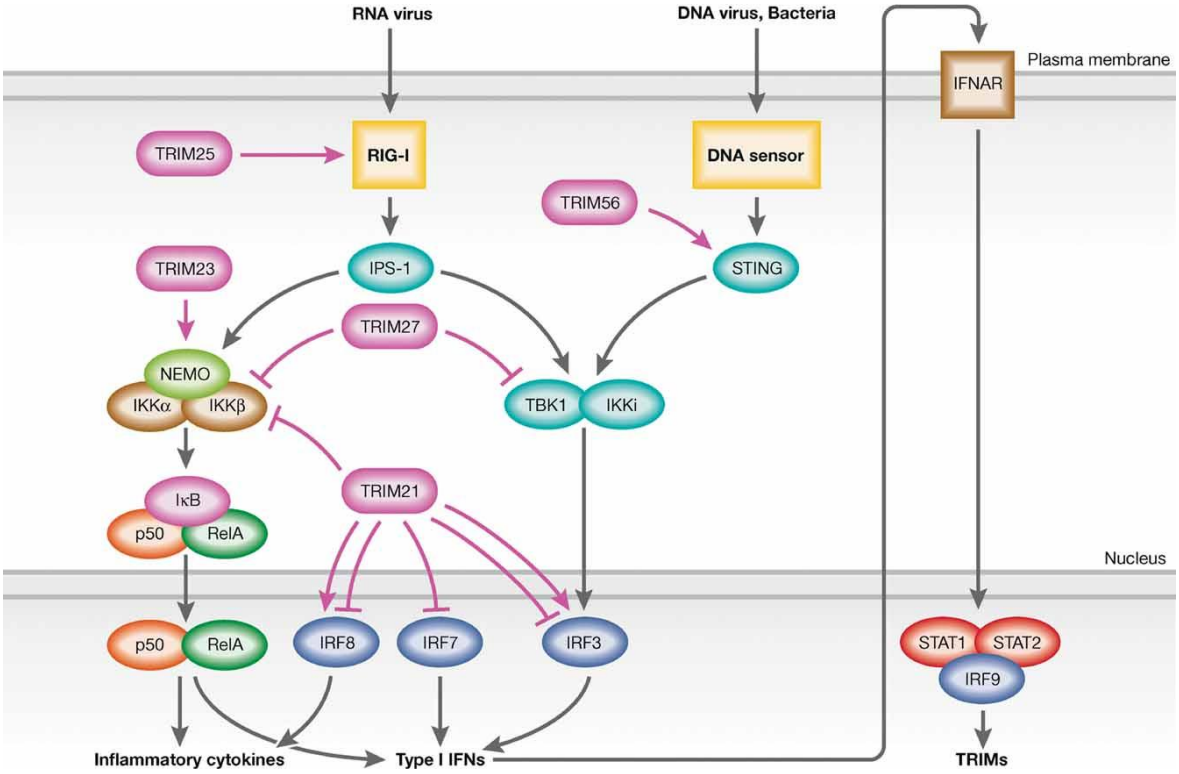

Figure 4: Regulation of RIG-I and DNA sensor signaling by TRIM proteins.

TRIM25, TRIM23, and TRIM56 positively regulate RIG-I, NEMO, and STING, respectively. TRIM27 negatively regulates IKK complex or TBK1 activity. TRIM21 shown to inhibit NEMO-IKK complex and IRF7 activity and able to regulate both positively or negatively IRF8 and IRF3 activity As adapted from (Kawai and Akira, 2011)

1.2 Interferon response

As a result of viral recognition and downstream signaling, fibroblast and monocytes secrete IFN-I. IFN-Is bind the cell surface receptor IFN-α/β receptor (IFNAR1/2) heterodimer, which then recruits, two JAK molecules. JAK phosphorylates IFNAR and STAT, which then dimerize and enter the nucleus and transcribe ISGs. Several ISGs directly inhibit virus infection by targeting the early or late stage of the viral life cycle in the host. This fast and amplified response combats viral infection (Schneider et al., 2014) .

1.2.1 Interferon types and receptors

Type I IFNs comprise the most significant IFN class, and all human cells are capable of IFN-I production(Siegal et al., 1999) . This class involves IFN-α, IFN-β, IFN-ε, IFN-κ, and IFN-ω, which are all grouped on chromosome 9. IFN-I is recognized by the heterodimeric receptor complex containing IFNAR1 and IFNAR2 subunits (Figure 5). The different types of IFN-I show differential tissue expression level and binding affinity for the IFNAR1/2 receptor complex (Pestka et al., 2004) .

There is only one type II IFN, IFN-γ. It is a homodimeric protein recognized by the IFN-γ receptor complex (IFNGR). Two IFNGR1 subunits initiate binding to IFN-γ followed

by the recruitment of two auxiliary IFNGR2 subunits and results in receptor enactment (Walter et al., 1995) . IFN-γ production is to a great extent confined to immune cells. However, the IFNGR1/2 receptors are broadly distributed, and almost all cell types are responsive to IFN-γ (Valente et al., 1992) . Two primary functions of IFN-II are immune regulation and connecting innate immune responses to adaptive immunity. Broadly, IFN-II is involved in up-regulation of pathogen recognition, antigen processing and presentation, antiviral state, inhibition of cellular proliferation and effects on apoptosis, activation of microbicidal effector functions, immunomodulation, and leukocyte trafficking (Schroder et al., 2004) .

The more recently discovered IFN-III subfamily is comprised of IFNL1/ IFNλ1/ interleukin (IL)-29, IFNL2/ IFNλ2/ IL-28A, IFNL3/ IFNλ3/ IL-28B. All three IFN-λs signal through the same heterodimer receptor complex composed of IFNLR1 and interleukin -10 receptor 2 (IL-10R2) (Sheppard et al., 2003) . IFN-λs may interfere with virus infection by various mechanisms including direct antiviral effect, or as a modulator of IFN-α-induced signaling via the suppressor of cytokine signaling 1 (SOCS) and the ubiquitin-specific peptidase 18 (USP18) inhibitory feedback loops (Syedbasha and Egli, 2017) . IFN-III showed potent antiviral Encephalomyocarditis virus (EMCV) activity in vitro but was unable to reduced infection in the murine model when treated singularly. On the other hand, IFN-III treatment prevents the disease pathogenesis by blocking herpes simplex virus-2 (HSV-2) replication in the vaginal mucosa (Ank et al., 2006) . IL28B contributes to Hepatitis C virus (HCV) resistance and is known to be upregulated by interferon and by RNA virus infection (Suppiah et al., 2009) .

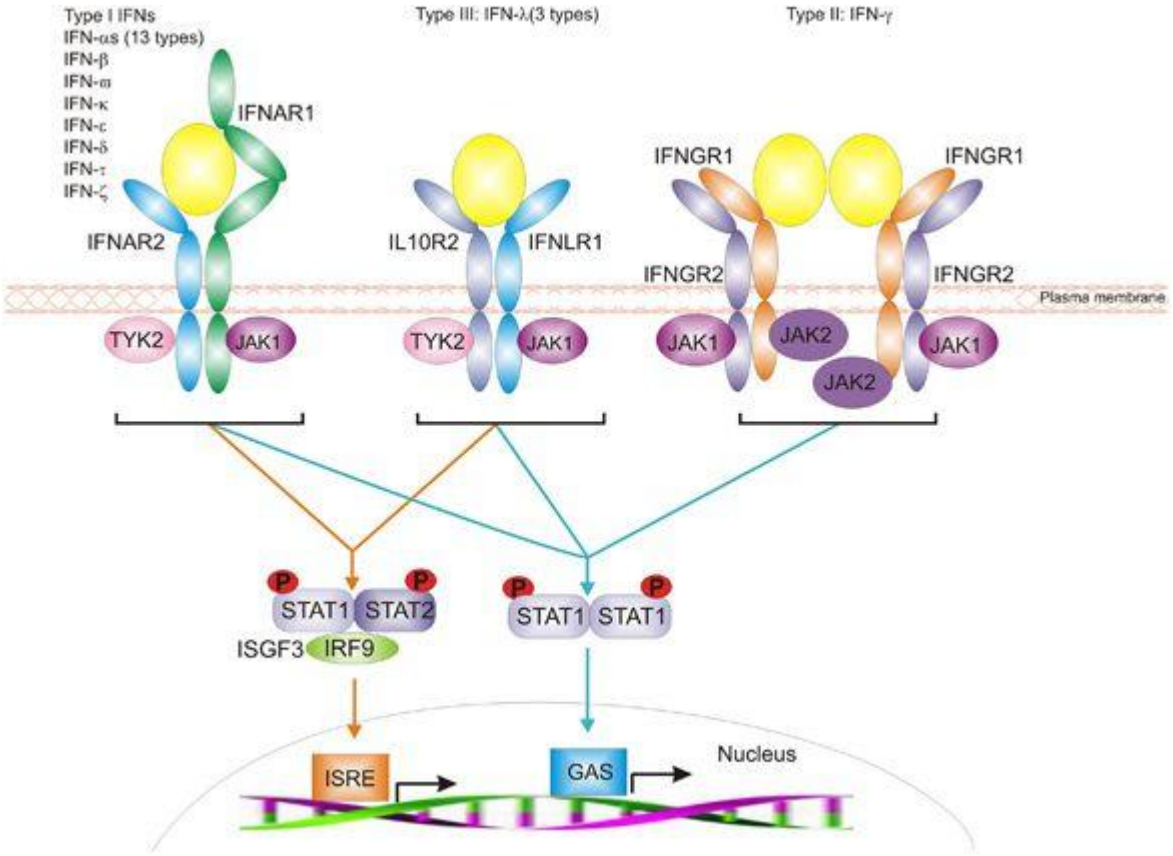

Figure 5: IFN-I, IFN-II, and IFN-III signaling.

IFN-I, IFN-II, and IFN-III bind to distinct receptors namely IFNAR1- IFNAR2 dimer, IFNGR1-IFNGR2 tetramer, and IFNLR1-IL10R2 dimer, respectively. Association of IFN with the receptor complex activates TYK2 and JAK1 kinases, which phosphorylate and dimerize STAT1 and STAT2. Phosphorylated STAT1-STAT2 dimer in association with IRF9 generates the ISGF3 complex. The IFN and receptor binding could also generate phosphorylated STAT1 dimer as a transcription factor. The transcription factors, ISGF3 or STAT1 dimer, translocate to the nucleus and bind to ISRE to activate transcription of several ISGs. As adapted from (https://www.creative-diagnostics.com/blog/index.php/interferons-and-interferon-receptors/)

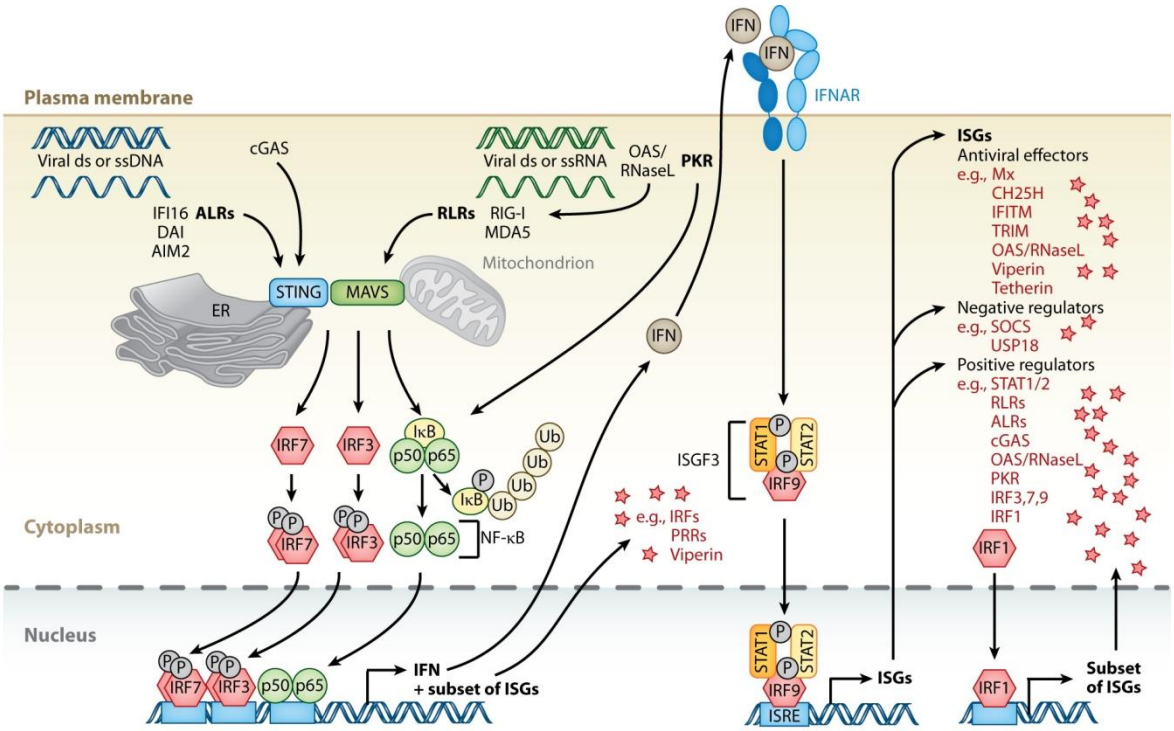

Figure 6: Antiviral innate immune signaling involves three following significant events.

First, recognition of viral DNA/ RNA by PRRs to activate IFN production. Second, the association of secreted interferon with IFNR to express hundreds of ISGs. Third, the action of ISGs as antiviral effectors or regulate these two pathways positively or negatively As adapted from (Schneider et al., 2014)

1.2.2 Interferon response- JAK-STAT pathway

Association of IFN with the receptor complex activate JAK-STAT signaling pathway (Figure 6). Briefly, IFNRs specifically recognize IFN and dimerize two receptor subunits, which activates TYK2 and JAK1 kinases, which phosphorylate and dimerize STAT1 and STAT2. Phosphorylated STAT1-STAT2 dimer in association with IRF9 generates the ISGF3 complex. The IFN and receptor binding could also generate phosphorylated STAT1 dimer as a transcription factor. The transcription factors, ISGF3 or STAT1 dimer, translocate to the nucleus and bind to ISRE to activate transcription of several ISGs.

1.2.2.1 Janus Kinases (JAKs)

The known JAKs include JAK1, JAK2, JAK3, and TYK2 (Kawamura et al., 1994) (Stark et al., 1998) . They comprise the catalytic kinase domain and regulatory pseudo-kinase domain (Ke Shuai and Liu, 2003) .

1.2.2.2 STAT

There are seven known mammalian STATS, STAT1, STAT2, STAT3, STAT4, STAT5A, STAT5B, and STAT6. They have homologous regions of SRC homology 2 (SH2) domain, DNA-binding domain, and a transactivation domain. The amino-terminal region of

STATs is involved in regulating STAT activity, such as the formation of STAT tetramers (Xu et al., 1996) and tyrosine dephosphorylation (K. Shuai et al., 1996) .

1.2.2.3 Interferon-stimulated genes: ISG

ISGs are involved in various effector function including directly targeting molecules required during the pathogen life cycle, maintaining cellular homeostasis by regulating antiviral state, pro-apoptotic proteins leading to cell death (Schneider et al., 2014) . ISGs are capable of enhancing pathogen recognition properties as well as regulating signaling through the JAK-STAT pathway. Some PRRs and IRFs expression is amplified by IFN, leading to enhanced pathogen recognition. A subset of ISGs is capable of IFN-independent activation to counteract pathogen-mediated innate immune evasion strategies (Iwasaki, 2012) .

A recent study aimed to decipher molecular mechanisms of ISG network identified 104 ISGs interactions and 1401 cellular partners. Various ISGs interact with some shared partners suggesting their central role in ISG mediated antiviral immune response. While few others attribute to specific interactome, suggesting a discreet role in particular viral infection (Hubel et al., 2019) .

Interferon-induced transmembrane protein-1 (IFITM1), IFITM2, and IFITM3 coordinate to induce antiviral activity in the interferon-stimulated cell. Endosomal IFITM3 combines with entering viral particle and inhibits viral fusion with lysosomal membrane

and thus release of the viral genome to the cytoplasm for replication. IFITM3 binding to the virus is specific and require s-palmitoylation (Ritz et al., 2011) . Although S-palmitoylation enhances IFITM3 membrane affinity and antiviral activity, ubiquitination decreases its localization with endolysosomes and antiviral activity in influenza infection (Yount et al., 2012) .

Oligoadenylate synthetase (OAS) detects cytosolic PAMPs leading to the synthesis of 2'-5'-oligoadenylates, which then act as intracellular second messengers to activate latent RNaseL. Activated RNase L degrades viral RNA, which can be sensed by RLRs, ultimately amplifying IFN response (Chakrabarti et al., 2011) .

They are two Myxovirus resistance (Mx) proteins, Mx1/ MxA, and Mx2/ MxB, which are related to dynamin-like large guanosine triphosphatases (GTPases) family of protein. Mx proteins are found to potently block viral entry by trapping incoming viral nucleotides and preventing its cellular movement. Mx1 contains a central stalk domain and a GTPase effector domain, which are both essential for self-oligomerization and formation of ring-like structures that bind to and impose conformational changes on the target protein (Klockow et al., 2002) . Mx2 potently inhibits human immunodeficiency virus 1 (HIV-1) and HIV-2 entry (Kane et al., 2013) . It keeps the reverse-transcribed genome from reaching its nuclear destination, thereby ultimately inhibiting chromosomal integration, which is an essential event of the HIV-1 replication cycle (Z. Liu et al., 2013) .

IFN stimulation induces several TRIM family of proteins. TRIMs are composed of 60 members and mainly function as an E3 ubiquitin ligase (K. Ozato et al., 2008b) . One of

the most studied TRIM as an ISG is TRIM5α, a potent inhibitor of HIV-1 entry (Stremlau et al., 2004) . TRIM5α binds to HIV-1 capsid, uncoating and exposing the viral nucleoprotein complex (Campbell et al., 2008) . Another protein TRIM22 inhibits expression of the HIV-1 long terminal repeats (Tissot and Mechti, 1995) . It also inhibits trafficking of the HIV-1 Gag protein to the host cell plasma membrane, resulting in reduced viral production (Barr et al., 2008) . TRIM22 has also been shown to inhibit multiple viruses by various mechanisms. It inhibits transcription from the core promoter of hepatitis B virus (HBV), blocks EMCV replication by promoting ubiquitination of the viral 3C protease, and targets influenza A virus nucleoprotein for proteasomal degradation (Schneider et al., 2014) .

Activation of dsRNA dependent PKR via IFN stimulation leads to a significant reduction in host mRNA production/ translation. In contrast, PKR is found to be crucial for the integrity of newly synthesized IFN mRNA to generate an optimal host antiviral immune response. Also, PKR is involved in the degradation of the inhibitor of κB (IκB), resulting in activation of the NF-κB signaling pathway (Munir and Berg, 2013) .

1.2.2.4 IFN desensitization

Interferon stimulation induces transcription of two genes, IFN-IND1 and IFN-IND2 within 30 minutes to 2 hours. Shortly after that cells undergo an IFN- desensitized state. It allows cells to recover from the IFN signaling expenditure (Larner et al., 1986) . Diverse

mechanisms achieve this negative regulation; some are cell intrinsic, while others are ISG mediated.

1.2.2.5 Regulation of interferon response by Post-translation modifications

PTM activates/ deactivates proteins rapidly leading to a quick response in signal transduction. PTM regulating JAKs and STATs functions includes phosphorylation, methylation, ubiquitination, and ISGylation.

Tyrosine phosphorylation of JAK2 is required for its efficient ubiquitination. JAK2 is ubiquitinated and rapidly degraded, which can be enhanced by IL-3 and IFN-γ. The SOCS box of SOCS1, which interacts with elongins B and C, is required for the ubiquitination of JAK2. So, the stability of JAK2 seems to be regulated by a SOCS1-mediated ubiquitin-proteasome pathway (Ke Shuai and Liu, 2003) .

In a process known as ISGylation, a small IFN-induced gene 15 (ISG15) that is ubiquitin-like protein is covalently attached to target proteins through a series of steps that mirror the ubiquitination pathway. ISG15 ISGylates JAK1 and STAT1 to regulate their function (Malakhova et al., 2003) . The removal of ISG15 conjugates (de-ISGylation) is performed by the isopeptidase activity of an ISG, USP18. (Malakhov et al., 2002) USP18 is a chief player in maintaining long-lasting desensitization of IFN-I signaling by ISGylation-dependent and independent manner. In an ISGylation independent mechanism, USP18 binds to the intracellular domain of IFNAR2, which prevents the binding of JAK1 (Malakhova et al., 2006) .

The intracellular conserved domain of IFN receptor, Serine 532, is phosphorylated and subsequently ubiquitinated by Skp, Cullin, F-box protein (SCF) E3 ubiquitin ligases.

However, the exact mechanism and outcome of ubiquitination are not clearly understood.

The tyrosine phosphorylation of JAKs and STATs catalyzes their activation. Independently, serine phosphorylation is observed on STAT1, STAT3, STAT4, STAT5A, and STAT5B (Levy and Darnell, 2002) . STAT1 is phosphorylated on Serine 727 by one of several kinases including extracellular signal-regulated protein kinase (ERK), p38, JUN N-terminal kinase (JNK), and protein kinase Cδ (PKCδ) (Decker and Kovarik, 2000) .

The arginine 31 methylation of STAT1 occurs constitutively, independently of tyrosine or serine phosphorylation. It increases the DNA-binding activity of STAT1, possibly due to inhibition of the interaction of PIAS1 with non-methylated STAT1 (Mowen et al., 2001) . The ubiquitin-proteasome pathway regulates polyubiquitination of STAT1 (T. K. Kim and Maniatis, 1996) . It has been shown that STAT1 can be modified by small ubiquitin-related modifier (SUMO)lyation on Lys703, which can be strongly enhanced by PIAS proteins (Rogers et al., 2003) .

1.2.2.6 Regulation of IFN response by host proteins

Three primary JAK-STAT regulators include Suppressors of Cytokine Signaling (SOCS), Protein Inhibitors of Activated STATs (PIAS) and Protein Tyrosine Phosphatases (PTPs) (Figure 7).

There are eight known SOCS proteins including CIS (cytokine-inducible SH2 domain protein) and SOCS1–SOCS7 (Hilton, 1999) . SOCS proteins bind to phosphorylated tyrosine residues, on either the JAKs or IFNRs, inhibiting JAK activity and STAT-binding. The C terminus of SOCS recruits proteins involved in receptor ubiquitination and proteasome degradation. SOCS proteins are induced early in the IFN response and play an essential role in early IFN desensitization (Hong and Carmichael, 2013) . The SOCS box can also bind to ubiquitin E3 ligase elongins B and C, suggesting that it targets signaling proteins for proteasomal degradation (Zhang et al., 1999) .

The mammalian PIAS family consists of four members including PIAS1, PIAS3, PIASX, and PIASY (K. Shuai, 2000) . PIAS has been shown to inhibit STAT-mediated gene activation by three possible mechanisms. PIAS1 and PIAS3 prevent the binding of the STAT dimers to DNA. While PIASX and PIASY might act as transcriptional co-repressors of STAT by recruiting other co-repressor proteins such as histone deacetylase (HDAC). PIAS proteins can regulate STAT1 by SUMO-lyation (Ke Shuai and Liu, 2003) .

PTPs regulate JAKs and exhibit specificity to negative regulation. Two SH2 domains-containing PTPase is SH-PTP1 and SH-PTP2 (Neel, 1993) . Another PTP, known as CD45 can directly bind and dephosphorylate all JAKs (Irie-Sasaki et al., 2001) . Two related PTPs, PTP1B and T cell protein tyrosine phosphatase (TCPTP), were shown to dephosphorylate JAKs, mainly TYK2 and JAK2 and regulate their activity (Myers et al., 2001) .

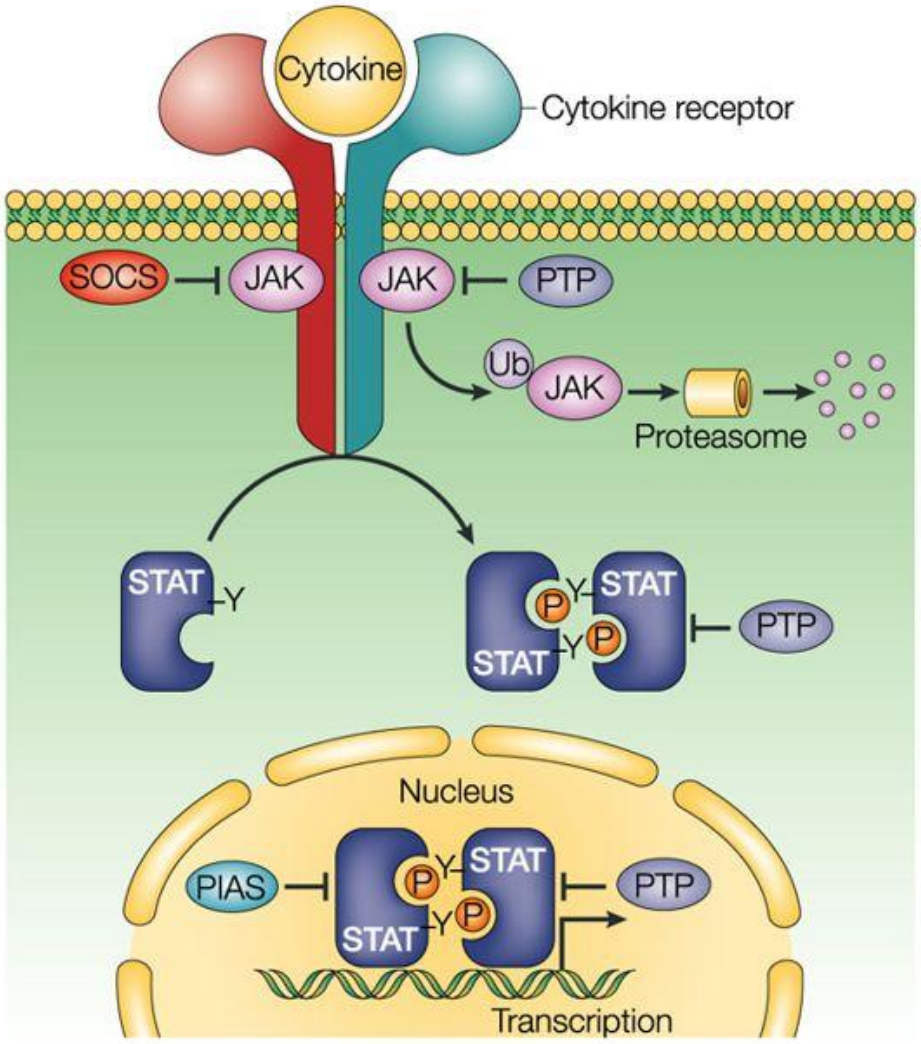

Figure 7: Regulators of the JAK-STAT pathway.

suppressor of cytokine signaling (SOCS) proteins, protein tyrosine phosphatases (PTPs), and Protein inhibitor of activated STAT (PIAS) As adapted from (Ke Shuai and Liu, 2003)

1.3 UBXNs

The human genome encodes at least 13 ubiquitin-regulatory-X (UBX)-domain-containing proteins (UBXN) (Alexandru et al., 2008) (Figure 8). Throughout the species, individual UBXNs are well conserved. Based on their protein domain composition, the human UBXNs are sub-classified into two main groups: the ubiquitin-associated (UBA)-UBX proteins and UBX-only proteins. The UBA domain motifs are predicted to interact with target proteins for nonredundant proteasomal degradation. The UBX domain of all UBXNs might bind and influence the function of an ATPase associated with diverse cellular activities (AAA)-ATPase, p97, which is also called as valosin-containing protein (VCP) (Schuberth and Buchberger, 2008) . VCP is a multifunctional protein involved in cellular processes like Endoplasmic-reticulum-associated protein degradation (ERAD), autophagy, endosomal sorting, mitochondrial and cytoplasmic protein degradation (Chapman et al., 2011) . The UBA-UBX domain proteins could bind to E3 ligase and recognize K-11 and K-48 polyubiquitin chains, demonstrating their role in ubiquitin-dependent proteasomal degradation pathway. Association of UBXNs with the binding partners like p97 and E3 ubiquitin ligases strongly suggests their role in the regulation of global protein turnover and cellular signaling.

Ubiquitin-dependent proteasomal degradation is one of the most studied protein degradation mechanisms. The role of VCP in ERAD is well established in this process. Proteomic networking analysis of VCP and its UBX domain cofactors revealed that various UBA-UBX domain-containing proteins form complexes with VCP and are also associated

with E3 ubiquitin ligases. UBXNs have diverse roles, and the substrate-specific degradation is carried out via specific UBXN-VCP complex. Interaction of VCP, nuclear protein localization protein 4 (NPL4), and Ubiquitin Recognition Factor In ER-Associated Degradation 1 (UFD1) with the substrate hypoxia-induced factor 1-α (HF-1α) and E3 ligase requires UBXN7. In the native state, the UBA and UBX domains are bound to each other. The UBX domain serves as a binding platform for VCP only when the UBA domain is associated with a ubiquitinated substrate (Alexandru et al., 2008) .

The N-terminal domain of VCP binds multiple regulatory cofactors including the UFD1/NPL4 heterodimer and UBXNs. The crystal structure of the UBXN3A/ FAS-associated factor 1 (FAF1), UBX domain in complex with the VCP N domain, reveals that the signature Phe-Pro-Arg motif known to be crucial for interactions of UBX domains with VCP adopts a cis-proline configuration. Moreover, UBXN3A and UBXD7 only bind to VCP-UFD1/NPL4, but not free VCP, thus demonstrating a hierarchy in VCP-cofactor interactions (Hanzelmann et al., 2011) .

The connections among VCP and the PUB [PNGase (peptide N-glycosidase)/ubiquitin-associated] area of PNGase, the UBX space of p47, and the UBD (ubiquitin D) space of NPL4 have been fundamentally described. The UBX and UBD are auxiliary homologs that share comparable VCP-restricting modes. It is conceivable that different proteins that contain a UBX/UBX-like space likewise associate with VCP using comparable systems. Moreover, a few short VCP-collaborating themes, for example, VCP-binding motif (VBM), VCP-interacting motif (VIM) and SHP, have been recognized as of

late and are additionally shared between VCP connectors, implying that proteins having the equivalent VCP-restricting theme may likewise share standard VCP-restricting components (Yeung et al., 2008) .

The overview of each UBXN including its aliases, size, domains and functions are discussed further (Table 1).

1.3.1 UBXN1

Various UBXNs were found to be involved in decreased lentiviral and retroviral production. UBXN1, UBXN9, and UBXN11 interfere with NF-κB pathway by binding to Cullin 1 (CUL 1), which inhibits the inhibitor of kappa B (IκBα) degradation. UBXN1 was found in being involved in murine embryonic cell development, cell adhesion, immune response pathways (Hu et al., 2017) .

UBXN1 was shown to interfere with RNA virus-induced IFN-I response while potentially increasing replication of viruses such as vesicular stomatitis virus (VSV), Sendai, West Nile, and dengue virus. At the molecular level, UBXN1 targets MAVS and blocks MAVS oligomerization, and disrupts the MAVS/TRAF3/TRAF6 signalosome, ultimately affecting IFN production (P. Wang et al., 2013) . Similarly, UBXN1 was found to regulate NF-κB signaling. UBXN1, which contained both ubiquitin-associated and ubiquitin regulatory X (UBX) domains acts as a negative regulator of TNFα-triggered NF-κB activation. Over-expression of UBXN1 inhibited TNFα-triggered NF-κB activation, although knockdown of UBXN1 had the opposite effect. UBX domain-containing proteins usually

act as VCP cofactors. However, knockdown of VCP barely affected UBXN1-mediated NF-κB inhibition. At the same time, we found that UBXN1 interacted with cellular inhibitors of apoptosis proteins (cIAPs), E3 ubiquitin ligases of RIP1 in the TNFα receptor complex. UBXN1 competitively bound to cIAP1, blocked cIAP1 recruitment to TNF receptor 1 (TNFR1), and sequentially inhibited receptor-interacting serine/threonine protein kinase 1 (RIPK1) polyubiquitination in response to TNFα. These findings demonstrate that UBXN1 is an essential negative regulator of the TNFα-triggered NF-κB signaling pathway by mediating cIAP recruitment independent on VCP (Y. B. Wang et al., 2015) .

A recent study demonstrated that the induction of interferon is potentially suppressed by Nipah virus V protein via UBXN1. Briefly, Nipah virus V protein interacts with the UBX domain of UBXN1 via its proximal zinc-finger motif in the C-terminal domain. Also, the level of UBXN1 is increased in Nipah infection, by suppressing its proteolysis. Additionally, Nipah virus V protein suppressed RIG-I and MDA5-dependent interferon signaling by stabilizing UBXN1 and increasing the interaction between MAVS and UBXN1 (Uchida et al., 2018) .

UBXN1 was shown to negatively modulate ERAD. This requires the ability of UBXN1 to bind both polyubiquitin and VCP. Moreover, the binding of UBXN1 with VCP is positively regulated by polyubiquitin binding of the UBX protein. It was found that UBXN1 also negatively regulate the VCP-dependent processing required for degradation of a cytosolic, non-ERAD, substrate. Additionally, UBXN1 protect polyubiquitin from the activity of deubiquitinases, such as ataxin-3, that are necessary for efficient ERAD. Thus,

UBXN1 inhibits protein degradation mediated by VCP complexes by protecting polyubiquitin chains from deubiquitination (LaLonde and Bretscher, 2011) .

Another recent study demonstrates that UBXN1 is negatively regulated by epidermal growth factor receptor mutation vIII (EGFRvIII), which play a significant role in glioblastoma cancer. The upregulation of H3K27me3 mediates the down-regulation of UBXN1 in the presence of EGFRvIII. EGFRwt/vIII activate NF-κB by suppressing UBXN1 expression (Huang et al., 2017) . Another cancer study revealed that UBXN1 polypeptide recognizes auto-ubiquitinated breast cancer type 1 susceptibility protein (BRCA1) via the UBA domain. The recognition is made in a bipartite interaction in which the UBA domain of UBXN1 binds K6-linked polyubiquitin chains conjugated to BRCA1 and the C-terminal domain of UBXN1 bind the BRCA1/ BRCA1 Associated RING Domain 1 (BARD1) heterodimer in a ubiquitin-independent fashion. The E3 ligase activity of BRCA1/BARD1 is drastically reduced in the presence of UBXN1. Thus, UBXN1 regulates the enzymatic function of ubiquitinated BRCA1 (Wu-Baer et al., 2010) .

1.3.2 UBXN2A

UBXN2A binds to Mortalin (mot2) and prevents p53-mot2 complex formation. Mot 2 inactivates the tumor silencer p53's transcriptional and apoptotic function by cytoplasmic sequestration of p53 in select malignancies. Interrupted p53-mot 2 interactions can control the development of disease cells in colon cancer. The interaction

also discharges p53 from cytosolic sequestration, safeguarding the tumor silencer elements of p53. Thus UBXN2A acts as a home defense response protein, which can reconstitute inactive p53-dependent apoptotic pathways. Inhibition of mot2-p53 interaction by UBXN2A is an attractive therapeutic target in mot2-elevated colon cancer (Sane et al., 2014) .

UBXN2A also binds to alpha3, alpha4 subunits of neuronal nicotinic acetylcholine receptors (nAChRs). This binding affects alpha3 ubiquitination and proteasomal degradation. Thus, UBXN2A affects the stability and cell surface number of these receptors (Rezvani et al., 2009) .

1.3.3 UBXN2B

VCP complexes with UBXN2B in the cytosol and localizes to the Golgi and Endoplasmic reticulum (ER). VCP-UBXN2B complex showed membrane fusion activity (Uchiyama et al., 2006) . Another study showed that phosphorylation of UBXN2B on Serine-56 and Threonine-59 by Cdc2 at mitosis, and this phosphorylated UBXN2B does not bind to Golgi membranes.

UBXN2B phosphorylation inhibits the VCP/UBXN2B pathway. These results demonstrate that UBXN2B phosphorylation on Serine-56 and Threonine-59 is essential for Golgi disassembly at mitosis (Kaneko et al., 2010) .

UBXN2B regulates the orientation of the spindle, which is a crucial step in cell division process and determines tissue morphogenesis and development of an organism. Briefly, spindle orientation is regulated via Gαi-LGN- nuclear mitotic apparatus protein (NuMA) complex. UBXN2B inhibits cortical NuMA levels via the protein phosphatase 1 (PP1) and its regulatory subunit Repo-Man. In metaphase, UBXN2B negatively regulates the accumulation of NuMA, resulting in lower cortical NuMA levels and correct spindle orientation (B. H. Lee et al., 2018) .

PP1 exhibits different functional reaction with many substrates by the assembly of alternative PP1 holoenzymes. Newly formed holoenzyme needs to be disassembled by the VCP AAA-ATPase to promote exchange for the substrate. UBXN2B acts as an adaptor in this process. The UBXN2B shp1, eyc, and p47 (SEP) domain interact with inhibitor-3 (I3) without the need for ubiquitination. Thus, VCP-UBXN2B complex function in a ubiquitin-independent manner in PPI biogenesis (Weith et al., 2018) .

In a recent study, VCP inhibitor analogs were evaluated for their ability to inhibit the ATPase activity against VCP, VCP-UBXN2B or VCP- Npl4-Ufd1 heterodimer (NU). The protein sequence of UBXN2B is 50 % identical to that of p47. However, unlike p47, UBXN2B does not significantly change the potencies of most of the tested analogs, suggesting complex -specific VCP inhibitors need to be developed (Gui et al., 2016) .

1.3.4 UBXN3A

UBXN3A associates with Fas-associated death domain protein (FADD) and caspase 8. The death effector domains (DEDs) of caspase-8 and FADD interacts with the amino acid 181-381 region of UBXN3A. Its over-expression in Jurkat cells causes apoptotic death. It is suggested that UBXN3B is a member of multiple Fas-death-inducing signaling complex (Fas-DISC), acting upstream to caspase 8 (Ryu et al., 2003) . Also, UBXN3B can drive breast cancer metastasis. UBXN3A destabilizes transforming growth factor β receptor II (TGF-βRII) on the cell surface by recruiting the VCP/E3 ligase complex. AKT phosphorylates UBXN3B at ser582, which abrogates UBXN3A activity and increases cell surface receptor availability. It leads to heightened TGF-β response and epithelial-to-mesenchymal transition (EMT) and metastasis (Xie et al., 2017) .

UBXN3A positively regulates RNA virus-induced antiviral responses. Briefly, it competitively binds with NLRX1, which liberates MAVS from NLRX1-inhibited state. The free MAVS can bind to RIG-I and activate downstream signaling (J. H. Kim et al., 2017) . UBXN3A can also regulate MAVS activity by a different mechanism. TRIM31 is an E3 ligase that catalyzes lysine 63-linked poly-ubiquitination of MAVS. UBXN3A can antagonize the poly-ubiquitination and aggregation of MAVS by competing with TRIM31. Also, viral infection triggers the kinase IKKε directly which phosphorylates serine 556 of UBXN3A and triggers UBXN3A de-aggregation. Moreover, Ser556 phosphorylation promotes UBXN3A lysosomal degradation, consequently relieving UBXN3A-dependent suppression of MAVS (Dai et al., 2018) .

The UBXN3A N-terminal UBA domain recognizes Lys(48)-ubiquitin linkage to recruit polyubiquitinated proteins and its C-terminal UBX domain interacts with VCP. VCP association to the C-terminal UBX domain regulates ubiquitin binding to the N-terminal UBA domain. The VCP-Npl4-Ufd1 complex is known as the machinery required for endoplasmic reticulum-associated degradation. UBXN3A binds to VCP-Npl4-Ufd1 complex via its UBX domain and polyubiquitinated proteins via its UBA domain to promote ERAD (J. J. Lee et al., 2013) .

UBXN3A is involved in negative regulation of NF-kappaB activation. UBXN3A binds to NF-kappaB p65 via its death effector domain (DED)-interacting domain (amino acids 181-381), where DEDs of the Fas-associated death domain protein and caspase-8 interact (M. Y. Park et al., 2004) .

1.3.5 UBXN3B

UBXN3B plays a role in the regulation of lipid metabolism. UBXN3B is capable of sensing unsaturated fatty acids (FAs). This exposure alters UBXN3B structure. It ultimately results in the inhibition of the synthesis of triglyceride (TGs) from diacylglycerols (DAGs) (J. N. Lee et al., 2010) . Another study showed that trafficking of UBXN3B to lipid droplets (LD) is restricted when it associates with ER-resident pseudo-protease UBA domain containing 2 (UBAC2). Also, LD size is increased when VCP is recruited to LD via UBXN3B association. This has resulted from an inhibition of adipose triglyceride lipase (ATGL)

activity and dissociation of co-activator comparative gene identification (CGI-58) (Olzmann et al., 2013) .

Hepatocyte-specific UBXN3B knockout mice on a high-fat diet showed significantly lower serum triglyceride and secreted very low-density lipoprotein (VLDL) as compared to wild type mice. Lipidated apolipoprotein B (ApoB) was accumulated in lipid droplet of UBXN3B knockout mice hepatocytes. The accumulation could ultimately result in periportal macrovascular steatosis (Imai et al., 2015) . UBXN3B was shown to target HMG-CoA reductase (HMGCR) to its proteasomal degradation. It affects rate-limiting enzymatic catalysis of the mevalonate pathway. Thus, UBXN3B is also capable of regulating de novo sterol biosynthesis to control cholesterol synthesis (Loregger et al., 2017) .

Our recent study demonstrated that UBXN3B positively regulates STING signaling. STING was first identified as a DNA sensor and recently shown to be involved in anti-viral responses against RNA viruses also. *Ubxn3b* knockout mice, like *Sting* knockout mice, are highly susceptible to lethal herpes simplex virus 1 (HSV-1) and VSV infection, which is correlated with deficient immune responses. Functional studies demonstrate that UBXN3B interacts with both STING and activate STING signaling via ubiquitination, dimerization, trafficking. Thus, UBXN3B is involved in the positive regulation of STING signaling (Yang et al., 2018) .

1.3.6 UBXN4

UBXN4/UBXD2/erasin is an ER and nuclear envelope integral membrane protein with both its N- and C-termini facing the cytoplasm or nucleoplasm. A single 21-amino-acid sequence located near the C-terminus is necessary and sufficient for localization of UBXN4 to the ER. UBXN4 protein expression increases during stress. It binds VCP via its UBX domain and triggers ERAD substrate CD3delta. Also, UBXN4 was found to accumulates preferentially in neurons undergoing neurofibrillary degeneration in Alzheimer's disease (Liang et al., 2006) . Knockdown of UBXN4, which serves a binding platform for VCP and ubiquitin in human cells slowed the degradation of two classical ERAD substrates. In *Caenorhabditis elegans*, ubiquitin and UBXN4 are ER stress-response genes that are regulated by the ire-1 branch of the unfolded protein response pathway. Loss of ubiquitin or UBXN4 activates ER stress, increases the accumulation of polyubiquitinated proteins, and shortens the lifespan of worms. These results demonstrate a role for this complex in ERAD and the regulation of ER stress (Lim et al., 2009) .

1.3.7 UBXN6

UBXN6 is one of the essential cofactors of VCP involved in the endolysosomal localization leading to autophagy. Upon endosome and lysosome rupture, VCP is recruited along with cofactors UBXN6, phospholipase A-2-activating protein (PLAA), and deubiquitinating enzyme YOD1. This endo-lysosomal response complex acts downstream of K-63 ubiquitination and p62 recruitment. It stimulates autophagy by selectively

removing K-48 ubiquitinated proteins from damaged lysosomal repertoire (Papadopoulos et al., 2017) .

VCP in the association of several co-factors involved in the cellular processes that maintain homeostasis. Mutations at the interface between the N-terminus and the first of two ATPase areas (D1 and D2) in VCP deregulate the ATPase action and cause a multisystem degenerative disorder, inclusion body myopathy in Paget disease of bone and frontotemporal dementia/amyotrophic lateral sclerosis. These mutations found to prominently weaken the VCP- UBXN6 interaction during caveolin-1 (CAV-1) endolysosomal sorting. The N-terminus of UBXN6 is critical and can be classified as intrinsically disordered. The N-terminal helices 1 and 2 of UBXN6 bind with VCP motifs.

Additionally, two distant epitopes on the VCP N-domain that include disease-associated residues and additional interaction between UBXN6-N terminus and the D1D2 barrel of VCP were identified. Functionally, binding of UBXN6 to VCP led to a reduction of ATPase activity and partial protection from proteolysis. Together, this study indicates that UBXN1 N terminus intercalates into the VCP and UBXN6-N terminal D1 interface, thereby modulating interdomain communication of VCP domains and its activity (Trusch et al., 2015) .

CAV1 is a plasma membrane-resident sorted to endosome and lysosome by VCP-UBXN6 complex. Six lysine residues in the N-terminal region of CAV1 get ubiquitinated, which then bind and recruit VCP-UBXN6 complex to endosomes (Kirchner et al., 2013) . VCP missense mutation leads to degenerative disease in humans, in which muscle-specific

caveolin-3 accumulates in sarcoplasmic pools and specifically delocalizes from the sarcolemma. The formation of CAV-VCP-UBXN6 complex is compromised by a disease-associated mutation, which leads to defective endosomal sorting of ubiquitylated CAV-1. Thus UBXN6 activity was found to be affected by VCP mutation (Ritz et al., 2011) .

VCP, in association with the Ufd1-Npl4 heterodimer as an adaptor, plays an essential role in ERAD. Several UBXNs recruit ubiquitinated substrates to VCP/Cdc48 by binding both VCP/Cdc48 and other ERAD components such as ubiquitin ligases. UBXN6 is involved in ERAD process. UBXN6 is a cytosolic protein that interacts with VCP and Derlin-1. UBXN6 overexpression in cells causes selective dissociation of Ufd1 from VCP, resulting in inhibition of mutant cystic fibrosis transmembrane conductance regulator (CFTR) degradation by ERAD (Nagahama et al., 2009) .

The AAA ATPase complex is known as VCP in mammals, and the yeast homolog is Cdc48. It is involved in various cellular pathways, including membrane fusion, protein folding, protein degradation and activation of membrane-bound transcription factors. This broad range of cellular involvement is executed via specific co-factors of VCP. UBXN6 is one of the co-factor of VCP. It localizes to the cytoplasm and nucleus and is highly expressed in centrosomes. Phosphorylation of the penultimate tyrosine residue in VCP completely abolishes UBXN6 interaction. Ternary complexes of UBXN6, p47 and VCP were detected in vitro. Inhibition of UBXN6 expression by siRNA did not affect the degradation of bulk protein or a model substrate of the ERAD pathway, indicating that UBXN6 directs VCP activity to specialized functions in vivo (Madsen et al., 2008) .

UBXN6 is a cofactor of VCP and possesses two binding domain namely UBX and PUB. The PUB domain mediates robust binding to the C-terminus of VCP, while the UBX domain does not contribute to VCP binding. Also, VCP possesses additional binding site in UBXD1 that competes with the p47 cofactor for binding to the N domain of VCP. This bipartite binding mode suggests that UBXN6 could be an effective regulator of VCP cofactor interactions (Kern et al., 2009) .

UBXN6 shows a relationship with lectin mannose-binding 1, also called as ER-Golgi intermediate compartment 53 kDa protein (ERGIC-53), a hexameric type I integral film protein. The UBXD1-ERGIC-53 association requires the N-terminal ten deposits of UBXD1 and the C-terminal cytoplasmic 12 amino corrosive tail of ERGIC-53. Utilization of VCP and E1 protein inhibitors show that development among UBXD1 and ERGIC-53 requires the ATPase movement of VCP, however not ubiquitin change. Moreover, a UBXD1-Rab3GAP affiliation requires the ERGIC-53 restricting space ofUBXN6. Confinement contemplates showing that UBXD1 modules the sub-cell dealing of ERGIC-53, including elevating development to the cell film. Thus, VCP-UBXD1 tweaks the dealing of ERGIC-53-containing vesicles by controlling the connection of transport factors with the cytoplasmic tail of ERGIC-53 (Haines et al., 2012) .

In Huntington disease mitochondrial outer membrane protein Myeloid cell Leukemia sequence-1(MCL1) is degraded extensively via VCP. UBXN6 specifically recognizes and bind to targets MCL1 and co-factors with VCP to extract MCL1 from mitochondria. In the mutant Huntington gene, VCP-UBXN6 complex can significantly degrade the MCL1 (Guo and Qi, 2017) .

1.3.8 UBXN7

UBXN7 can participate in the degradation of misfolded or damaged proteins in the VCP-mediated ubiquitin-proteasome system (UPS). UBXN7 binds to ubiquitinated substrates via its UBA domain and interacts with VCP N-terminal domain through its UBX domain to recruit VCP or the VCP core complex (VCP/NPL4/UFD1). The crystal structural superpositions suggest that dimerization of UBXN7 via an intermolecular disulfide bond could interfere with the formation of the VCP-UBXN7 complex. Interestingly, UBXN7 may have a cooperative effect on VCP interaction with UFD1 (Z. H. Li et al., 2017) .

Human UBXN7 mediates VCP interaction with the transcription factor HIF1α that is actively ubiquitylated in normoxic cells by a CUL2-based E3 ligase, CRL2. UBXN7 interaction with cullins is independent of ubiquitin- and substrate-binding. Instead, it relies on the ubiquitin-interacting motif (UIM) in UBXN7 that directly engages the NEDD8 modification on cullins. It leads to accumulation of HIF1α, a CUL2 substrate that uses UBXN7/VCP as a ubiquitin-receptor on its way to proteasome-mediated degradation. Also, HIF1α carrying long ubiquitin-chains can recruit alternative ubiquitin-receptors, lacking VCP's ATP-dependent segregase activity. Thus by sequestering CUL2 in its NEDD-lated form, UBXN7 negatively regulates the ubiquitin-ligase activity of CRL2, and this might prevent recruitment of ubiquitin-receptors other than VCP to nuclear HIF1α (Bandau et al., 2012) .

1.3.9 UBXN8

HBV integration into the human genome has been considered as one of the major causative factors to hepato-carcinogenesis. Analysis of in hepatocellular carcinoma tissues revealed that *UBXN8* was significantly down-regulated, particularly the tissue with HBV integration within the intron of UBXN8. Further, the tumor suppressive activity of UBXN8 is dependent on a cell cycle negative regulator tumor protein 53 (TP53). Thus, UBXN8 is identified as a new tumor suppressor candidate (X. Li et al., 2014) .

Mouse UBXN8 expression was found to be highly tissue-specific and abundant in gonads. In testes, it is expressed in post-meiotic round spermatids, whereas in ovaries it is expressed in granulosa cells. UBXN8 associates directly with VCP via its UBX domain. It was shown that UBXN8 is a transmembrane protein that localizes to the ER membrane with its UBX domain facing the cytoplasm. Knock-down of UBXN8 expression in human cells leads to a decreased association of VCP with the ER membrane and concomitantly a slow degradation of misfolded ER-derived proteasome substrates. Thus, UBXN8 tethers VCP to the ER membrane for efficient ER-associated degradation (Madsen et al., 2011) .

1.3.10 UBXN9

UBXN9 interact directly with VCP and also exhibit species, mutation and ATP-dependent differences in the binding affinities. Also, UBXN9 efficiently disassembled wild-

type, but to a lesser extent, mutant VCP hexamers into monomers (Rijal et al., 2016) . Another group found similar observations that UBXN9 promotes VCP hexamer disassembly, resulting in the formation of stable VCP-UBXN9 heterotetramers. An extended UBX domain (eUBX) in UBXN9 is critical for this association. The overproduction of UBXN9 disrupts VCP hexamer function in ERAD, and that engineered eUBX polypeptides can induce cell death, providing a rationale for developing anti-cancer polypeptide inhibitors that may target VCP activity (Arumughan et al., 2016) .

Alveolar soft part sarcoma (ASPS) is a rare tumor. In a study, UBXN9 -TFE3 fusion transcripts were observed in all 12 ASPS case and determined as its oncogenic significant fusion product. The UBXN9-TFE3 fusion replaces the N-terminal portion of TFE3 by the fused UBXN9 sequences while retaining the TFE3 DNA-binding domain, implicating transcriptional deregulation in the pathogenesis of this tumor (Ladanyi et al., 2001) .

1.3.11 UBXN10

UBXN10 localizes to cilia in a VCP-dependent manner, and both VCP and UBXN10 are required for ciliogenesis. Pharmacological inhibition of VCP destabilized the intraflagellar transport B (IFT-B) complex and increased trafficking rates. Depletion of UBXN10 in zebrafish embryos causes defects in left-right asymmetry, which depends on functional cilia (Raman et al., 2015) .

1.3.12 UBXN11

UBXN11/ Colon antigen-1 (COA-1) was recently identified as a novel antigen of colorectal cancer encoded by the UBXD5 gene. UBXN11-specific and tumor-reactive T lymphocytes were isolated from all studied colorectal cancer patients with the progressive disease but not in patients with early-stage tumor and healthy donors, suggesting that the immune response against this antigen is associated with the progression of colorectal cancer. UBXN11- and tumor-specific T lymphocytes displayed a CD3+CD4+CD69+CD45RA+ phenotype, compatible with the activated effector-type T-cell subset, and most of them exerted cytotoxic activity against HLA-matched and UBXN11+ tumor cells. UBXN11-specific T cells could also be isolated by in vitro stimulation of peripheral blood mononuclear cells with autologous dendritic cells loaded with tumor lysate, suggesting that this antigen can generate a dominant immunologic response against colorectal cancer cells. Notably, UBXN11-derived epitopes binding to HLA-A*0201 molecules elicited antigen- and tumor-specific CD8+ T-cell-mediated responses in colorectal cancer patients (Maccalli et al., 2008) .

1.3.13 p47

p47 is a cofactor of VCP, and it is the best-studied UBXN. In the animal cells, p47 is required to be associated with VCP for budding of cisternae from mitotic Golgi fragments. In budding yeast cells, it is essential or the process called karyogamy/ outer membrane

fusion reaction (Kondo et al., 1997) . The p47 phosphorylation on Serine-140 by Cdc2 results in mitotic inhibition of the VCP/p47 pathway (Uchiyama et al., 2003) .

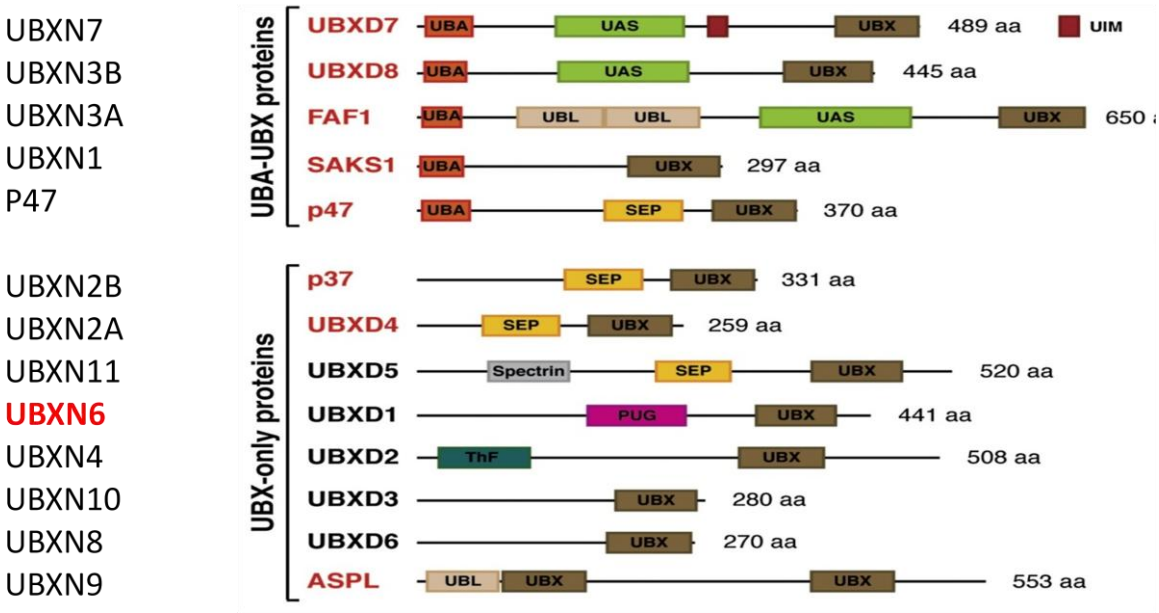

Figure 8: Types of UBXNs and its domains.

UBXNa are primarily divided into two groups depending on their domain. The first group consists of UBA-UBX domain-containing proteins and the second group consists of only UBX domain-containing proteins As adapted from (Alexandru et al., 2008)

Table 1: Overview of UBXNs

Protein	Aliases	Size	Domain	Function	Reference
UBXN1	UBXD10, SAPK1, SAS1	33	UBA-UBX	Interference of RIG-I signaling Negatively regulate NF-κB signaling Interact with Nipah virus V protein and interfere with IFN-β induction Negatively regulate ERAD EGFR activates NF-κB via negatively downregulating UBXN1, role in glioblastoma Negatively regulate BRACA1 enzymatic action	(P. Wang et al., 2013) (Y. B. Wang et al., 2015) (Uchida et al., 2018) (LaLonde and Bretscher, 2011) (Huang et al., 2017) (Wu-Baer et al., 2010)
UBXN2A	UBXD4	29	UBX	Promote cell death in colon cancer Regulation of nicotinic acetylcholine receptor	(Sane et al., 2014) (Rezvani et al., 2009)
UBXN2B	NSFL1. cofactor3	37	UBX	Membrane fusion	(Uchiyama et al., 2006)

	7, p37			Spindle orientation	(B. H. Lee et al., 2018)
UBXN3A	UBXD12, FAF1, CGI-03	74	UBA-UBX	Death-inducing signaling complex Cancer metastasis ERAD	(Ryu et al., 2003) (Xie et al., 2017) (J. J. Lee et al., 2013)
UBXN3B	UBXD8, FAF2, ETEA, KIAA0887	52	UBA-UBX	Lipid metabolism regulation Positive regulator of STING mediated antiviral immune response	(Imai et al., 2015) (Yang et al., 2018)
UBXN4	UBXD2, UBXDC1, Erasin, KIAA0242	57	UBX	ERAD	(Liang et al., 2006)
UBXN6	UBXD1, UBXDC2, CTB-50L17.16	50	UBX	Lysosome clearance by autophagy Endolysosomal sorting of caveolin-1 ERGIC-53 trafficking MCL1 degradation-Huntington disease	(Papadopoulos et al., 2017) (Ritz et al., 2011) (Haines et al., 2012) (Guo and Qi, 2017)

UBXN7	UBXD7, KIAA0794	55	UBA-UBX	HI1-α accumlation	(Bandau et al., 2012)
UBXN8	UBXD6, D8S2298E	30	UBX	Tumor suppressor ERAD	(X. Li et al., 2014) (Madsen et al., 2011)
UBXN9	UBXD9, ASPL, TUG	60	UBX	Monomerization of VCP hexamer TEF3 fusion in ASPS	(Rijal et al., 2016) (Arumughan et al., 2016) (Ladanyi et al., 2001)
UBXN10	UBXD3	30	UBX	Ciliogenesis	(Raman et al., 2015)
UBXN11	UBXD5, CoA-1, Socius, SOC-1, PP2243	57	UBX	Colorectal cancer	(Maccalli et al., 2008)
P47	UBXD10, UBXN2C, NSFL1C		UBA-UBX	Regrowth of Golgi cisternae	(Kondo et al., 1997)

2 Materials and methods

2.1 Materials

2.1.1 Cell lines

Human embryonic kidney 293 cells transformed with T antigen of SV40 (HEK293T, # CRL-3216), Vero cells (monkey kidney epithelial cells, # CCL-81) were purchased from American Type Culture Collection (ATCC) (Manassas, VA20110, USA). A 2fGTH cell line stably expressed an ISRE-luciferase reporter. It was used previously (Jinzhu Ma et al., 2018a) . HEK293T, Vero cells, and 2fGTH cells were grown in DMEM and trophoblast were grown in RPMI 1640 (Gibco) supplemented with 10% FBS, glutamine, antibiotics, and mycozap (Lonza).

2.1.2 Viruses

Encephalomyocarditis virus (EMCV, VR129-B) and Zika virus FLR strain (Cat# VR-1844) were purchased from American Type Culture Collection (ATCC) (Manassas, VA20110 USA). The Indiana strain of VSV was tagged with Green fluorescence protein (GFP) to generate VSV-GFP. All viruses were propagated in Vero cells.

2.1.3 Plasmid construction

FLAG-Myc-UBXN2A (Cat # MR203340), -2B (Cat# MR204884) were purchased from Origene (Rockville, MD 20850, USA). FLAG-UBXN1 was constructed previously in our lab. The additional FLAG-UBXNs (which include FLAG-UBXN3A, FLAG-UBXN3B, FLAG-UBXN4, FLAG-UBXN6, FLAG-UBXN7, FLAG-UBXN8, FLAG-UBXN9, FLAG-UBXN10, FLAG-UBXN11, P47) were a kind gift of Dr. Raymond J. Deshaies at California Institute of Technology, USA.

2.1.4 Ligand treatment conditions

PRR ligand 100 ng of ΔRIG-I plasmid or 4 μg/ml poly (I: C) (Invivogen #tlrl-pic) were transfected into cells with Lipofectamine 2000. Human IFN-β (PeroTech #300-02BC-5UG) or human IFN-λ1 (PeroTech #300-02L-5UG) were added to the growth medium without serum at the final concentration of 10ng/ml of medium. The cells were incubated for 0, 30, 60 minutes following treatment, for the determination of JAK-STAT molecules. The incubation was for 16-24hrs for determining the ISG mRNA levels after stimulation.

2.1.5 Lipofectamine transfection protocol

24 well plate seeded with 50,000 HEK-293T cells/well and incubated at 37^0 C with 5% CO_2. After 16-24 hrs, cells were 50-80% confluent. The cell culture medium was

changed to serum-free DMEM. Plasmids with required concentration were added to serum-free DMEM in 1.5 ml microcentrifuge tube. In another 1.5 ml microcentrifuge tube, Lipofectamine 2000 reagent was added to serum-free DMEM. Both mixtures were incubated for 5 minutes separately and then added and incubated for 20 minutes at room temperature. The prepared DNA + Lipofectamine 2000 transfection mix was added to cells in a dropwise manner. Cells were incubated at 37^0C with 5% CO_2. After 6-10 hours, the culture medium was changed to DMEM with 10% serum.

2.1.6 Virus infection conditions

The viruses were allowed to infect cells for two hours in the serum-free medium; the cells were then washed with 1× phosphate-buffered saline (PBS) once and incubated with pre-warmed medium with 10% serum. The MOI and infection conditions were specified for each experiment in the figure legend.

2.2 Methods

2.2.1 Dual-Luciferase reporter assay

2.2.1.1 Rationale

Dual Luciferase reporter system is developed to measure renilla and firefly luciferase activity in the same sample (Figure 9) (Grentzmann et al., 1998) . Firefly luciferase is a 61kDa and *Renilla* luciferase a 36kDa protein. Both are monomeric, and neither requires post-translational processing so that they can function as genetic reporters immediately upon translation.

The activity of the primary reporter gene is proportional to the specific treatment, while the control reporter gene provides internal control to normalize results. The advantage of dual glow system is the establishment of the internal control, which reduce sample variation by reducing false negative or false positive readouts caused by non-specificity (Promega, 2019) .

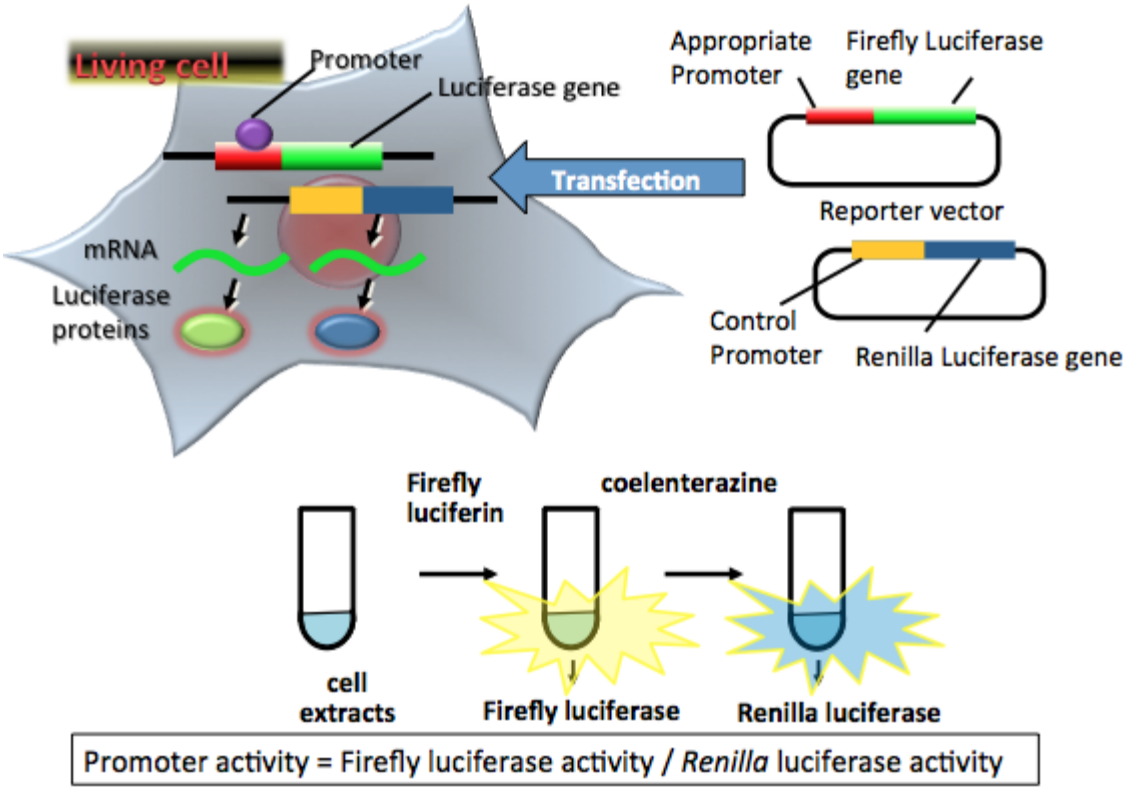

Figure 9: The principle of a dual nonsecreted luciferase reporter assay.

Transfection of two reporter plasmid vectors consist of the firefly luciferase gene sequence downstream to target promoter (ISRE in our system), and the Renilla luciferase gene sequence with the constitutive promoter sequence as a control. The promoter region regulates the expression of the luciferase genes in living cells. Firefly luciferase protein catalyzes the externally provided substrate luciferin in the presence of Mg^{2+} and ATP to produce a yellow-green light. This reaction is stopped by the inhibitor, and subsequent renilla luciferase activity is measured as proportional to the production of blue light by catalysis of substrate coelenterazine. As adapted from (Ohmiya)

2.2.1.2 Protocol

24 well plate seeded with 50,000 HEK-293T cells/well. After 16-24 hrs, 50-80% confluent HEK293T cells were transfected with Calcium phosphate transfection method. Briefly, a combination of 3 plasmids including 100 ng of pGL3-ISRE luciferase reporter (firefly luciferase; experimental reporter) plasmid, 10ng of Actin-Renilla reporter (renilla luciferase; internal control), and each UBXN expressing plasmid are mixed with 100µL 0.25M CaCl2 and incubated at room temperature for 15 minutes. Then 100µL 2xHBS added dropwise with aeration. They were incubated at room temperature for 20 minutes. 200µL of plasmid- Calcium phosphate Complex is added to each well. After 10-12 hours 10ng/mL hIFNβ or hIFNλ was added. 16 hrs after transfection, luciferase activity was measured using a Promega Dual- Glow Luciferase assay system (Cat# E2920).

Briefly, media were removed from multiwell plates. Cells were washed with 500 µL cooled 1X PBS and lysed by adding 50 µL of 1X passive lysis buffer to each well. To 5 µL of cell lysate is aliquoted to 1.5 mL microcentrifuge tube, 30 µL Dual-Glo Luciferase Reagent was added, and firefly luciferase activity was measured in terms of luminescence produced by a luminometer. To the same sample, 30 µL STOP-Glo Luciferase Reagent was added and mixed, and *Renilla* luciferase activity was measured in terms of luminescence produced by a luminometer.

2.2.1.3 Data analysis

The luminescence values and the ratio of luminescence from the ISRE reporter to luminescence from the control Renilla reporter were noted. This ratio was normalized to the ratio of a control well of non-stimulated vector control. Relative Response Ratios was calculated from IFN stimulated Vector samples to the IFN stimulated UBXNs samples.

2.2.2 Biochemical Assay for IFN-I bioavailability

IFN-I concentration in the cell culture supernatant was measured by 2fGTH reporter cell line. This cell line stably expresses the ISRE-luciferase reporter, which is activated in proportion to IFN concentration (Jinzhu Ma et al., 2018a) . Briefly, 1×10^5 2fGTH cells were seeded in each well of 24-well plate and grown in complete DMEM supplemented with 10% FBS and antibiotics/antimycotics at 37°C, 5% CO_2overnight. Two hundred microliters of samples of pre-stimulated HEK293T culture medium were added to the 2fGTH-ISRE-Luc cells and incubated at 37°C, 5% CO_2 for ten hours. A serial two-fold dilution of recombinant human IFN-β served as positive controls and was used for a standard curve plot. Unstimulated HEK293T cell culture medium served as a negative control. After ten hours of stimulation, luciferase activity was measured by Luciferin substrate (Promega).

2.2.3 Generation of gene knockout cell lines with CRISPR-Cas9 technology

2.2.3.1 Background

CRISPR technology was used to generate knockout cells (Figure 10). We co-expressed an endonuclease- Cas9 and a guide RNA (gRNA) specific to the *UBXN6* gene exon2 sequence. The 20 nucleotide DNA sequence of the target was chosen based on two characteristics:

1. The target sequence was unique compared to the rest of the genome.
2. A Protospacer Adjacent Motif (PAM)/ NGG sequence was present immediately adjacent to the chosen target sequence.

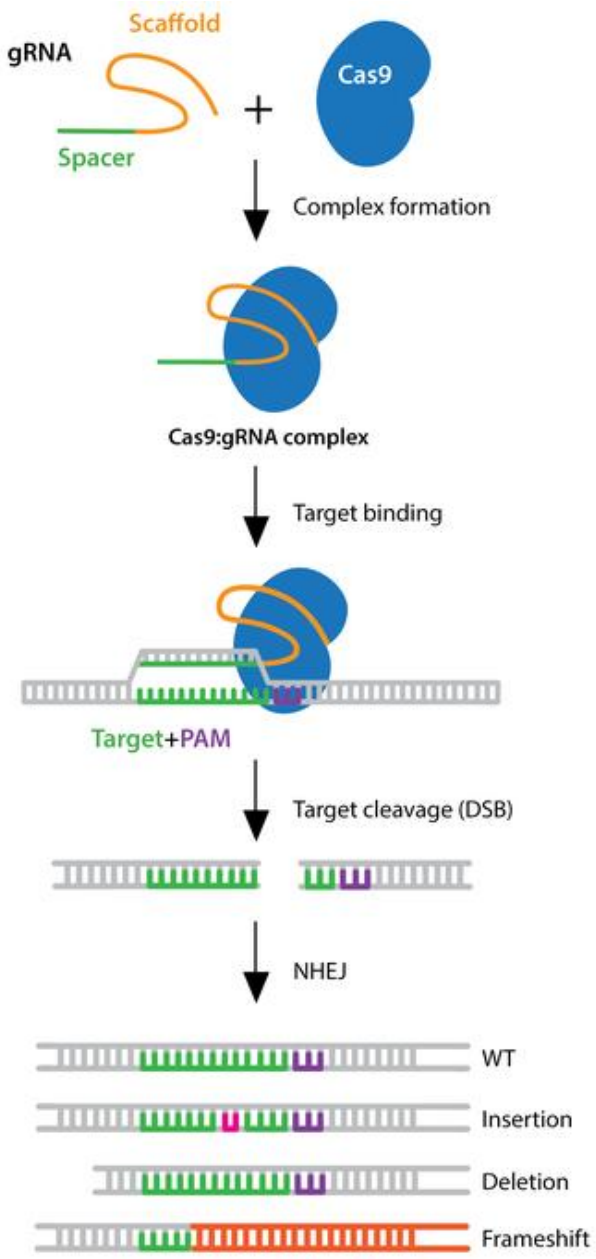

Figure 10: The mechanism of CRISPR-Cas9 technology.

The expressed Cas9 protein and gRNA form a ribonucleoprotein complex through interactions between the gRNA scaffold and surface-exposed positively-charged grooves on Cas9. The Cas9 + gRNA complex undergoes a conformational change, in which the active Cas9 bind to DNA, whereas the spacer region of the gRNA, remains free to interact with target DNA. The Cas9 nuclease has two functional endonuclease domains: RuvC and

HNH. Cas9 undergoes a second conformational change upon target binding that positions the nuclease domains to cleave opposite strands of the target DNA. The result of Cas9-mediated DNA cleavage is a double-strand break (DSB) within the target DNA (~3-4 nucleotides upstream of the PAM sequence). The resulting DSB is then repaired by one of two general repair pathways:

1. The efficient but error-prone **non-homologous end joining (NHEJ) pathway**
2. The less efficient but high-fidelity **homology-directed repair (HDR) pathway**

The NHEJ repair pathway is the most effective repair mechanism, and it frequently causes small nucleotide insertions or deletions (indels) at the DSB site. The randomness of NHEJ-mediated DSB repair has important practical implications because a population of cells expressing Cas9 and a gRNA will result in a diverse array of mutations.

In most cases, NHEJ gives rise to small indels in the target DNA that result in amino acid deletions, insertions, or frameshift mutations leading to premature stop codons within the open reading frame (ORF) of the targeted gene. The typical result is a loss-of-function mutation within the targeted gene. As adapted from (Addgene, 2019)

2.2.3.2 Protocol:

Well established CRISPR-Cas9 protocol was used to create gene knockout (Figure 11) (Ran et al., 2013)

2.2.3.2.1 Designing gRNA:

The 20 nucleotides long gRNA specific to the *UBXN6* gene exon2 sequence were designed based on the unique target sequence and PAM/ NGG sequence adjacent to target sequence (Table 2).

Table 2: Two sequences of human UBXN6 gene at exon-2 were targeted by designing a pair of gRNA.

Gene	gRNA Primer sequence
UBXN6_CRISPR-F1	CAC CGT CGG ATG GTG TCC TGC GAT G
UBXN6_CRISPR-R1	AAA CCA TCG CAG GAC ACC ATC CGA C
UBXN6_CRISPR-F2	CAC CGG CTG GTT GGG CTT CTC TTT G
UBXBN6_CRISPR-R2	AAA CCA AAG AGA AGC CCA ACC AGC C

2.2.3.2.2 Cloning

The primer pairs were annealed and cloned into Lenti-CRISPR V2 plasmid separately (Sanjana et al., 2014) . The cloned g-RNA was confirmed by sequencing using the LKO.1 primer with the sequence 5'-GAC TAT CAT ATG CTT ACC GT-3.'

2.2.3.2.3 Production of packaging Lentivirus particles:

The g-RNA- Lenti-CRISPR V2 vector was co-transfected into HEK293T cells with the packaging plasmids pCMV-VSV-G (Addgene# 8545) and psPAX2 (Addgene# 12260) in ratio 1:2:2. The first harvest of supernatant Lentivirus particles was collected after two days of transfection. The second harvest was after 4 days of transfection. The medium was centrifuged, and the supernatant was stored at -80^{o} C.

2.2.3.2.4 Transduction and selection of knock-out clone:

HEK293Tcells, trophoblasts were then transduced by lentiviral particles for three days. The efficiency of transduction was increased by adding polybrene. The wild type (WT) control was lentiCRISPRv2 vector only. The puromycin (1 µg/ml) selection applied to transduced cells for both HEK293T cells and trophoblasts. The non-transduced cells died of puromycin, while all transduced cells were survived. Immunoblotting confirmed the successful knockout clones. For RT-PCR, the primer pair to find the gene deletion was

designed which target the selected sgRNA sequence and the sequence 100 nucleotides apart (Table 3).

Table 3: The designing of primer pairs for detection of *UBXN6* deletion by qPCR.

Gene	Primer sequence
UBXN6-QPCR1-FWD	AGG CCC ACA AAG AGA AGC
UBXN6-QPCR1-REV	TGG GGC CCC AGG CCC GGG
UBXN6-QPCR2-FWD	GGC CCC ACA TCG CAG GAC
UBXN6-QPCR2-REV	GGG CAG AGC CTT CCT CTC

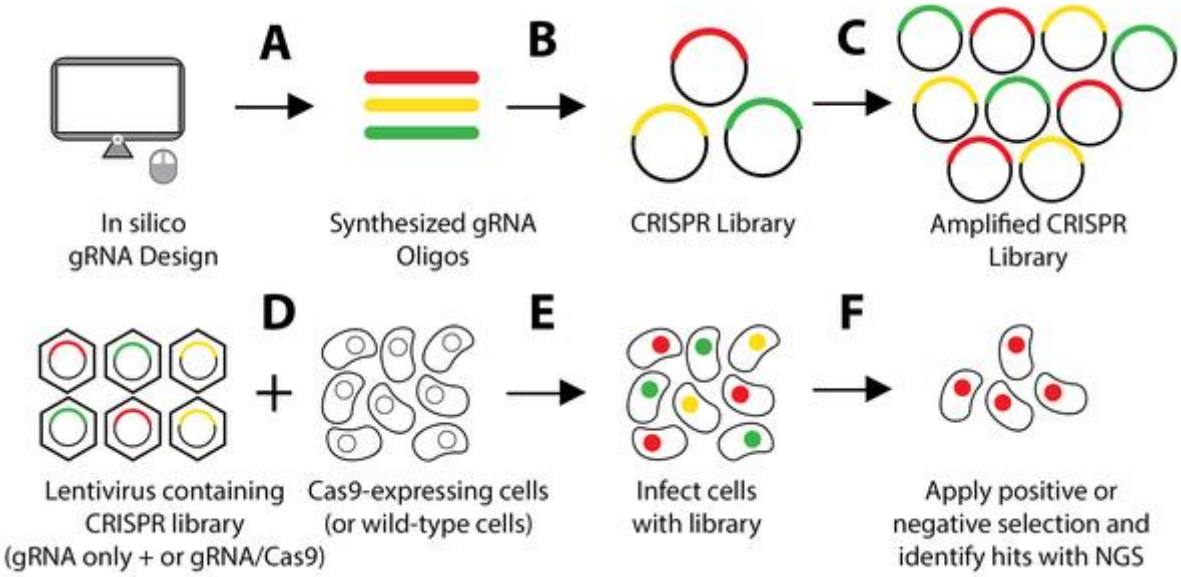

Figure 11: Protocol for the generation of gene knockout by CRISPR technology.

Briefly, the target-specific gRNA was designed and cloned into Lenti-CRISPR V2 plasmids. The CRISPR-Cas9 + gRNA library was amplified and packaged into lentivirus particle and used to transduce target cells. The transduced cells were selected by puromycin survival. The knockout of the target gene was confirmed by immunoblotting As adapted from (Addgene, 2019) .

2.2.4 Reverse transcription and quantitative PCR (qPCR)

The cells were washed with 1X PBS and lysed in 350µl of RLT buffer containing β-mercaptoethanol (QIAGEN RNeasy mini kit). The total RNA was extracted following the QIAGEN RNeasy manufacturer's instructions. Reverse-transcription of RNA into cDNA was performed using the BIO-RAD iScript cDNA Synthesis Kit. qPCR was performed with gene-specific primers and SYBR Green. Results were calculated using the –ΔΔCt method and a housekeeping gene as an internal control. The qPCR primers were listed in the Previous study (Yang et al., 2018) . The housekeeping gene controls were beta-actin (ACTB). These primer sequences are listed (Table 4).

Fold induction was the change in gene expression after infection or stimulation. It was calculated as the ratio of induced (infected/stimulated) to basal (non-infected/stimulated) levels.

Table 4: The primers used for detection of gene expression by qPCR.

Gene	Primer sequence
hOAS1-F	AGGAAAGGTGCTTCCGAGGTAG
hOAS1-R	GGACTGAGGAAGACAACCAGGT
hIFIT-1-F	GCCTTGCTGAAGTGTGGAGGAA
hIFIT-1-R	ATCCAGGCGATAGGCAGAGATC
hISG15-F	CTCTGAGCATCCTGGTGAGGAA
hISG15-R	AAGGTCAGCCAGAACAGGTCGT
hIL28-F	TCGCTTCTGCTGAAGGACTGCA
hIL28-R	CCTCCAGAACCTTCAGCGTCAG
hIL29-F	AACTGGGAAGGGCTGCCACATT
hIL29-R	GGAAGACAGGAGAGCTGCAACT
hTNF-F	CTCTTCTGCCTGCTGCACTTTG
hTNF-R	ATGGGCTACAGGCTTGTCACTC
hIFNB -F	CAGCAATTTTCAGTGTCAGAAGCT
hIFNB -R	TCATCCTGTCCTTGAGGCAGT
ACTB-F	ATCCTGGCCTCGCTGTCCAC
ACTB-R	GGGCCGGACTCGTCATAC
VSV-F	CATGTCACTGCAAGGCCTAAGA
VSV-R	GGCAGTATCGTGAATTCGATGC
ZIKV-F	CCGCTGCCCAACACAAG
ZIKV-R	CCACTAACGTTCTTTTGCAGACAT
EMCV-F	CCTCTTAATTCGACGCTTGAA
EMCV-R	GGCAAGCATAGTGATCGAG

2.2.5 PCR array of human IFN-I Response

Isolated RNA was reverse transcribed using a cDNA kit. The cDNA was used on the real-time RT Profiler PCR Array (Table 5) (QIAGEN, Cat. no. PAHS-016Z) in combination with SYBR Green qPCR Mastermix (Cat. no. 330529). CT values were exported to an Excel file to create a table of CT values. This table was then uploaded on to the data analysis web portal at http://www.qiagen.com/geneglobe. Samples were assigned to controls and test groups. CT values were normalized based on a/an Automatic selection from HKG panel of reference genes.

The data analysis web portal was used to calculate the fold change/regulation by the delta-delta CT method. Briefly, delta CT is calculated between the gene of interest (GOI) and an average of reference genes (HKG), followed by delta-delta CT calculations (delta CT (Test Group)-delta CT (Control Group)). Fold Change is then calculated using two ^ (-delta delta CT) formula. The data analysis web portal also plots scatter plot, volcano plot, clustergram, and heat map. This data analysis report was exported from the QIAGEN web portal at GeneGlobe.

Table 5: The design of the PCR array plate for human IFN-I response gene.

Position	Unigene	Refseq	Symbol	Description
A01	Hs.12341	NM_001111	ADAR	Adenosine deaminase, RNA-specific
A02	Hs.523309	NM_004281	BAG3	BCL2-associated athanogene 3
A03	Hs.118110	NM_004335	BST2	Bone marrow stromal cell antigen 2
A04	Hs.2490	NM_033292	CASP1	Caspase 1, apoptosis-related cysteine peptidase (interleukin 1, beta, convertase)
A05	Hs.74034	NM_001753	CAV1	Caveolin 1, caveolae protein, 22kDa
A06	Hs.303649	NM_002982	CCL2	Chemokine (C-C motif) ligand 2
A07	Hs.514821	NM_002985	CCL5	Chemokine (C-C motif) ligand 5
A08	Hs.501497	NM_001252	CD70	CD70 molecule
A09	Hs.838	NM_005191	CD80	CD80 molecule
A10	Hs.171182	NM_006889	CD86	CD86 molecule
A11	Hs.238990	NM_004064	CDKN1B	Cyclin-dependent kinase inhibitor 1B (p27, Kip1)
A12	Hs.701991	NM_000246	CIITA	Class II, major histocompatibility complex, transactivator
B01	Hs.709456	NM_000567	CRP	C-reactive protein, pentraxin-related
B02	Hs.632586	NM_001565	CXCL10	Chemokine (C-X-C motif) ligand 10
B03	Hs.190622	NM_014314	DDX58	DEAD (Asp-Glu-Ala-Asp) box polypeptide 58
B04	Hs.131431	NM_002759	EIF2AK2	Eukaryotic translation initiation factor 2-alpha kinase 2
B05	Hs.62661	NM_002053	GBP1	Guanylate binding protein 1, interferon-inducible
B06	Hs.181244	NM_002116	HLA-A	Major histocompatibility complex, class I, A
B07	Hs.77961	NM_005514	HLA-B	Major histocompatibility complex, class I, B
B08	Hs.650174	NM_005516	HLA-E	Major histocompatibility complex, class I, E
B09	Hs.512152	NM_002127	HLA-G	Major histocompatibility complex, class I, G
B10	Hs.380250	NM_005531	IFI16	Interferon, gamma-inducible protein 16
B11	Hs.532634	NM_005532	IFI27	Interferon, alpha-inducible protein 27
B12	Hs.14623	NM_006332	IFI30	Interferon, gamma-inducible protein 30
C01	Hs.730125	NM_002038	IFI6	Interferon, alpha-inducible protein 6
C02	Hs.163173	NM_022168	IFIH1	Interferon induced with helicase C domain 1
C03	Hs.20315	NM_001548	IFIT1	Interferon-induced protein with tetratricopeptide repeats 1
C04	Hs.437609	NM_001547	IFIT2	Interferon-induced protein with tetratricopeptide repeats 2
C05	Hs.47338	NM_001549	IFIT3	Interferon-induced protein with tetratricopeptide repeats 3

C06	Hs.458414	NM_003641	IFITM1	Interferon induced transmembrane protein 1 (9-27)
C07	Hs.709321	NM_006435	IFITM2	Interferon induced transmembrane protein 2 (1-8D)
C08	Hs.374650	NM_021034	IFITM3	Interferon induced transmembrane protein 3
C09	Hs.37026	NM_024013	IFNA1	Interferon, alpha 1
C10	Hs.211575	NM_000605	IFNA2	Interferon, alpha 2
C11	Hs.1510	NM_021068	IFNA4	Interferon, alpha 4
C12	Hs.529400	NM_000629	IFNAR1	Interferon (alpha, beta and omega) receptor 1
D01	Hs.708195	NM_000874	IFNAR2	Interferon (alpha, beta and omega) receptor 2
D02	Hs.93177	NM_002176	IFNB1	Interferon, beta 1, fibroblast
D03	Hs.682604	NM_176891	IFNE	Interferon, epsilon
D04	Hs.73010	NM_002177	IFNW1	Interferon, omega 1
D05	Hs.193717	NM_000572	IL10	Interleukin 10
D06	Hs.168132	NM_000585	IL15	Interleukin 15
D07	Hs.654458	NM_000600	IL6	Interleukin 6 (interferon, beta 2)
D08	Hs.436061	NM_002198	IRF1	Interferon regulatory factor 1
D09	Hs.654566	NM_002199	IRF2	Interferon regulatory factor 2
D10	Hs.289052	NM_001571	IRF3	Interferon regulatory factor 3
D11	Hs.521181	NM_001098629	IRF5	Interferon regulatory factor 5
D12	Hs.166120	NM_001572	IRF7	Interferon regulatory factor 7
E01	Hs.1706	NM_006084	IRF9	Interferon regulatory factor 9
E02	Hs.458485	NM_005101	ISG15	ISG15 ubiquitin-like modifier
E03	Hs.459265	NM_002201	ISG20	Interferon stimulated exonuclease gene 20kDa
E04	Hs.207538	NM_002227	JAK1	Janus kinase 1
E05	Hs.656213	NM_004972	JAK2	Janus kinase 2
E06	Hs.80395	NM_002371	MAL	Mal, T-cell differentiation protein
E07	Hs.132966	NM_000245	MET	Met proto-oncogene (hepatocyte growth factor receptor)
E08	Hs.153837	NM_002432	MNDA	Myeloid cell nuclear differentiation antigen
E09	Hs.517307	NM_002462	MX1	Myxovirus (influenza virus) resistance 1, interferon-inducible protein p78 (mouse)
E10	Hs.926	NM_002463	MX2	Myxovirus (influenza virus) resistance 2 (mouse)
E11	Hs.82116	NM_002468	MYD88	Myeloid differentiation primary response gene (88)
E12	Hs.54483	NM_004688	NMI	N-myc (and STAT) interactor

F01	Hs.709191	NM_000625	NOS2	Nitric oxide synthase 2, inducible
F02	Hs.524760	NM_002534	OAS1	2'-5'-oligoadenylate synthetase 1, 40/46kDa
F03	Hs.414332	NM_002535	OAS2	2'-5'-oligoadenylate synthetase 2, 69/71kDa
F04	Hs.654583	NM_033238	PML	Promyelocytic leukemia
F05	Hs.496255	NM_002744	PRKCZ	Protein kinase C, zeta
F06	Hs.375217	NM_002818	PSME2	Proteasome (prosome, macropain) activator subunit 2 (PA28 beta)
F07	Hs.349094	NM_002351	SH2D1A	SH2 domain containing 1A
F08	Hs.521482	NM_003028	SHB	Src homology 2 domain containing adaptor protein B
F09	Hs.50640	NM_003745	SOCS1	Suppressor of cytokine signaling 1
F10	Hs.642990	NM_007315	STAT1	Signal transducer and activator of transcription 1, 91kDa
F11	Hs.530595	NM_005419	STAT2	Signal transducer and activator of transcription 2, 113kDa
F12	Hs.463059	NM_003150	STAT3	Signal transducer and activator of transcription 3 (acute-phase response factor)
G01	Hs.731555	NM_000593	TAP1	Transporter 1, ATP-binding cassette, sub-family B (MDR/TAP)
G02	Hs.29344	NM_182919	TICAM1	Toll-like receptor adaptor molecule 1
G03	Hs.522632	NM_003254	TIMP1	TIMP metallopeptidase inhibitor 1
G04	Hs.657724	NM_003265	TLR3	Toll-like receptor 3
G05	Hs.659215	NM_016562	TLR7	Toll-like receptor 7
G06	Hs.660543	NM_138636	TLR8	Toll-like receptor 8
G07	Hs.87968	NM_017442	TLR9	Toll-like receptor 9
G08	Hs.379754	NM_198282	TMEM173	Transmembrane protein 173
G09	Hs.478275	NM_003810	TNFSF10	Tumor necrosis factor (ligand) superfamily, member 10
G10	Hs.510528	NM_003300	TRAF3	TNF receptor-associated factor 3
G11	Hs.75516	NM_003331	TYK2	Tyrosine kinase 2
G12	Hs.73793	NM_003376	VEGFA	Vascular endothelial growth factor A
H01	Hs.520640	NM_001101	ACTB	Actin, beta
H02	Hs.534255	NM_004048	B2M	Beta-2-microglobulin
H03	Hs.592355	NM_002046	GAPDH	Glyceraldehyde-3-phosphate dehydrogenase
H04	Hs.412707	NM_000194	HPRT1	Hypoxanthine phosphoribosyltransferase 1
H05	Hs.546285	NM_001002	RPLP0	Ribosomal protein, large, P0
H06	N/A	SA_00105	HGDC	Human Genomic DNA Contamination
H07	N/A	SA_00104	RTC	Reverse Transcription Control
H08	N/A	SA_00104	RTC	Reverse Transcription Control

H09	N/A	SA_00104	RTC	Reverse Transcription Control
H10	N/A	SA_00103	PPC	Positive PCR Control
H11	N/A	SA_00103	PPC	Positive PCR Control
H12	N/A	SA_00103	PPC	Positive PCR Control

2.2.6 ELISA (enzyme-linked immunosorbent assay)

A commercial ELISA kit was used to measure the interferon levels in the cell culture supernatants. The levels of IFN-λ2 (Cat # RHF333CK) and IFN-β (Cat# RHF842CK, from Antigenix America, INC) were quantified. Briefly, the plate was prepared by adding 100 uL of the diluted capture antibody with 0.05M Carbonate buffer (or PBS) to concentration 1.0 ug/mL. The plate was sealed and incubated overnight at room temperature. All liquid was removed, and plates were washed four times using 300 uL of wash buffer per well. After last wash, 200 uL ANTIGENIX AMERICA ELISA coating stabilizer cat # EA150) was added and incubated for 60 minutes at room temperature. The standard was serially diluted from 10.0 ng/mL to zero, and 100 uL of standard or undiluted samples were added to each well in triplicate and incubated at room temperature for 2 hours. The plate was aspirated and washed four times. 100 uL per well detection (Biotin Tracer) antibody in the diluent to the concentration of 0.20 ug/mL was added and incubated at room temperature for 1 hour. The plate was aspirated and washed four times. 100 uL per well Streptavidin-HRP conjugate 1:1,000 in diluent was added and incubated for 30 minutes at room temperature. The plate was aspirated and washed four times. 100 uL per well substrate solution was added and incubated for 10 minutes at room temperature. 100 uL stop solution was added to stop color development. The plate was read at @ 450 nm in ELISA plate reader spectrophotometer.

2.2.7 Immunoblotting

Samples were prepared from cultured cells after washing with ice-cold 1X PBS. Cold Triton lysis buffer was added to well/ plate/ flask. Lysates were kept on ice with constant agitation for 30 minutes. The microcentrifuge tubes containing lysates were centrifuged at 12,000 rpm for 20 minutes at 4^{o}C. The supernatant was transferred to a new tube, mixed with SDS loading dye with freshly added β-mercaptoethanol and used for electrophoresis. Equal amounts of protein were loaded into the wells of the SDS-PAGE gel, along with molecular weight marker. The gel was run for 1–2 h at 100 V. Next, the proteins were transferred from gel to nitrocellulose membrane by wet transfer method. The membrane was washed and blocked for one h at room temperature in the 1% milk as blocking buffer. The membrane was incubated with appropriate dilutions of primary antibody in blocking buffer overnight at 4°C (Table 6). The membrane was washed three times in TBST 10 min each and incubated with the recommended in HRP-conjugated secondary antibody in blocking buffer at room temperature for one h. An enhanced chemiluminescent (ECL) substrate (ThermoFisher Cat# 32106) was applied, and images were acquired using darkroom development techniques.

Table 6: List of antibodies used for immunoblotting.

Antibody	Species reactivity	Mol wt(kDa)	Dilution	Source	Catalog number
Flag (1mg/ml)			1-1000	mouse	collaborator
GAPDH (1mg/ml)	H M R	36	0.1-0.2µg/ml	rabbit	sigma G9545
Tubulin(DM1A)	H M R Mk	52	1-1000	mouse	Cell signal 3873ing
UBXD1/ UBXN6	H M R	50	1-1000	rabbit-polyclonal	Proteintech 14706-1-AP
phospho-Stat1(Tyr701)	H M	84, 91	1-1000	rabbit	Cell Signaling 9167
Stat1	H M R Mk	84, 91	1-1000	rabbit	Cell Signaling 9172

2.2.8 Co-immunoprecipitation.

2.2.8.1 Rationale:

ANTI-FLAG M2 Magnetic Beads (Sigma # M8823) is composed of the ANTI-FLAG M2 monoclonal antibody attached to superparamagnetic iron impregnated, 4% agarose beads. The M2 antibody binds to fusion proteins containing the FLAG peptide sequence (Brizzard et al., 1994) . Additionally, the M2 antibody recognizes the FLAG octapeptide sequence (N-Asp-Tyr-Lys-Asp-Asp-Asp-Asp-Lys-C) at the N-terminus, Met-N-terminus, or C-terminus locations of a fusion protein in mammalian and bacterial extracts. Hence, they are used to detect and capture of fusion proteins containing a FLAG peptide sequence by commonly used immunoprecipitation procedures (Safarik and Safarikova, 2004) .

2.2.8.2 Sample Preparation:

1x107 HEK293T cells were transfected with either empty vector or expression plasmids (FLAG-UBXN6) using Lipofectamine 2000. After 24 hours, transfected cells were treated with human IFN-β (10ng/ml) for 60 minutes. The four experiemental groups were:

1. IP1-Vector control
2. IP2-Vector + IFNλ
3. IP3- FLAG-UBXN6
4. IP4- FLAG-UBXN6 + IFNλ

Whole cell lysates were prepared from transfected cells in 1ooμl lysis buffer. The lysates were cleared by centrifugation at 10,000g for 20min at 4°C. Whole cell lysates were immunoprecipitated with FLAG antibody-conjugated magnetic beads as detailed below.

2.2.8.3 Binding

The resin was thoroughly resuspended and transferred to a microcentrifuge tube. The beads were equilibrated by resuspending with five packed gel volumes of TBS (50 mM Tris HCl, 150 mM NaCl, pH 7.4) for five times. The cleared lysates were incubated with the Beads with gentle agitation at 4°C overnight. Once the binding step was complete, the magnetic beads were collected by placing the tube in the appropriate magnetic separator (Promega # Z5434) and removed the supernatant. The resin beads were washed with TBS buffer to remove all of the nonspecifically bound proteins. The beads were washed five times in ice-cold 1X wash buffer. The bound proteins were eluted by competition with the FLAG Peptide by adding five packed gel volumes of a solution containing the 3X- FLAG peptide (Sigma# F 4799) in TBS buffer. The supernatants were incubated with gentle shaking on a rotator for 30 minutes at room temperature. The supernatants were collected by placing the tubes in the magnetic separator. The supernatants were stored at -20o C, used for SDS-PAGE analysis with Coomassie blue staining and sent for Mass spectrometry evaluation at the Proteomics and Metabolomics facility, University of Connecticut, Storrs, Connecticut.

A Thermo Q Exactive HF Orbitrap mass spectrometer coupled to a Dionex Ultimate RSLCnano UPLC was used for the analysis at the Proteomics and Metabolomics facility, University of Connecticut, Storrs, Connecticut. All data was processed with the MaxQuant search algorithm and visualized with Scaffold Q+S.

2.2.8.4 Data analysis of Mass Spectrometry:

The results obtained from the Mass spectrometry evaluation identified total 522 proteins in four IP samples; denoted with their name, accession number, alternate ID, molecular weight, protein grouping ambiguity and total spectrum count of each group.

A spectrum count is a single MS/MS spectrum that has been matched to a single peptide sequence from any given identified protein. The acquisition method samples the most abundant peptide ions first, so spectral counts are a rough estimate of overall protein abundance (most abundant proteins will have the highest number of spectral counts), with a few caveats.

The first fifty proteins, which shows highest total spectrum count were tabulated. The total spectrum counts of bound proteins were normalized to input UBXN6 counts. Amongst the fifty identified proteins three UBXN6-interacting proteins with the highest normalized value were considered to hypothesized UBXN6-interacting protein under IFNλ stimulation.

2.2.9 Quantification of infectious viral particles by Plaque-forming assay

The 6-well plates were seeded with Vero cells in DMEM with 10% FBS, antibiotics and glutamine so that cells were 90% confluent on the day of the assay ($2.5x10^5$ cells/well). The virus dilutions were made in DMEM without serum by making serial 10-fold dilutions. The medium was changed to pre-warmed DMEM without serum. The 100ul/well serial dilutions of the supernatant were added to confluent Vero cells in duplicates and incubated at 37 °C for two h. The inoculum was then replaced with warm 2 ml of DMEM complete medium with 1% SeaPlaque agarose (Cat# 50100, Lonza). Plates were incubated at 37 °C, 5% CO2 and plaques were monitored under the microscope each day. The second overlay of Neutral red (Sigma-Aldrich) solution and agarose were added after incubation. Plaques were visualized as clear zones in red background.

2.2.10 RNA Interference by siRNA

1×10^5 HEK293 were plated into polyornithine-coated 24-well cell culture plates. Sixteen hours later, cells were transfected with 40 pmol of siRNA mix directed against human *UBXN6* (three 27-mer siRNAs from Origene) or scramble control, by Lipofectamine 2000 (Invitrogen). Cells were transfected again with luciferase reporter plasmids (100 ng ISRE-Luc and ten ng Act-Renilla per well) 36 hr after siRNA transfection. Cells were transfected with ΔRIG-I plasmids 48 hr after siRNA transfection. Cells were washed gently

with PBS and lysed for Dual Glow Luciferase assay following the manufacturer's instructions (Promega) 16 hr after infection.

2.3 Graphing and statistics

Graph Pad Prism 7 software was used for graphs and statistical analyses. For all the graphs, data were expressed as mean ± s.e.m. A standard two-tailed unpaired Student's t-test was calculated in Microsoft Excel.

P values ≤ 0.05 were considered significant and denoted with **, while P values ≤ 0.01 were denoted with *. The sample sizes (biological replicates), specific statistical tests used, and the main effects of statistical analysis for each experiment were detailed in each figure legend.

3 Aims

Aim 1: To identify a UBXN proteins that acts as a positive regulators of RNA virus-induced innate immune responses.

Our previous studies characterized the role of UBXN1 in negative regulation of RNA virus-induced innate immune responses and a role of UBXN3B as a positive regulator of the innate immune response to DNA virus infections. Hence, in this project, we will screen all UBXNs to determine the positive regulator of RNA virus-induced immune responses.

Sub-aim 1.1: To screen for the UBXN that positively regulates type I IFN responses.

Sub-aim 1.2: To validate the UBXN screening for the role of UBXN6 in the regulation of IFN-stimulated responses.

Aim 2: To characterize the function of UBXN6 in viral pathogenesis and host innate immune responses.

The screening from Aim 1 suggests that UBXN6 positively regulates RNA virus-induced IFN-I/III responses. To validate the results from the UBXN6 overexpression studies, we evaluated IFN-I/III expression and viral replication in UBXN6 deficient cells. Two approaches were undertaken for gene abrogation; gene knockdown by siRNA and gene knock out by CRISPR-Cas9 technology. We have established the protocol for the generation of knockout cells by CRISPR technology. The HEK293 and trophoblast knockout cells (indicated as *UBXN6*$^{-/-}$ hereafter) were used to explore the function of this gene in IFN-I/III responses and viral replication.

Sub-aim 2.1: To determine the role of UBXN6 in host immune responses by siRNA knockdown of *UBXN6*.

Sub-aim 2.2: To generate UBXN6 knockout in HEK293 and trophoblast cells by CRISPR-Cas9 technology and to examine host immune responses as well as a viral infection in knockout cells.

Aim 3: To find out the molecular mechanism by which UBXN6 resists viral infections and regulates the immune responses.

UBXN6 was shown to induce hIFN-β-, and hIFN-λ-stimulated ISRE promoter activity (from Aim 1-screen). This also indicates that the activity of Type I/III interferon-

induced JAK/STAT signaling pathway is enhanced by UBXN6. Hence, we hypothesize that UBXN6 can regulate IFN- JAK-STAT signaling pathway.

Sub-aim 3.1: To test if recombinant hIFN-λ-induced ISG response is deficient in *UBXN6*$^{-/-}$ cells.

Sub-aim 3.2: To identify UBXN6-interacting partners during IFN-I/III responses.

4 Results

The roles of UBXNs in the regulation of antiviral immune responses have not been much explored. Previous work in our lab identified UBXN1 as a negative regulator of the RLR pathway and UBXN3B as a positive regulator of STING-mediated immune responses. In this study, we aimed to determine the member of UBXNs as a positive regulator of RNA virus infection-induced innate immune responses. By using an ISRE-driven luciferase reporter assay that monitors the activity of type I/III IFN-induced JAK-STAT signaling, we identified that UBXN6 overexpression synergized with RIG-I, IFN-β or IFN-λ to enhance antiviral immune responses. We further used siRNA and CRISPR-Cas9 technology to abrogate UBXN6 function, which was used to establish the function of UBXN6 in viral infection and JAK-STAT signaling. By PCR array we found that UBXN6-deficiency led to a reduction in type I/III IFN-induced gene expression, which was validated by qPCR. Also, RNA virus replication was increased in UBXN6-deficient when compared to UBXN6-sufficient cells, which was accompanied by a significant reduction in IFN-β and IFN-λ. Lastly, we decoded the mechanism by which UBXN6 regulates the JAK-STAT pathway. We observed that IFN-β-stimulated STAT1 phosphorylation was impaired in UBXN6-deficient cells. By co-immunoprecipitation techniques and mass spectrometry analysis, we identified that following IFN-β stimulation UBXN6 interacted with PRMT5, a protein methyl transferase known to modify and interact with JAK1/2. Our results demonstrate that UBXN6 positively regulates JAK1-STAT1/2 signaling to combat viral infections.

4.1 Aim 1: To identify a member of UBXN proteins as a positive regulator of RNA virus-induced innate immune responses.

Our previous studies characterized the role of UBXN1 in negative regulation of RNA virus-induced innate immune responses and a role of UBXN3B as a positive regulator of the innate immune response to DNA virus infections. Hence, in this project, we will screen all UBXNs to determine the positive regulator of RNA virus-induced immune responses.

4.1.1.1 Sub-aim 1.1: To screen for the UBXN that positively regulates type I IFN responses.

We performed a screening in human embryonic kidney 293 cells transformed with T antigen of SV40 (HEK293T) cells for UBXNs that enhanced ΔRIG-I-stimulated ISRE reporter activity. ΔRIG-I is the 2CARD domain open conformation of RIG-I. It is constitutively active. ΔRIG-I stimulated a robust ISRE activity in vector control and UBXN6 enhanced ISRE by ~2 times compared to the treated vector control. UBXN6 was the only UBXN that potentiated the RIG-I-induced interferon effect (**Figure 12**). Next, we screened the anti-RNA virus activity of all known UBXNs using VSV as a model RNA virus, which specifically stimulate RIG-I signaling. Amongst all tested UBXNs, overexpression of UBXN6 repressed VSV replication most dramatically as identified by Western blotting of VSV-G protein (**Figure 13**).

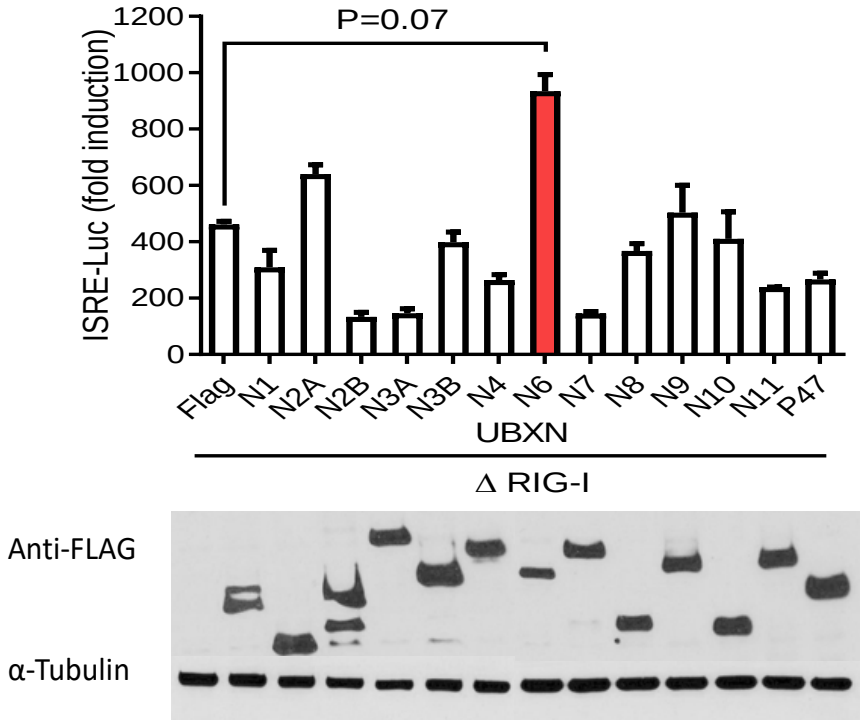

Figure 12: Ectopic expression of UBXN6 enhances RIG-I- induced IFN-I response.

(A) Quantification of ISRE promoter activities by a Dual-Luciferase assay in HEK293T cells transfected with either 100ng of vector or 100ng of individual FLAG-UBXN plasmids together with reporter plasmids 16hr after ΔRIG-I transfection.

The immunoblot of whole cell lysates depicts the expression levels of FLAG-UBXN proteins, and α-Tubulin serves as a housekeeping protein control.

Data represent the mean ± SEM (n = 3), Student's t-Test: two tailed distribution, two-sample unequal variance (*$p < 0.05$; ** $p < 0.01$)

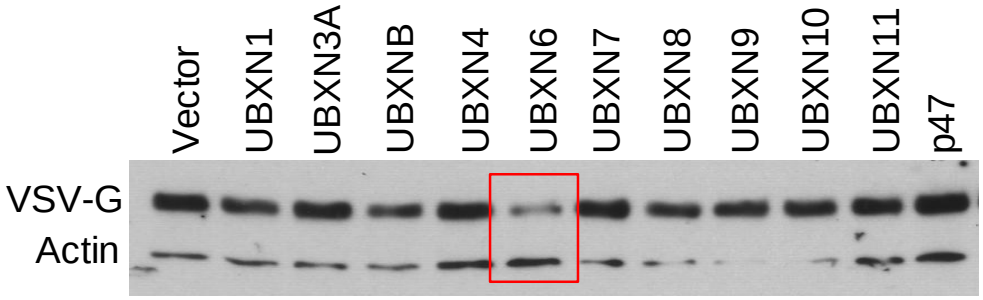

Figure 13: Immunoblot of VSV-G in the whole cell lysates prepared from HEK293T cells.

Cells were transfected with either vector or individual FLAG-UBXN plasmid and infected with VSV-GFP. Actin serves as a housekeeping protein control. The results are representative of 2 independent experiments.

4.1.1.2 Sub-aim 1.2: To validate the UBXN screening for the role of UBXN6 in the regulation of IFN stimulated responses.

The primary immune response in the innate immunity is characterized by viral RNA recognition by RLRs. This recognition is transduced downstream to generate IFN-I/IIIs. The secreted IFN-I/IIIs further act on IFN receptor-bearing cells to activate JAK-STAT signaling, which stimulates several hundreds of ISGs to interfere with viral processes directly and also augmentIFN-I/III production. The activation of primary IFN-I and secondary JAK-STAT pathways was measured by total ISRE activity. Hence, we performed another screening in human embryonic kidney 293 cells transformed with T antigen of SV40 (HEK293T) cells for UBXNs that enhanced type I/III IFN- stimulated response element (ISRE) reporter activity. We observed that expression of UBXN6 increased basal ISRE by ~2.5 times compared to the empty vector control (**Figure 14A).** Both recombinant IFN-β and IFN-λ stimulated a robust ISRE activity (Vector + IFN v.s Vector alone) and interestingly UBXN6 further enhanced ISRE by ~2.5-3.4 times compared to the treated vector control, respectively (**Figure 14 B, C**).

The ability of UBXN6 to activate ISRE was dose-dependent (**Figure 15A)**. We further confirmed the ISRE reporter assay by quantitative reverse transcription PCR (q-RT-PCR). UBXN6 potentiated the mRNA expression of two well-established ISGs, including *OAS1A* and *ISG15* (**Figure 15B, C**). These results demonstrate that UBXN6 is a unique UBXN that regulates optimal JAK-STAT activity.

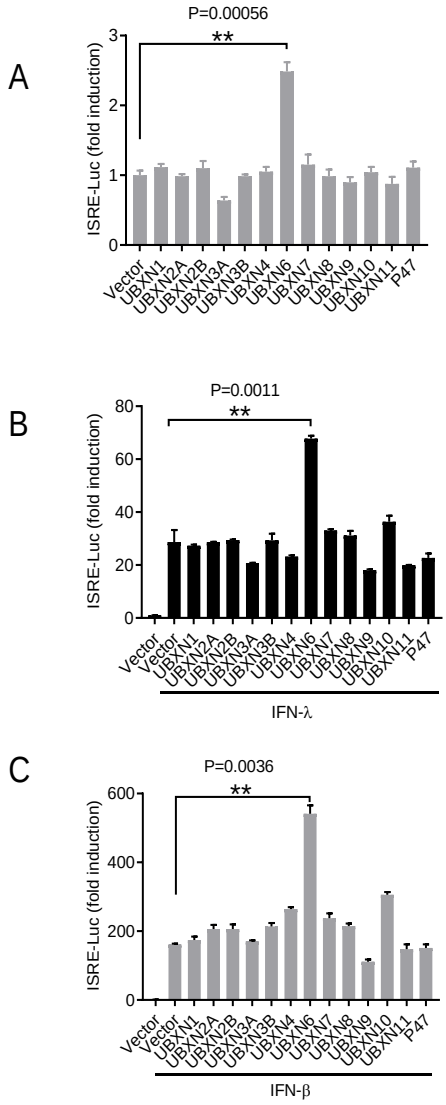

Figure 14: Ectopic expression of UBXN6 enhances recombinant IFN induced ISRE activity.

(A) Quantification of ISRE promoter activities by Dual-Luciferase assay in HEK293T cells transfected with either 100ng of vector or 100ng of individual FLAG-UBXN plasmids.

The immunoblot of whole cell lysates depicts the expression levels of FLAG-UBXN proteins, and α-Tubulin serves as a housekeeping protein control.

(B) Quantification of ISRE promoter activities by Dual-Luciferase assay in HEK293T cells transfected with either 100ng vector or 100ng individual FLAG-UBXN plasmids 16hr after 10ng/ ml of human IFN- λ1 stimulation.

(C) Quantification of ISRE promoter activities by Dual-Luciferase assay in HEK293T cells transfected with either 100ng vector or 100ng individual FLAG-UBXN plasmids 16hr after 10ng/ ml of human IFN- β1 stimulation.

Data represent the mean ± SEM (n = 3), Student's t-Test: two tailed distribution, two-sample unequal variance (** $p < 0.01$)

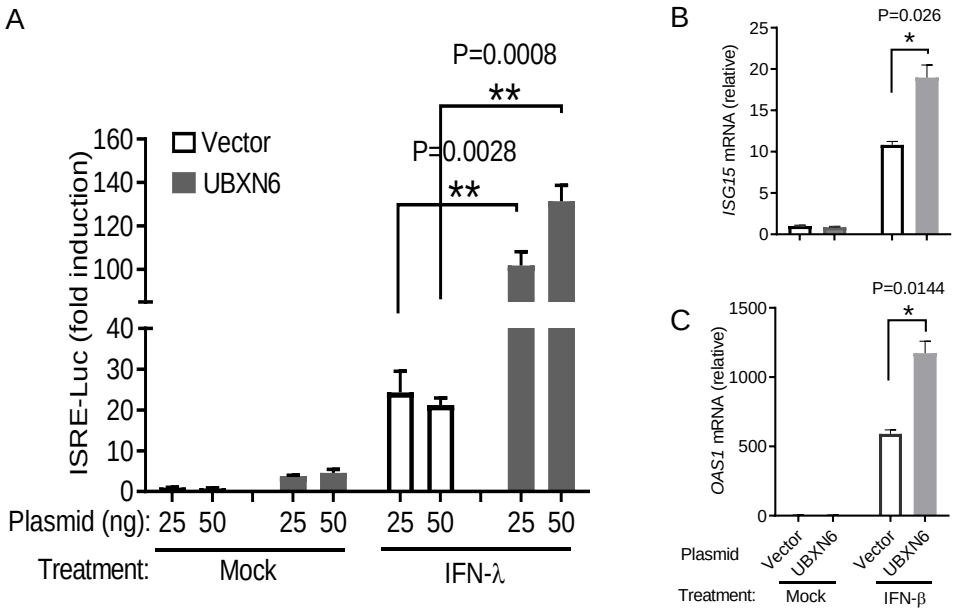

Figure 15: Ectopic expression of UBXN6 enhances IFN-I/III-induced ISRE activity and ISG expression in a dose-dependent manner.

(A) Quantification of ISRE promoter activities by Dual-Luciferase assay in HEK293T cells transfected with either increasing doses of vector or increasing doses of FLAG-UBXN6 plasmid 16hr after 10ng/ ml of human IFN-λ stimulation.

(B, C) mRNA expression of interferon-stimulated gene *ISG15* and *OAS1A* 16hrs after IFN-β stimulation as quantified by qPCR analysis.

Data represent the mean ± SEM (n = 3), Student's t-Test: two tailed distribution, two-sample unequal variance (*$p < 0.05$; ** $p < 0.01$; *** $p < 0.001$)

4.2 Aim 2: To characterize the function of UBXN6 in viral pathogenesis and host innate immune responses.

The screening from Aim 1, I hypothesized that UBXN6 positively regulates RNA virus-induced IFN-I/III responses. To validate the results from the UBXN6 overexpression studies, we evaluated IFN-I/III expression and viral replication in UBXN6 deficient cells. Two approaches were undertaken for gene silencing; gene knockdown by siRNA and gene knockout by CRISPR-Cas9 technology. We have established the protocol for the generation of knockout cells by CRISPR technology. The HEK293 and trophoblast knockout cells (indicated as *UBXN6*$^{-/-}$ hereafter) were used to explore the function of this gene in IFN-I/III responses and viral replication.

4.2.1 Sub-aim 2.1: To determine the role of UBXN6 in host immune responses by siRNA knockdown of *UBXN6*.

We depleted UBXN6 by three individual siRNAs against UBXN6 and MAVS as a control, followed by transfection with ΔRIG-I. We observed a moderate decrease in ISRE activity in UBXN6-depleted cells (**Figure 16A**). The knockdown efficiency of specific siRNA was about 50% (**Figure 16B**). Hence, we next used a mixture of all three siRNA for transfecting HEK293. We overexpressed MDA5, MAVS, and TBK1 of the RLR pathway to activate *IFNB1* transcription in UBXN6-depleted cells. We observed a nonsignificant decrease in ISRE activity in UBXN6-depleted cells. Also, the *IFNB1* mRNA levels were not

significantly reduced in UBXN6-depleted cells (**Figure 17**), suggesting that UBXN6 is not essential for RLR signaling.

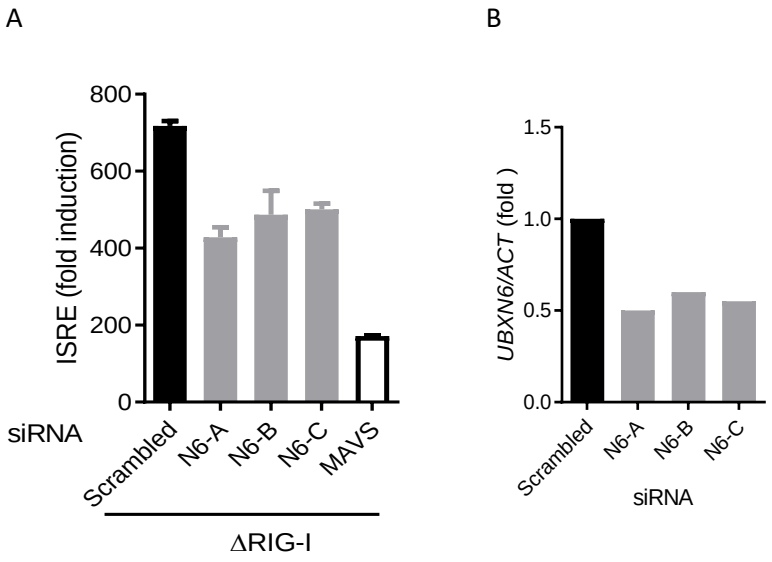

Figure 16: RNA interference of UBXN6 moderately affects RIG-I-induced ISRE activity.

(A) Quantification of ISRE promoter activities by Dual-Luciferase assay. HEK293T cells were transfected with either scrambled (control) or UBXN6-specific siRNA, and after 48 hours the cells were transfected again with either vector or Δ RIG-I and reporter plasmids. Luciferase activity was measured 16 hrs after the second transfection.
(B) Quantification of siRNA knockdown efficiency as measured by qPCR using UBXN6 specific primers.

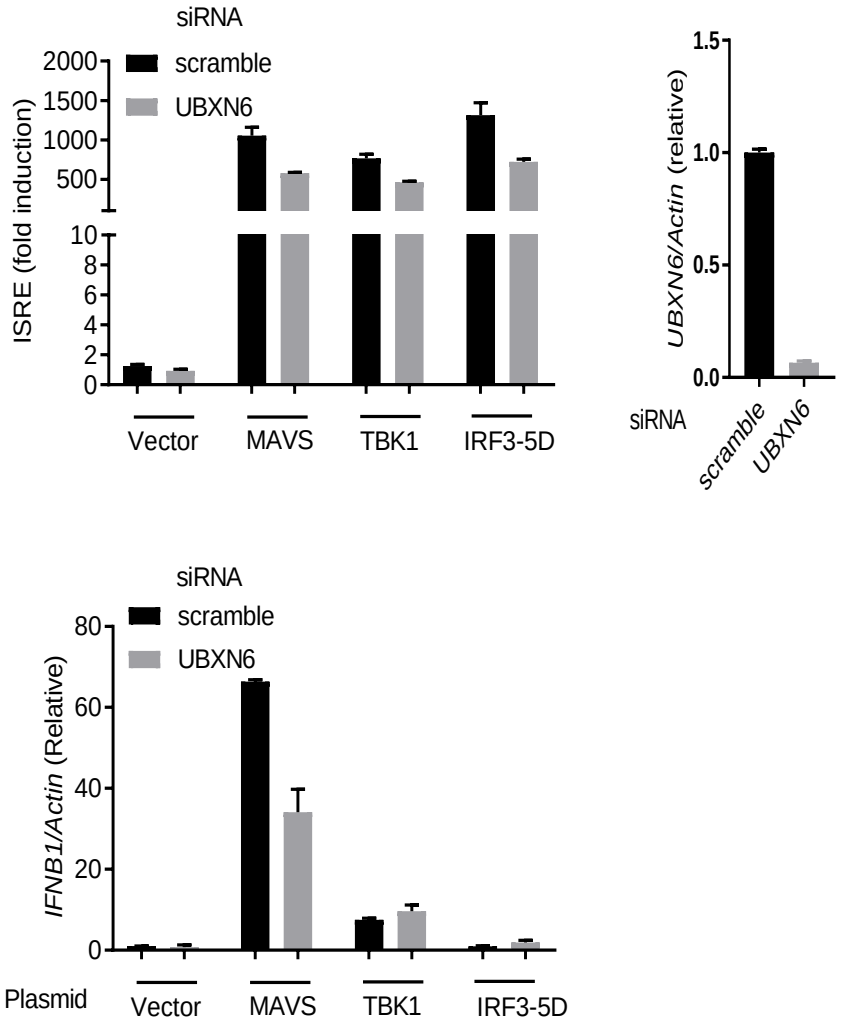

Figure 17: RNA interference of UBXN6 modestly affects the primary RLR pathway.

(A) Quantification of ISRE promoter activities by Dual-Luciferase assay in HEK293T cells transfected with either scrambled (control) or UBXN6 specific siRNA and after 48 hours transfected again with either vector or MAVS, TBK1, IRF3-5D.

Quantification of siRNA knockdown efficiency as measured by qPCR using UBXN6 specific primers.

(B) Expression of IFNB1 in whole cell lysate from (A) as quantified by qPCR.

4.2.2 Sub-aim 2.2: To generate UBXN6 knockout in HEK293 and trophoblast cells by CRISPR-Cas9 technology and to examine host immune response as well as a viral infection in *UBXN6* knockout cells.

We next generated UBXN6 knockout in HEK293T and human trophoblasts cell lines using the CRISPR-Cas9 technology. Western blotting shows successful loss of UBXN6 protein expression (**Figure 18**). Thus, the knockout efficiency at protein level was established.

Next, we employed two models of RNA viruses, VSV and EMCV, to study the UBXN6 antiviral function. Both viruses induce IFN-I/III and ISGs primarily via the RLRs. A transcriptional unit encoding green fluorescent protein (GFP) is incorporated into the VSV genome upstream of the L polymerase to facilitate viral detection by fluorescence microscopy (Dalton and Rose, 2001) . *UBXN6*$^{-/-}$ cells produced more intracellular VSV-GFP as observed by Fluorescent microscopic images (**Figure 19**). Consistently, *UBXN6*$^{-/-}$ cells produced more intracellular VSV RNA as measured by qPCR and increased extracellular infectious viral particles than *UBXN6*$^{+/+}$ cells as quantified by plaque assay (**Figure 20**). IFN-β and IFN-λ concentrations produced by *UBXN6*$^{-/-}$ cells were much lower than *UBXN6*$^{+/+}$ cells in VSV infected cells (**Figure 21**).

Similar results were noted with EMCV infection. *UBXN6*$^{-/-}$ cells produced more intracellular EMCV RNA as measured by qPCR and increased extracellular infectious viral particles than *UBXN6*$^{+/+}$ cells as quantified by plaque assay (**Figure 22**).

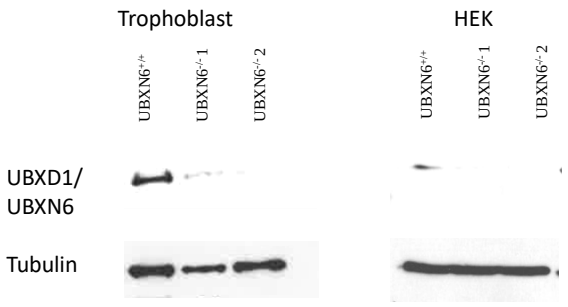

Figure 18: Abrogation of UBXN6 protein in trophoblast and HEK.

Immunoblots showing UBXN6 and housekeeping Tubulin in *UBXN6$^{+/+}$, UBXN6$^{-/-}$ 1* and *UBXN6$^{-/-}$ 2* trophoblast and HEK293T cells.

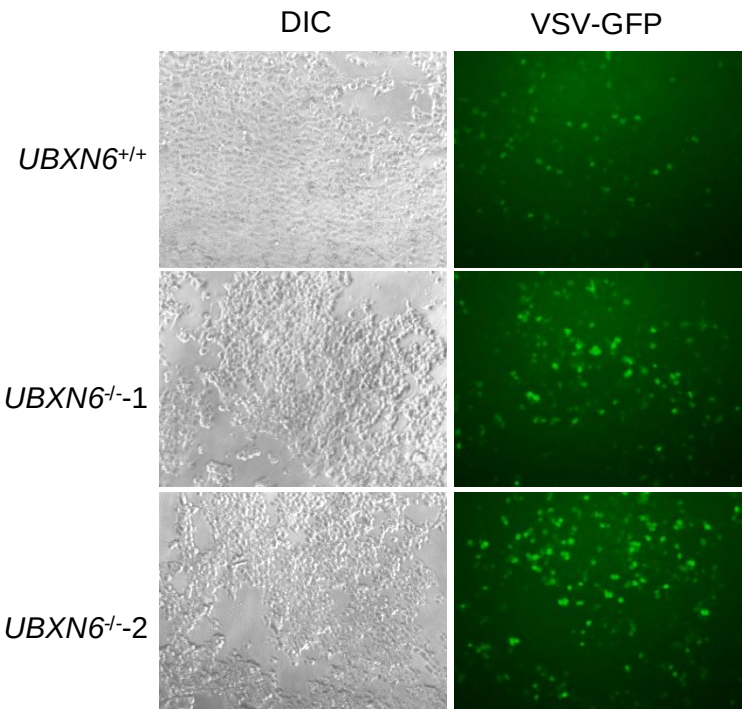

Figure 19: UBXN6 interferes with VSV infection.

Fluorescent microscopic images of *UBXN6$^{+/+}$, UBXN6$^{-/-}$ 1* and *UBXN6$^{-/-}$ 2* trophoblasts infected with VSV-GFP (MOI=0.01) for 12 hrs. Objective 5x, scale bar 10 µm.

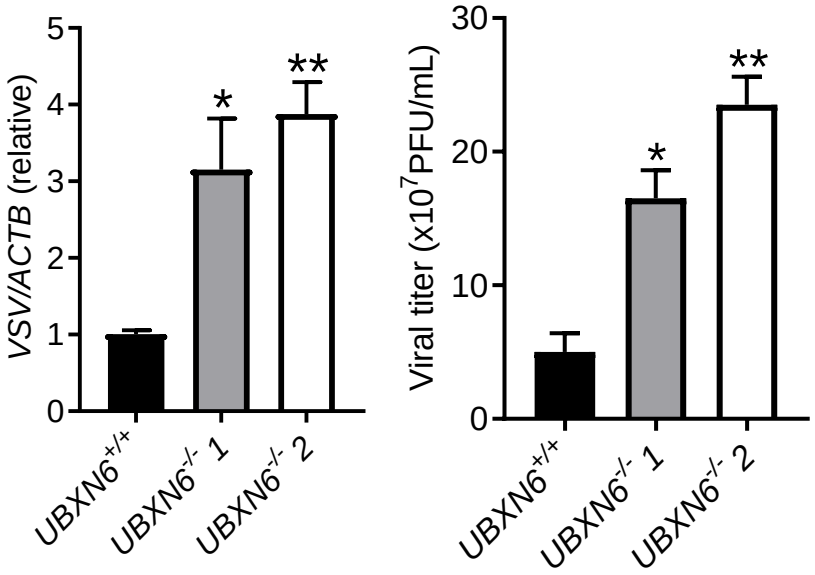

Figure 20: Viral replication is increased in *UBXN6*$^{-/-}$ trophoblasts.

(A) Quantification of intracellular VSV RNA at 12 hours after infection by qPCR.

(B) Quantification of the viral titers at 12hrs after VSV infection by plaque assay.

Data represent the mean ± SEM (n = 3), Student's t-Test: two tailed distribution, two-sample unequal variance (*$p < 0.05$; ** $p < 0.01$). All experiments were repeated 3 times.

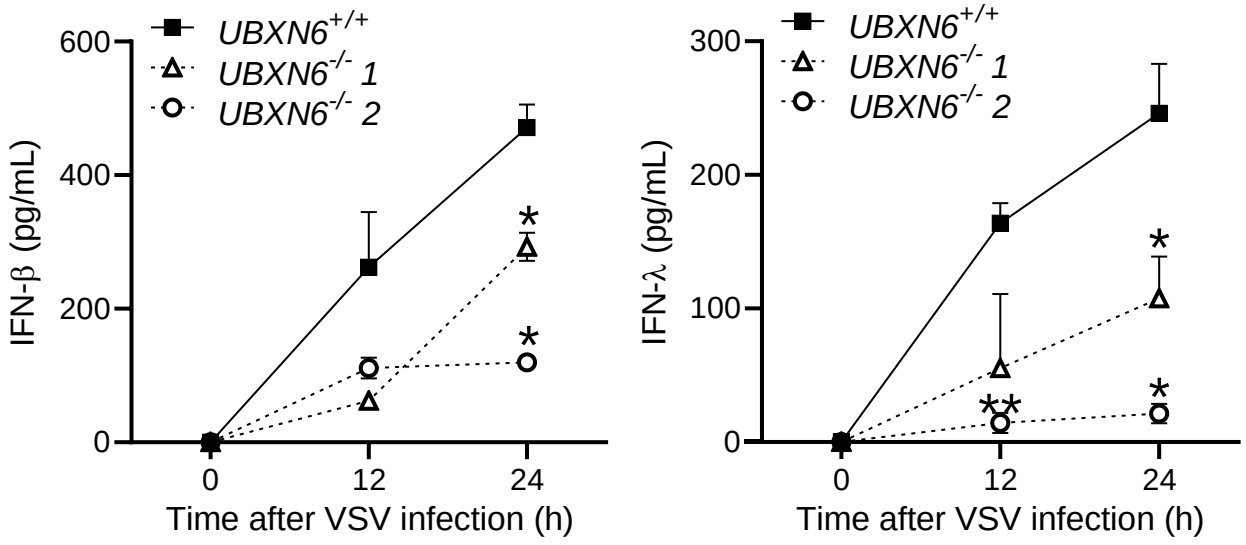

Figure 21: IFN-I/III induction by VSV is impaired in *UBXN6*$^{-/-}$ trophoblasts.

(A) ELISA of IFN-β1 secreted from *UBXN6*$^{+/+}$, *UBXN6*$^{-/-}$ *1* and *UBXN6*$^{-/-}$ *2* trophoblasts 0, 12, and 24 hours after VSV infection.

(B) ELISA of IFN-λ2 secreted from *UBXN6*$^{+/+}$, *UBXN6*$^{-/-}$ *1* and *UBXN6*$^{-/-}$ *2* trophoblasts 0, 12, and 24 hours after VSV infection.

Data represent the mean ± SEM (n = 3), Student's t-Test: two tailed distribution, two-sample unequal variance (*$p < 0.05$; ** $p < 0.01$)

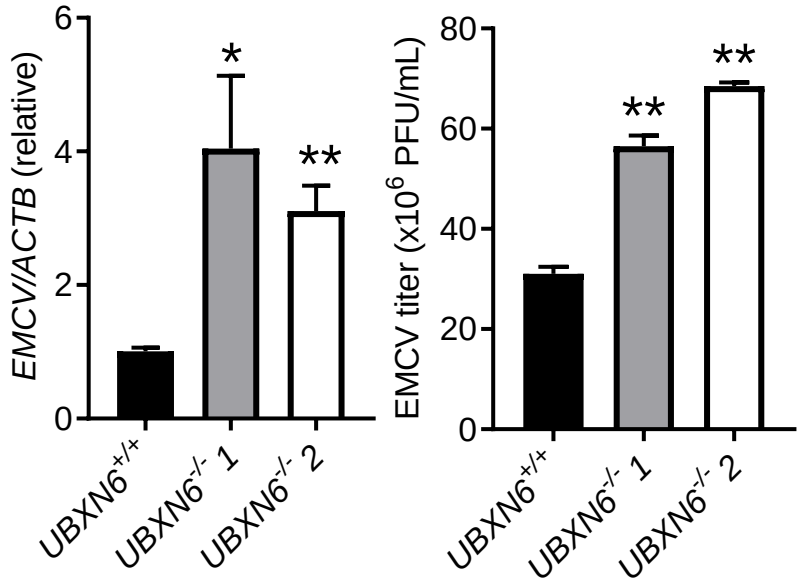

Figure 22: EMCV replication is increased in *UBXN6*$^{-/-}$ trophoblasts.

(A) Quantification of intracellular viral RNA at 12 hours after infection by qPCR.

(B) Quantification of the viral titers at 12 hrs after infection by plaque assay.

Data represent the mean ± SEM (n = 3), Student's t-Test: two tailed distribution, two-sample unequal variance (*$p < 0.05$; ** $p < 0.01$)

4.3 Aim 3: To find out the molecular mechanism by which UBXN6 resists viral infections and regulates the immune responses.

UBXN6 was shown to induce hIFN-β-, and hIFN-λ-stimulated ISRE promoter activity (from Aim 1-screen). This also indicates that the activity of Type I/III interferon-induced JAK/STAT signaling pathway is enhanced by UBXN6. Hence, we hypothesize that UBXN6 can regulate IFN- JAK-STAT signaling pathway.

4.3.1.1 Sub-aim 3.1: To test if recombinant hIFN-λ-induced ISG response is deficient in UBXN6$^{-/-}$ cells.

We analyzed the expression of 84 genes related to IFN-I/III responses by PCR array in *UBXN6*$^{+/+}$ and *UBXN6*$^{-/-}$trophoblasts (Table 7). The fold change with each gene was shown in table 1. The volcano plot, heat map, and cluster-grams were used to identify changes in gene expression (**Figure 23 A, B, D**). Expression of ~20 ISGs including well-characterized *IFIT1, OAS1/2*, *IFITM1, ISG15* and *DDX58* (encodes RIG-I) was >1.5 fold lower in *UBXN6*$^{-/-}$ than *UBXN6*$^{+/+}$ cells treated with recombinant IFN-λ for 6 hours. Three genes (*IL6, VEGF, IFNE*) that are not conventional ISGs were upregulated (**Figure 23 C**). The reduction in *IFIT1* and *OAS1* expression in HEK293 and trophoblasts was further validated by qPCR (**Figure 24**).

Table 7: The relative fold changes in all the tested genes from human IFN-I PCR array from *UBXN6*$^{+/+}$ and *UBXN6*$^{-/-}$ *2* trophoblast cells 6hrs after 10ng/mL IFN-λ1 treatment.

The down-regulated genes are highlighted in blue, up-regulated in red.

Gene Symbol	Fold Change (UBXN6$^{-/-}$/UBXN6$^{+/+}$)			Gene Symbol	Fold Change (UBXN6$^{-/-}$/UBXN6$^{+/+}$)		
	Fold	95% CI	P value		Fold	95% CI	P value
ADAR	0.89	(0.61, 1.17)	0.480	IL6	3.48	(2.71, 4.26)	0.000
BAG3	1.24	(0.94, 1.53)	0.159	IRF1	0.84	(0.61, 1.07)	0.287
BST2	1.29	(0.97, 1.60)	0.110	IRF2	1.24	(0.91, 1.57)	0.191
CASP1	0.88	(0.67, 1.08)	0.336	IRF3	1.20	(0.86, 1.55)	0.323
CAV1	0.50	(0.40, 0.61)	0.010	IRF5	1.28	(0.57, 1.99)	0.455
CCL2	0.69	(0.57, 0.81)	0.010	IRF7	0.54	(0.36, 0.73)	0.051
CCL5	0.93	(0.73, 1.13)	0.536	IRF9	0.86	(0.60, 1.12)	0.377
CD70	1.09	(0.84, 1.34)	0.529	ISG15	0.31	(0.22, 0.40)	0.010
CD80	0.95	(0.56, 1.33)	0.740	ISG20	0.39	(0.29, 0.49)	0.008
CD86	0.97	(0.57, 1.38)	0.993	JAK1	1.03	(0.82, 1.24)	0.859
CDKN1B	1.02	(0.70, 1.34)	0.990	JAK2	1.14	(0.86, 1.42)	0.394
CIITA	1.02	(0.63, 1.40)	0.926	MAL	1.03	(0.62, 1.43)	0.949
CRP	0.87	(0.56, 1.18)	0.406	MET	0.94	(0.66, 1.22)	0.656
CXCL10	1.08	(0.34, 1.82)	0.915	MNDA	0.84	(0.59, 1.08)	0.283
DDX58	0.39	(0.31, 0.47)	0.005	MX1	0.65	(0.44, 0.86)	0.049
EIF2AK2	0.68	(0.51, 0.85)	0.066	MX2	0.33	(0.25, 0.40)	0.005
GBP1	0.63	(0.49, 0.78)	0.037	MYD88	0.97	(0.67, 1.28)	0.780
HLA-A	0.90	(0.65, 1.16)	0.493	NMI	0.72	(0.57, 0.87)	0.053
HLA-B	0.66	(0.43, 0.89)	0.110	NOS2	1.06	(0.81, 1.32)	0.703
HLA-E	0.86	(0.64, 1.08)	0.322	OAS1	0.43	(0.36, 0.50)	0.003
HLA-G	0.97	(0.62, 1.32)	0.797	OAS2	0.35	(0.24, 0.46)	0.015
IFI16	0.72	(0.58, 0.87)	0.053	PML	0.52	(0.38, 0.67)	0.021
IFI27	0.63	(0.42, 0.84)	0.079	PRKCZ	0.99	(0.68, 1.31)	0.881
IFI30	1.02	(0.68, 1.36)	0.957	PSME2	1.07	(0.80, 1.35)	0.713
IFI6	0.29	(0.17, 0.41)	0.023	SH2D1A	1.12	(0.80, 1.44)	0.514
IFIH1	0.56	(0.40, 0.72)	0.035	SHB	1.18	(0.94, 1.43)	0.198
IFIT1	0.20	(0.14, 0.26)	0.006	SOCS1	0.96	(0.77, 1.15)	0.676
IFIT2	0.32	(0.23, 0.40)	0.008	STAT1	0.58	(0.41, 0.76)	0.044
IFIT3	0.30	(0.20, 0.40)	0.016	STAT2	0.64	(0.46, 0.83)	0.076
IFITM1	0.44	(0.35, 0.53)	0.007	STAT3	1.02	(0.76, 1.29)	0.973
IFITM2	0.81	(0.66, 0.97)	0.115	TAP1	0.68	(0.49, 0.86)	0.079
IFITM3	0.71	(0.56, 0.87)	0.064	TICAM1	1.12	(0.86, 1.38)	0.433
IFNA1	1.20	(0.86, 1.54)	0.299	TIMP1	0.79	(0.58, 1.00)	0.186
IFNA2	1.04	(0.54, 1.54)	0.782	TLR3	1.26	(0.90, 1.63)	0.178
IFNA4	1.28	(0.95, 1.62)	0.135	TLR7	0.90	(0.19, 1.61)	0.700
IFNAR1	0.90	(0.69, 1.11)	0.416	TLR8	1.04	(0.69, 1.40)	0.740
IFNAR2	1.08	(0.79, 1.36)	0.712	TLR9	1.05	(0.64, 1.46)	0.796
IFNB1	1.43	(0.92, 1.94)	0.123	TMEM173	0.71	(0.54, 0.87)	0.064
IFNE	1.59	(0.99, 2.18)	0.064	TNFSF10	0.95	(0.56, 1.35)	0.819
IFNW1	1.07	(0.77, 1.37)	0.573	TRAF3	0.92	(0.63, 1.22)	0.580
IL10	1.23	(0.50, 1.96)	0.546	TYK2	1.01	(0.70, 1.32)	0.986
IL15	0.87	(0.69, 1.05)	0.276	VEGFA	1.69	(1.16, 2.21)	0.042

A

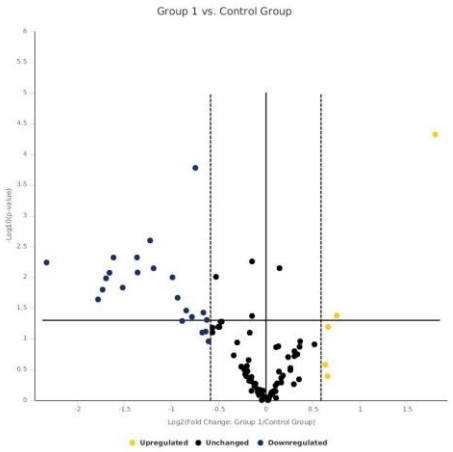
Group 1 vs. Control Group
Log2(Fold Change: Group 1/Control Group)
Upregulated
Unchanged
Downregulated

B

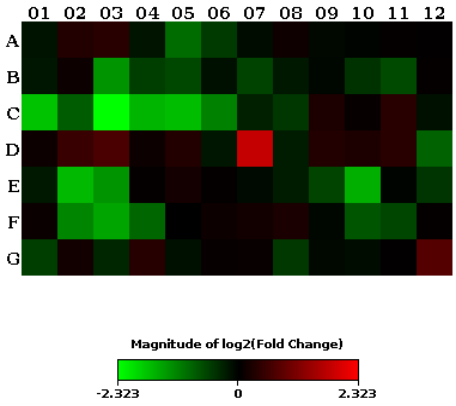
01 02 03 04 05 06 07 08 09 10 11 12
A
B
C
D
E
F
G
Magnitude of log2(Fold Change)
-2.323
0
2.323

C

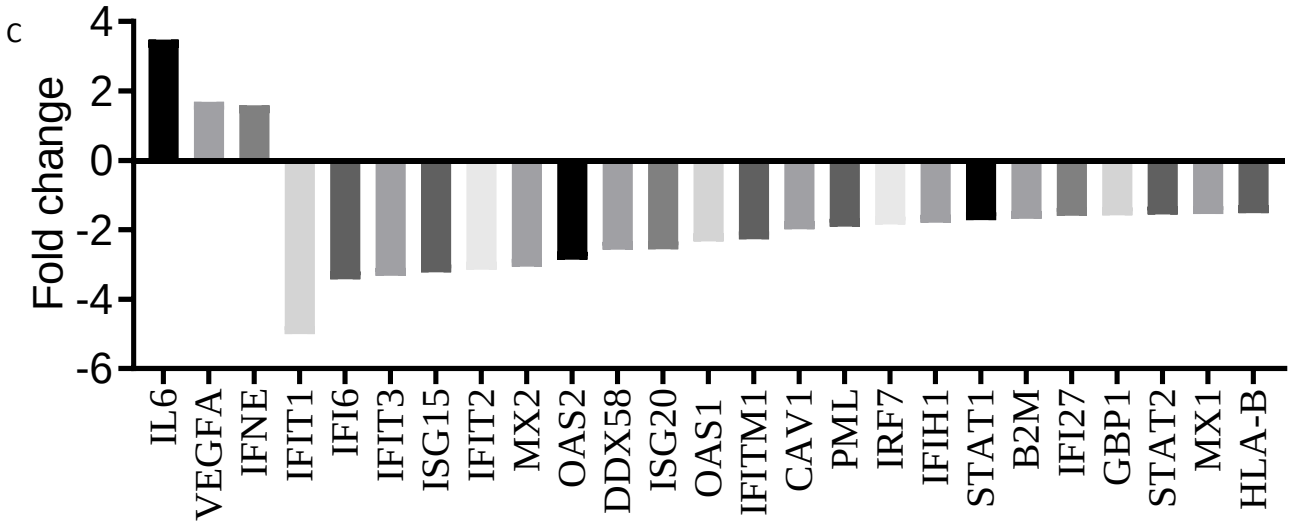
Fold change
4
2
0
-2
-4
-6
IL6
VEGFA
IFNE
IFIT1
IFI6
IFIT3
ISG15
IFIT2
MX2
OAS2
DDX58
ISG20
OAS1
IFITM1
CAV1
PML
IRF7
IFIH1
STAT1
B2M
IFI27
GBP1
STAT2
MX1
HLA-B

D

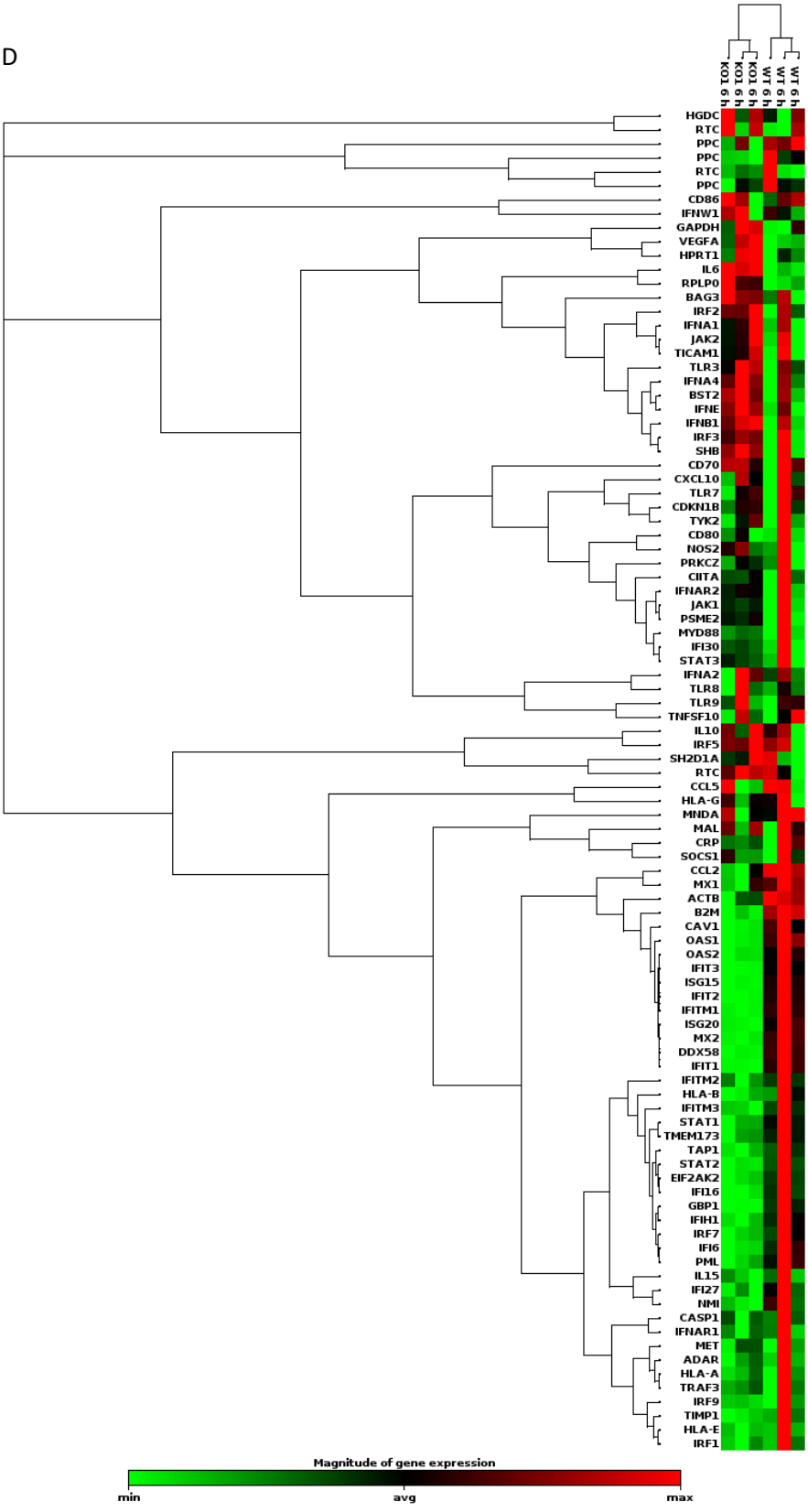
KO1 6 h
KO2 6 h
KO3 6 h
WT1 6 h
WT2 6 h
WT3 6 h
HGDC
RTC
PPC
PPC
RTC
PPC
CD86
IFNW1
GAPDH
VEGFA
HPRT1
IL6
RPLP0
BAG3
IRF2
IFNA1
JAK2
TICAM1
TLR3
IFNA4
BST2
IFNE
IFNB1
IRF3
SHB
CD70
CXCL10
TLR7
CDKN1B
TYK2
CD80
NOS2
PRKCZ
CIITA
IFNAR2
JAK1
PSME2
MYD88
IFI30
STAT3
IFNA2
TLR8
TLR9
TNFSF10
IL10
IRF5
SH2D1A
RTC
CCL5
HLA-G
MNDA
MAL
CRP
SOCS1
CCL2
MX1
ACTB
B2M
CAV1
OAS1
OAS2
IFIT3
ISG15
IFIT2
IFITM1
ISG20
MX2
DDX58
IFIT1
IFITM2
HLA-B
IFITM3
STAT1
TMEM173
TAP1
STAT2
EIF2AK2
IFI16
GBP1
IFIH1
IRF7
IFI6
PML
IL15
IFI27
NMI
CASP1
IFNAR1
MET
ADAR
HLA-A
TRAF3
IRF9
TIMP1
HLA-E
IRF1
Magnitude of gene expression
min
avg
max

Figure 23: PCR array of IFN response genes in *UBXN6*$^{+/+}$ and *UBXN6*$^{-/-}$ *2* trophoblast cells 6hrs after IFN-λ1 treatment.

(A) The volcano plot of relative fold change in all the tested genes.

(B) The heat map of relative fold change in all the tested genes.

(C) The bar graph of genes with a 1.5 or more-fold change in the expression (upregulation/ downregulation).

(D) The cluster-gram of relative fold change in all the tested genes.

Data represent the mean ± SEM (n = 3), Student's t-Test: two tailed distribution, two-sample unequal variance (*$p < 0.05$; ** $p < 0.01$)

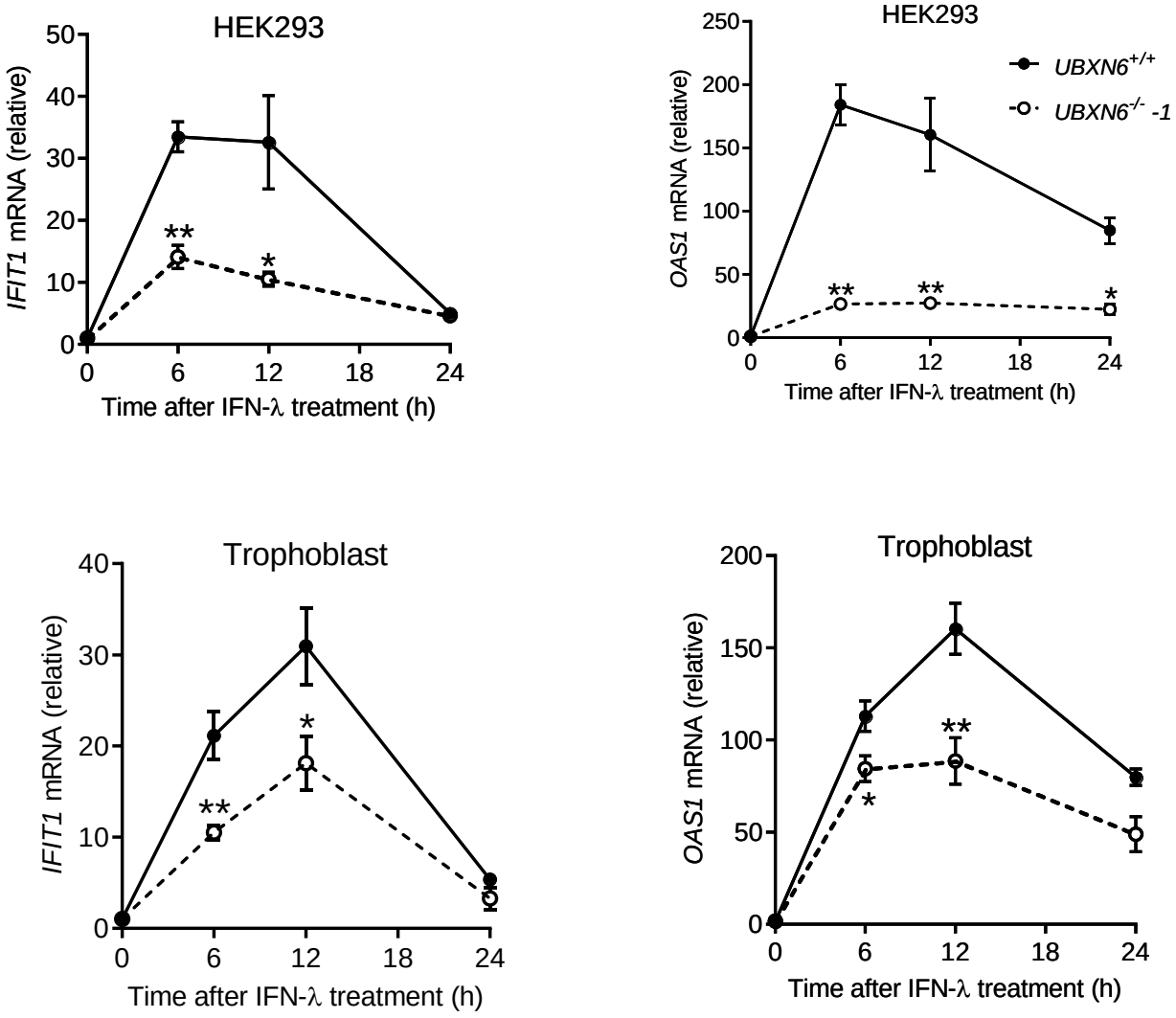

Figure 24: UBXN6 is critical for IFN-λ1 induced ISGs production in trophoblasts.

(A) mRNA expression of *IFIT1* and *OAS1A* at 0, 6, 12, 24 hrs after IFN-λ1 treatment in *UBXN6*$^{+/+}$ and *UBXN6*$^{-/-}$ *1* HEK293 cell.

(B) mRNA expression of *IFIT1* and *OAS1A* at 0, 6, 12, 24 hrs after IFN-λ1 treatment in *UBXN6*$^{+/+}$ and *UBXN6*$^{-/-}$ *2* trophoblasts.

Data represent the mean ± SEM (n = 3), Student's t-Test: two tailed distribution, two-sample unequal variance (*$p < 0.05$; ** $p < 0.01$)

4.3.2 Sub-aim 3.2: To identify the molecular mechanism by which UBXN6 regulates IFN-I/III responses.

As the data mentioned above established the role of UBXN6 in positive regulation of IFN-I/III responses, we next investigated the mechanism by which it acts on the JAK-STAT pathway. The STAT1 phosphorylation was significantly reduced in *UBXN6*$^{-/-}$ trophoblast than *UBXN6*$^{+/+}$ cells treated with recombinant IFN-λ for 60 minutes (**Figure 25**).

Next, we performed immune-precipitation and mass spectrometry analysis to identify the UBXN6-interacting protein, which could be helpful for us to pinpoint the molecular mechanism (Table 8). Consistent with a previous report (Alexandru et al., 2008) UBXN6 bound to VCP with the highest affinity. Intriguingly, UBXN6 also pull-down CFL and PRMT5 with/without IFN-λ treatment. IFN-λ treatment slightly increased UBXN6-PRMT5/CFL/VCP interaction. Of great interest, PRMT5 is an arginine methyltransferase that interacts with JAK1/2-TYK2 (Pollack et al., 1999) . It is thus possible that UBXN6 could regulate JAK1-STAT1/2 signaling via PRMT5.

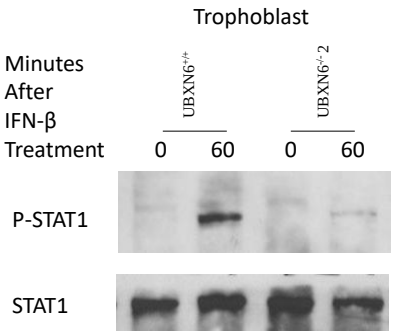

Figure 25: UBXN6 regulates STAT1 phosphorylation.

Immunoblot of p-STAT1 and STAT1 in the whole cell lysates of *UBXN6*$^{+/+}$ and *UBXN6*$^{-/-}$ *2* trophoblasts after 60 minutes of treatment with 10ng/ml IFNβ.

Table 8: Identification of UBXN6-interacting proteins by immunoprecipitation and mass spectrometry analysis.

HEK293T cells were transfected with either vector or FLAG-UBXN6 plasmid and treated with human IFN-β (10ng/ml) for 60 minutes. Whole cell lysates were immunoprecipitated with FLAG antibody-conjugated magnetic beads and the bound proteins were identified by mass spectrometry t. The total spectrum counts of bound proteins were normalized to input UBXN6 counts. Fifty identified proteins were listed below, and three UBXN6-interacting proteins with the highest confidence were highlighted in yellow.

							Total Spectrum Count						
							IP1-Vec	IP2-Vec-+IFN-L	IP3-FLAG-UBXN6	IP4-FLAG-UBXN6+IFN-L	Normalized to input		
#	Visible?	Identified Proteins (522)	Accession Number	Alternate ID	Molecular Weight (kDa)	Protein Grouping Ambiguity					UBXN6	UBXN6+IFN-L	Confidence
1	TRUE	Transitional endoplasmic reticulum ATPase OS=Homo sapiens GN=VCP PE=1 SV=4	TERA_HUMAN	VCP	89		2	1	33	23	1.65	1.91	****
2	TRUE	Cluster of Heat shock protein HSP 90-alpha OS=Homo sapiens GN=HSP90AA1 PE=1 SV=5 (HS90A_HUMAN)	HS90A_HUMAN [3]	HSP90AA1	85	TRUE	7	3	23	6			
3	TRUE	Immunoglobulin kappa variable 2-29 OS=Homo sapiens GN=IGKV2-29 PE=3 SV=2	KV229_HUMAN (+2)	IGKV2-29	13	TRUE	13	13	23	11			
4	TRUE	THO complex subunit 4 OS=Homo sapiens GN=ALYREF PE=1 SV=1	E9PB61_HUMAN (+1)	ALYREF	28		10	9	20	17	1	1.41	
5	TRUE	FLAG-UBXN6 OS=Homo sapiens GN=fUBXN6 PE=1 SV=1	A12345_HUMAN	fUBXN6	52		0	0	20	12	1	1	
6	TRUE	Heat shock 70 kDa protein 1B OS=Homo sapiens GN=HSPA1B PE=1 SV=1	A0A0G2JIW1_HUMAN (+2)	HSPA1B	70	TRUE	13	6	18	16			
7	TRUE	Cluster of Tubulin beta chain OS=Homo sapiens GN=TUBB PE=1 SV=1 (Q5JP53_HUMAN)	Q5JP53_HUMAN [3]	TUBB	48	TRUE	4	1	15	5			
8	TRUE	CON__P02769	CON__P02769		?		13	7	15	4			

9	TRUE	Actin, cytoplasmic 2 OS=Homo sapiens GN=ACTG1 PE=1 SV=1	ACTG_HUMAN	ACTG1	42		6	5	14	6			
10	TRUE	Pyruvate kinase PKM OS=Homo sapiens GN=PKM PE=1 SV=4	KPYM_HUMAN	PKM	58		7	7	13	8			
11	TRUE	Alpha-enolase OS=Homo sapiens GN=ENO1 PE=1 SV=2	ENOA_HUMAN	ENO1	47		2	1	13	2			
12	TRUE	Protein arginine N-methyltransferase 5 OS=Homo sapiens GN=PRMT5 PE=1 SV=4	ANM5_HUMAN	PRMT5	73		3	1	11	7	0.55	0.58	***
13	TRUE	Cluster of Elongation factor 1-alpha 1 OS=Homo sapiens GN=EEF1A1 PE=1 SV=1 (EF1A1_HUMAN)	EF1A1_HUMAN [3]	EEF1A1	50	TRUE	7	4	11	6			
14	TRUE	Cluster of Heat shock cognate 71 kDa protein OS=Homo sapiens GN=HSPA8 PE=1 SV=1 (HSP7C_HUMAN)	HSP7C_HUMAN [2]	HSPA8	71	TRUE	7	4	11	5			
15	TRUE	SCY1-like protein 2 OS=Homo sapiens GN=SCYL2 PE=1 SV=1	SCYL2_HUMAN	SCYL2	104		4	0	11	4			
16	TRUE	Elongation factor 2 OS=Homo sapiens GN=EEF2 PE=1 SV=4	EF2_HUMAN	EEF2	95		1	0	11	1			
17	TRUE	Eukaryotic translation initiation factor 4B OS=Homo sapiens GN=EIF4B PE=1 SV=1	E7EX17_HUMAN (+1)	EIF4B	70		11	9	10	11			
18	TRUE	Protein phosphatase 1B OS=Homo sapiens GN=PPM1B PE=1 SV=1	PPM1B_HUMAN	PPM1B	53		4	6	10	7			
19	TRUE	78 kDa glucose-regulated protein OS=Homo sapiens GN=HSPA5 PE=1 SV=2	GRP78_HUMAN	HSPA5	72	TRUE	7	3	10	3			
20	TRUE	CON__P12763	CON__P12763		?		4	0	10	2			
21	TRUE	Tubulin alpha-1B chain OS=Homo sapiens GN=TUBA1B PE=1 SV=1	TBA1B_HUMAN	TUBA1B	50		6	2	9	7			
22	TRUE	Peroxiredoxin-6 OS=Homo sapiens GN=PRDX6 PE=1 SV=3	PRDX6_HUMAN	PRDX6	25		2	3	9	4			
23	TRUE	60S ribosomal protein L38 OS=Homo sapiens GN=RPL38 PE=1 SV=2	RL38_HUMAN	RPL38	8		3	4	9	3			
24	TRUE	6-phosphofructo-2-kinase/fructose-2,6-bisphosphatase 2 OS=Homo sapiens GN=PFKFB2 PE=1 SV=2	F262_HUMAN	PFKFB2	58	TRUE	2	0	9	1			
25	TRUE	Nucleolin OS=Homo sapiens GN=NCL PE=1 SV=3	NUCL_HUMAN	NCL	77		1	0	9	0			
26	TRUE	Cluster of Keratin, type II cytoskeletal 1 OS=Homo sapiens GN=KRT1 PE=1 SV=6 (K2C1_HUMAN)	K2C1_HUMAN [5]	KRT1	66	TRUE	10	0	8	16			
27	TRUE	Heterogeneous nuclear ribonucleoprotein K OS=Homo sapiens GN=HNRNPK PE=1 SV=1	HNRPK_HUMAN	HNRNPK	51		5	3	8	3			
28	TRUE	60 kDa heat shock protein, mitochondrial OS=Homo sapiens GN=HSPD1 PE=1 SV=2	CH60_HUMAN	HSPD1	61		3	4	8	2			
29	TRUE	Stress-70 protein, mitochondrial OS=Homo sapiens GN=HSPA9 PE=1 SV=2	GRP75_HUMAN	HSPA9	74		2	1	8	1			
30	TRUE	Cofilin-1 OS=Homo sapiens GN=CFL1 PE=1 SV=3	COF1_HUMAN (+1)	CFL1	19		0	0	7	5	0.35	0.41	****
31	TRUE	Polymerase delta-interacting protein 3 OS=Homo sapiens GN=POLDIP3 PE=1 SV=1	F6VRR5_HUMAN (+1)	POLDIP3	48		1	0	7	3			
32	TRUE	40S ribosomal protein S25 OS=Homo sapiens GN=RPS25 PE=1 SV=1	RS25_HUMAN	RPS25	14		3	3	7	1			
33	TRUE	Heat shock 70 kDa protein 4 OS=Homo sapiens GN=HSPA4 PE=1 SV=4	HSP74_HUMAN	HSPA4	94		1	1	7	1			

34	TRUE	ATP synthase subunit beta, mitochondrial OS=Homo sapiens GN=ATP5B PE=1 SV=3	ATPB_HUMAN	ATP5B	57		0	0	7	0			
35	TRUE	GTP-binding nuclear protein Ran OS=Homo sapiens GN=RAN PE=1 SV=1	B5MDF5_HUMAN (+1)	RAN	26		0	0	7	0			
36	TRUE	60S ribosomal protein L35 OS=Homo sapiens GN=RPL35 PE=1 SV=2	RL35_HUMAN	RPL35	15		5	4	7	5			
37	TRUE	Serine/threonine-protein kinase 38 OS=Homo sapiens GN=STK38 PE=1 SV=1	STK38_HUMAN	STK38	54	TRUE	4	3	6	5			
38	TRUE	Elongation factor Tu, mitochondrial OS=Homo sapiens GN=TUFM PE=1 SV=2	EFTU_HUMAN	TUFM	50		4	1	6	4			
39	TRUE	60S ribosomal protein L23a OS=Homo sapiens GN=RPL23A PE=1 SV=1	RL23A_HUMAN	RPL23A	18		6	5	6	3			
40	TRUE	40S ribosomal protein S3 OS=Homo sapiens GN=RPS3 PE=1 SV=2	RS3_HUMAN	RPS3	27		3	3	6	3			
41	TRUE	RNA binding motif protein 10, isoform CRA_d OS=Homo sapiens GN=RBM10 PE=1 SV=1	A0A0A0MR66_HUMAN (+1)	RBM10	110		4	1	6	3			
42	TRUE	ATP synthase subunit alpha, mitochondrial OS=Homo sapiens GN=ATP5A1 PE=1 SV=1	ATPA_HUMAN	ATP5A1	60		2	0	6	3			
43	TRUE	Histone H4 OS=Homo sapiens GN=HIST1H4A PE=1 SV=2	H4_HUMAN	HIST1H4A	11		4	4	6	2			
44	TRUE	60S ribosomal protein L27 OS=Homo sapiens GN=RPL27 PE=1 SV=2	RL27_HUMAN	RPL27	16		3	3	6	1			
45	TRUE	Heterogeneous nuclear ribonucleoproteins A2/B1 OS=Homo sapiens GN=HNRNPA2B1 PE=1 SV=2	ROA2_HUMAN	HNRNPA2B1	37		1	1	6	1			
46	TRUE	Multifunctional protein ADE2 (Fragment) OS=Homo sapiens GN=PAICS PE=1 SV=1	E9PBS1_HUMAN (+1)	PAICS	46		0	0	6	1			
47	TRUE	Endoplasmin OS=Homo sapiens GN=HSP90B1 PE=1 SV=1	ENPL_HUMAN	HSP90B1	92	TRUE	1	0	6	1			
48	TRUE	T-complex protein 1 subunit theta OS=Homo sapiens GN=CCT8 PE=1 SV=4	TCPQ_HUMAN	CCT8	60		1	0	6	0			
49	TRUE	Ubiquitin-like modifier-activating enzyme 1 OS=Homo sapiens GN=UBA1 PE=1 SV=3	UBA1_HUMAN	UBA1	118		0	0	6	0			
50	TRUE	CON__P00761	CON__P00761		?		4	3	6	7			

5 Discussion

UBXN6 belongs to a family of proteins that are putatively involved in VCP-mediated cellular processes. Recent studies suggest that UBXN6 participates in ERAD (Nagahama et al., 2009) , protein trafficking(Haines et al., 2012 ; Kirchner et al., 2013 ; Ritz et al., 2011) , clearance of ruptured lysosomes by autophagy (Papadopoulos et al., 2017) , degradation of mitochondrial outer membrane protein myeloid cell leukemia 1 (MCL1) in a model of Huntington's disease (Guo and Qi, 2017) . In this study, we identified that UBXN6 is the only positive regulator of JAK-STAT signaling amongst the 13 known UBXNs.

We present several pieces of evidence showing that UBXN6 positively regulates the JAK1-STAT1/2 signaling pathway. First, UBXN6 overexpression potentiates ISG induction by recombinant IFN-β or IFN-λ, which activates JAK1-STAT1/2 signaling via their respective receptors. Second, ISG expression and STAT1 phosphorylation stimulated by IFNs is impaired in UBXN6-deficient cells. Third, IFN/ISG expression activated by polyIC and viral infection is also reduced in UBXN6 overexpression.

Although our data suggest that UBXN6 regulates JAK1-STAT1/2 specifically, the observations that polyIC and virus-induced type I/III expression is also reduced in the UBXN6 deficient cells suggest a role of UBXN6 in the RLR signaling too. The two dominant polyIC/viral RNA receptors in human trophoblasts are melanoma differentiation-associated gene 5, MDA5 (encoded by IFIH1), and retinoic acid-inducible gene-1, RIG-I (encoded by DDX58) (J. Ma et al., 2018b) , which are also well characterized ISGs. Their

basal levels are generally very low and need to be induced via JAK1-STAT1/2 in the context of polyIC/virus stimulation. Thus, a deficiency in JAK1-STAT1/2 signaling may also negatively impact primary IFN responses. Indeed, STAT1/2 deficiency in mice led to a significant reduction in type I IFNs after dengue virus infection (Perry et al., 2011) . To clarify this point, we overexpressed the major molecules (MDA5/MAVS/TBK1) of the RLR pathway to activate *IFNB1* transcription independently of JAK1-STAT1/2. The results suggest that UBXN6 does not directly regulate the RLR pathway, rather directly targets JAK1-STAT1/2. This is further substantiated by the findings that JAK1/STAT1 phosphorylation activated directly by recombinant IFN-λ1 was impaired in *UBXN6*$^{-/-}$ cells.

Next, we investigated the molecular function of UBXN6. The significant reduction of STAT1 phosphorylation after IFN-β stimulation in UBXN6 deficient cells suggests that UBXN6 acts upstream in the pathway. By this hypothesis, we found that UBXN6 was able to bind to JAK-binding protein PRMT5, when over-expressed at a very low amount and stimulated with IFN-β. PRMT5 was identified as a JAK-binding protein and involved in arginine methyltransferase (Pollack et al., 1999) . PRMT5 was found to be involved in the regulation of NF-κB in TRAIL-induced apoptosis by competing with TRAIL to bind to DDR4. Another study reported that methylation of p65 subunit leads to the regulation of NF-κB activity (J. H. Kim et al., 2016) . However, we recognize that our current dataset cannot conclude a functional relationship between UBXN6, PRMT5, and JAK1/2. At present, work is underway to elucidate this. We hypothesize that PRMT5 could be a dominant negative binder of JAK1/2 and UBXN6 binding to PRMT5 directly or as a complex of PRMT5-UBXN6-VCP (As in **Figure 26**) liberates JAK from the PRMT5-bound state. The free

JAK may undergo conformational changes and expose the phosphorylation sites or may provide docking to STAT for its activation. It is also possible that methylation or demethylation of arginine on JAK1/2 residues may enhance JAK phosphorylation and the downstream signaling. Thus, increased STAT phosphorylation is a possible mechanism by which UBXN6 can positively regulate JAK-STAT signaling.

UBXN6 could also stimulate STAT phosphorylation by a PRMT5-JAK independent mechanism. UBXN6 may interact with TYK2, which is bound to the cytoplasmic domain of IFN receptors, resulting in enhanced kinase activity. Alternately, UBXN6-VCP complex may degrade inhibitors of JAK-STAT signalings, such as SOCSs, PTPs, and PIAs.

Another predicted mechanism of positive regulation of JAK-STAT signaling by UBXN6 is via IFN receptors trafficking/recycling/degradation. Following receptor agonism, the C-terminus of IFNAR is phosphorylated, followed by its ubiquitination and internalization. Internalization can result in degradation of the receptor, thereby reducing membrane expression, or it can result in the recycling of the receptor without an extended impact on membrane receptor levels. However, clathrin-mediated endocytosis may also serve to concentrate the IFNAR receptors and signaling components, thereby amplifying signaling (Claudinon et al., 2007) .

Many cells are responsive to type I IFNs because their receptors are ubiquitously expressed. In contrast, type III receptors are restricted to specific cell types such as mucosal epithelial, endothelial cells and human liver (Wack et al., 2015) . The trophoblasts act as a primary barrier of the placenta by constitutively secreting IFN-III. The medium from uninfected cells was found to protect nonplacental cells from Zika

infection. Trophoblast-derived IFN-III act as a barrier to Zika infection via autocrine as well as the paracrine mode and restrict viral entry to the fetal compartment (Bayer et al., 2016) . Indeed, we found that increased ISG production in trophoblasts by recombinant IFN-λ1 stimulation was impaired in *UBXN6*$^{-/-}$ cells; confirming our findings that UBXN6 positively regulates IFN-induced ISG production.

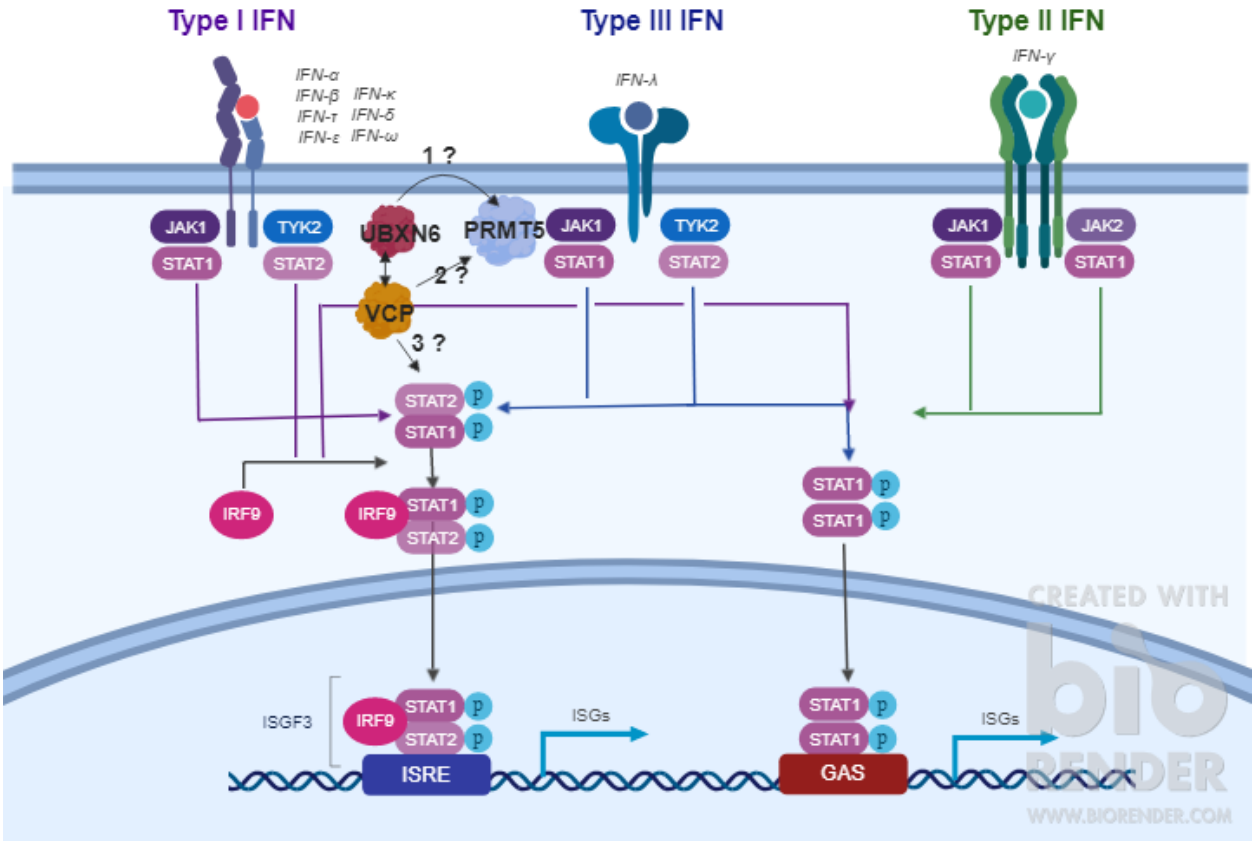

Figure 26: A model depicting UBXN6 association with the only PRMT5 or as a complex of PRMT5-UBXN6-VCP to act on JAK and STAT1 phosphorylation.

6 Conclusion

The UBX domain-containing proteins (UBXN) are involved in various cellular processes including ubiquitin-dependent protein degradation, vesicle fusion, and cell cycle control. However, their role in the regulation of the innate immune pathways has not been thoroughly explored. We demonstrate that the UBXN6 positively regulates type I/III interferons (IFN-I/III)- induced Janus kinase/signal transducers and activators of transcription (JAK/STAT) pathway. IFN-I/III induce expression of several ISGs through theJAK/STAT pathway to combat viral infections.

Amongst 13 known UBXNs, ectopic expression of UBXN6 highly enhances IFN-β and IFN-λ1-stimulated ISG. *UBXN6* $^{-/-}$ HEK293 and trophoblasts were deficient in ISG production upon IFN-λ1 stimulation. Also, RNA virus replication increased in *UBXN6* $^{-/-}$ cells compared to *UBXN6* $^{+/+}$ cells, and this was accompanied by a reduction in both IFN-I/III and ISG expression. The IFN responses to a dsRNA analogue polyinosinic-polycytidylic acid were also decreased. Phosphorylation of STAT1 induced by recombinant IFN-λ1 was impaired in UBXN6 deficient cells. These results demonstrate that UBXN6 restricts viral infection through optimal activation of JAK1-STAT1/2 signaling.

Mass spectrometry analysis revealed the association of UBXN6 with PRMT5, a JAK-binding protein. It is suggested that binding of UBXN6 to PRMT5 affect JAK activity and its downstream signaling. Further mechanistic studies are required to confirm the target of

UBXN6 in JAK-STAT signaling. Also, the role of PRMT5 when associated with UBXN6 needs to be explored in detail.

7 Citation

1. Addgene. (2019). from https://www.addgene.org/crispr/guide/
2. **Alexandru G , Graumann J , Smith GT , Kolawa NJ , Fang R , & Deshaies RJ**. Ubxd7 binds multiple ubiquitin ligases and implicates p97 in hif1alpha turnover. *Cell*, 2008; 134(5): 804-816.
3. **Ank N , West H , Bartholdy C , Eriksson K , Thomsen AR , & Paludan SR**. Lambda interferon (ifn-λ), a type iii ifn, is induced by viruses and ifns and displays potent antiviral activity against select virus infections in vivo. *Journal of Virology*, 2006; 80(9): 4501-4509.
4. **Arumughan A , Roske Y , Barth C , Forero LL , Bravo-Rodriguez K , Redel A, . . . Wanker EE**. Quantitative interaction mapping reveals an extended ubx domain in aspl that disrupts functional p97 hexamers. *Nat Commun*, 2016; 7: 13047.
5. **Bandau S , Knebel A , Gage ZO , Wood NT , & Alexandru G**. Ubxn7 docks on neddylated cullin complexes using its uim motif and causes hif1alpha accumulation. *BMC Biol*, 2012; 10: 36.
6. **Barr SD , Smiley JR , & Bushman FD**. The interferon response inhibits hiv particle production by induction of trim22. *PLoS Pathog*, 2008; 4(2): e1000007.
7. **Bayer A , Lennemann NJ , Ouyang Y , Bramley JC , Morosky S , Marques ET, Jr., . . . Coyne CB**. Type iii interferons produced by human placental trophoblasts confer protection against zika virus infection. *Cell Host Microbe*, 2016; 19(5): 705-712.
8. **Brizzard BL , Chubet RG , & Vizard DL**. Immunoaffinity purification of flag epitope-tagged bacterial alkaline phosphatase using a novel monoclonal antibody and peptide elution. *Biotechniques*, 1994; 16(4): 730-735.
9. **Campbell EM , Perez O , Anderson JL , & Hope TJ**. Visualization of a proteasome-independent intermediate during restriction of hiv-1 by rhesus trim5alpha. *J Cell Biol*, 2008; 180(3): 549-561.
10. **Castanier C , Zemirli N , Portier A , Garcin D , Bidere N , Vazquez A , & Arnoult D**. Mavs ubiquitination by the e3 ligase trim25 and degradation by the proteasome is involved in type i interferon production after activation of the antiviral rig-i-like receptors. *BMC Biol*, 2012; 10: 44.
11. **Chakrabarti A , Jha BK , & Silverman RH**. New insights into the role of rnase l in innate immunity. *J Interferon Cytokine Res*, 2011; 31(1): 49-57.
12. **Chapman E , Fry AN , & Kang M**. The complexities of p97 function in health and disease. *Mol Biosyst*, 2011; 7(3): 700-710.
13. **Claudinon J , Monier MN , & Lamaze C**. Interfering with interferon receptor sorting and trafficking: Impact on signaling. *Biochimie*, 2007; 89(6-7): 735-743.
14. **D'Cruz AA , Kershaw NJ , Hayman TJ , Linossi EM , Chiang JJ , Wang MK, . . . Nicholson SE**. Identification of a second binding site on the trim25 b30.2 domain. *Biochem J*, 2018; 475(2): 429-440.
15. **Dai T , Wu L , Wang S , Wang J , Xie F , Zhang Z, . . . Zhang L**. Faf1 regulates antiviral immunity by inhibiting mavs but is antagonized by phosphorylation upon viral infection. *Cell Host Microbe*, 2018; 24(6): 776-790 e775.
16. **Dalton KP , & Rose JK**. Vesicular stomatitis virus glycoprotein containing the entire green fluorescent protein on its cytoplasmic domain is incorporated efficiently into virus particles. *Virology*, 2001; 279(2): 414-421.
17. **Decker T , & Kovarik P**. Serine phosphorylation of stats. *Oncogene*, 2000; 19(21): 2628-2637.
18. **Dixit E , Boulant S , Zhang Y , Lee ASY , Odendall C , Shum B, . . . Kagan JC**. Peroxisomes are signaling platforms for antiviral innate immunity. *Cell*, 2010; 141(4): 668-681.

19. **Grentzmann G , Ingram JA , Kelly PJ , Gesteland RF , & Atkins JF**. A dual-luciferase reporter system for studying recoding signals. *RNA*, 1998; 4(4): 479-486.
20. **Gui L , Zhang X , Li K , Frankowski KJ , Li S , Wong DE, . . . Chou TF**. Evaluating p97 inhibitor analogues for potency against p97-p37 and p97-npl4-ufd1 complexes. *ChemMedChem*, 2016; 11(9): 953-957.
21. **Guo X , & Qi X**. Vcp cooperates with ubxd1 to degrade mitochondrial outer membrane protein mcl1 in model of huntington's disease. *Biochim Biophys Acta Mol Basis Dis*, 2017; 1863(2): 552-559.
22. **Haines DS , Lee JE , Beauparlant SL , Kyle DB , den Besten W , Sweredoski MJ, . . . Deshaies RJ**. Protein interaction profiling of the p97 adaptor ubxd1 points to a role for the complex in modulating ergic-53 trafficking. *Mol Cell Proteomics*, 2012; 11(6): M111 016444.
23. **Hanzelmann P , Buchberger A , & Schindelin H**. Hierarchical binding of cofactors to the aaa atpase p97. *Structure*, 2011; 19(6): 833-843.
24. **Heaton SM , Borg NA , & Dixit VM**. Ubiquitin in the activation and attenuation of innate antiviral immunity. *The Journal of Experimental Medicine*, 2016; 213(1): 1.
25. **Hilton DJ**. Negative regulators of cytokine signal transduction. *Cell Mol Life Sci*, 1999; 55(12): 1568-1577.
26. **Hong XX , & Carmichael GG**. Innate immunity in pluripotent human cells: Attenuated response to interferon-beta. *J Biol Chem*, 2013; 288(22): 16196-16205.
27. **Hu Y , O'Boyle K , Auer J , Raju S , You F , Wang P, . . . Sutton RE**. Multiple ubxn family members inhibit retrovirus and lentivirus production and canonical nfκβ signaling by stabilizing iκbα. *PLoS pathogens*, 2017; 13(2): e1006187-e1006187.
28. **Huang K , Yang C , Wang QX , Li YS , Fang C , Tan YL, . . . Kang CS**. The crispr/cas9 system targeting egfr exon 17 abrogates nf-kappab activation via epigenetic modulation of ubxn1 in egfrwt/viii glioma cells. *Cancer Lett*, 2017; 388: 269-280.
29. **Hubel P , Urban C , Bergant V , Schneider WM , Knauer B , Stukalov A, . . . Pichlmair A**. A protein-interaction network of interferon-stimulated genes extends the innate immune system landscape. *Nat Immunol*, 2019.
30. **Imai N , Suzuki M , Hayashi K , Ishigami M , Hirooka Y , Abe T, . . . Fujimoto T**. Hepatocyte-specific depletion of ubxd8 induces periportal steatosis in mice fed a high-fat diet. *Plos One*, 2015; 10(5).
31. **Irie-Sasaki J , Sasaki T , Matsumoto W , Opavsky A , Cheng M , Welstead G, . . . Penninger JM**. Cd45 is a jak phosphatase and negatively regulates cytokine receptor signalling. *Nature*, 2001; 409(6818): 349-354.
32. **Iwasaki A**. A virological view of innate immune recognition. *Annu Rev Microbiol*, 2012; 66: 177-196.
33. **Kane M , Yadav SS , Bitzegeio J , Kutluay SB , Zang T , Wilson SJ, . . . Bieniasz PD**. Mx2 is an interferon-induced inhibitor of hiv-1 infection. *Nature*, 2013; 502(7472): 563-566.
34. **Kaneko Y , Tamura K , Totsukawa G , & Kondo H**. Phosphorylation of p37 is important for golgi disassembly at mitosis. *Biochem Biophys Res Commun*, 2010; 402(1): 37-41.
35. **Kawai T , & Akira S**. Regulation of innate immune signalling pathways by the tripartite motif (trim) family proteins. *EMBO Mol Med*, 2011; 3(9): 513-527.
36. **Kawamura M , McVicar DW , Johnston JA , Blake TB , Chen YQ , Lal BK, . . . et al.** Molecular cloning of l-jak, a janus family protein-tyrosine kinase expressed in natural killer cells and activated leukocytes. *Proc Natl Acad Sci U S A*, 1994; 91(14): 6374-6378.
37. **Kern M , Fernandez-Saiz V , Schafer Z , & Buchberger A**. Ubxd1 binds p97 through two independent binding sites. *Biochem Biophys Res Commun*, 2009; 380(2): 303-307.

38. **Kim JH , Park ME , Nikapitiya C , Kim TH , Uddin MB , Lee HC, . . . Lee JS**. Fas-associated factor-1 positively regulates type i interferon response to rna virus infection by targeting nlrx1. *PLoS Pathog*, 2017; 13(5): e1006398.
39. **Kim JH , Yoo BC , Yang WS , Kim E , Hong S , & Cho JY**. The role of protein arginine methyltransferases in inflammatory responses. *Mediators Inflamm*, 2016; 2016: 4028353.
40. **Kim TK , & Maniatis T**. Regulation of interferon-gamma-activated stat1 by the ubiquitin-proteasome pathway. *Science*, 1996; 273(5282): 1717-1719.
41. **Kirchner P , Bug M , & Meyer H**. Ubiquitination of the n-terminal region of caveolin-1 regulates endosomal sorting by the vcp/p97 aaa-atpase. *J Biol Chem*, 2013; 288(10): 7363-7372.
42. **Klockow B , Tichelaar W , Madden DR , Niemann HH , Akiba T , Hirose K , & Manstein DJ**. The dynamin a ring complex: Molecular organization and nucleotide-dependent conformational changes. *EMBO J*, 2002; 21(3): 240-250.
43. **Kondo H , Rabouille C , Newman R , Levine TP , Pappin D , Freemont P , & Warren G**. P47 is a cofactor for p97-mediated membrane fusion. *Nature*, 1997; 388(6637): 75-78.
44. **Ladanyi M , Lui MY , Antonescu CR , Krause-Boehm A , Meindl A , Argani P, . . . Bridge J**. The der(17)t(x;17)(p11;q25) of human alveolar soft part sarcoma fuses the tfe3 transcription factor gene to aspl, a novel gene at 17q25. *Oncogene*, 2001; 20(1): 48-57.
45. **LaLonde DP , & Bretscher A**. The ubx protein saks1 negatively regulates endoplasmic reticulum-associated degradation and p97-dependent degradation. *J Biol Chem*, 2011; 286(6): 4892-4901.
46. **Larner AC , Chaudhuri A , & Darnell JE, Jr.** Transcriptional induction by interferon. New protein(s) determine the extent and length of the induction. *J Biol Chem*, 1986; 261(1): 453-459.
47. **Lee BH , Schwager F , Meraldi P , & Gotta M**. P37/ubxn2b regulates spindle orientation by limiting cortical numa recruitment via pp1/repo-man. *J Cell Biol*, 2018; 217(2): 483-493.
48. **Lee JJ , Park JK , Jeong J , Jeon H , Yoon JB , Kim EE , & Lee KJ**. Complex of fas-associated factor 1 (faf1) with valosin-containing protein (vcp)-npl4-ufd1 and polyubiquitinated proteins promotes endoplasmic reticulum-associated degradation (erad). *J Biol Chem*, 2013; 288(10): 6998-7011.
49. **Lee JN , Kim H , Yao H , Chen Y , Weng K , & Ye J**. Identification of ubxd8 protein as a sensor for unsaturated fatty acids and regulator of triglyceride synthesis. *Proceedings of the National Academy of Sciences of the United States of America*, 2010; 107(50): 21424-21429.
50. **Levy DE , & Darnell JE, Jr.** Stats: Transcriptional control and biological impact. *Nat Rev Mol Cell Biol*, 2002; 3(9): 651-662.
51. **Li X , Zhang J , Yang Z , Kang J , Jiang S , Zhang T, . . . Lu F**. The function of targeted host genes determines the oncogenicity of hbv integration in hepatocellular carcinoma. *J Hepatol*, 2014; 60(5): 975-984.
52. **Li ZH , Wang Y , Xu M , & Jiang T**. Crystal structures of the ubx domain of human ubxd7 and its complex with p97 atpase. *Biochem Biophys Res Commun*, 2017; 486(1): 94-100.
53. **Liang J , Yin C , Doong H , Fang S , Peterhoff C , Nixon RA , & Monteiro MJ**. Characterization of erasin (ubxd2): A new er protein that promotes er-associated protein degradation. *J Cell Sci*, 2006; 119(Pt 19): 4011-4024.
54. **Lim PJ , Danner R , Liang J , Doong H , Harman C , Srinivasan D, . . . Monteiro MJ**. Ubiquilin and p97/vcp bind erasin, forming a complex involved in erad. *J Cell Biol*, 2009; 187(2): 201-217.
55. **Liu F , & Gu J**. Retinoic acid inducible gene-i, more than a virus sensor. *Protein & Cell*, 2011; 2(5): 351-357.

56. **Liu S-Y , Sanchez DJ , & Cheng G**. New developments in the induction and antiviral effectors of type i interferon. *Current Opinion in Immunology*, 2011; 23(1): 57-64.
57. **Liu Z , Pan Q , Ding S , Qian J , Xu F , Zhou J, . . . Liang C**. The interferon-inducible mxb protein inhibits hiv-1 infection. *Cell Host Microbe*, 2013; 14(4): 398-410.
58. **Loregger A , Raaben M , Tan J , Scheij S , Moeton M , van den Berg M, . . . Zelcer N**. Haploid mammalian genetic screen identifies ubxd8 as a key determinant of hmgcr degradation and cholesterol biosynthesis. *Arteriosclerosis Thrombosis and Vascular Biology*, 2017; 37(11): 2064-+.
59. **Ma J , Ketkar H , Geng T , Lo E , Wang L , Xi J, . . . Wang P**. Zika virus non-structural protein 4a blocks the rlr-mavs signaling. *Frontiers in microbiology*, 2018a; 9: 1350-1350.
60. **Ma J , Ketkar H , Geng T , Lo E , Wang L , Xi J, . . . Wang P**. Zika virus non-structural protein 4a blocks the rlr-mavs signaling. *Front Microbiol*, 2018b; 9: 1350.
61. **Maccalli C , Di Cristanziano V , Fodale V , Corsi D , D'Agostino G , Petrangeli V, . . . Belardelli F**. Induction of both cd8+ and cd4+ t-cell-mediated responses in colorectal cancer patients by colon antigen-1. *Clin Cancer Res*, 2008; 14(22): 7292-7303.
62. **Madsen L , Andersen KM , Prag S , Moos T , Semple CA , Seeger M , & Hartmann-Petersen R**. Ubxd1 is a novel co-factor of the human p97 atpase. *Int J Biochem Cell Biol*, 2008; 40(12): 2927-2942.
63. **Madsen L , Kriegenburg F , Vala A , Best D , Prag S , Hofmann K, . . . Hartmann-Petersen R**. The tissue-specific rep8/ubxd6 tethers p97 to the endoplasmic reticulum membrane for degradation of misfolded proteins. *Plos One*, 2011; 6(9): e25061.
64. **Malakhov MP , Malakhova OA , Kim KI , Ritchie KJ , & Zhang DE**. Ubp43 (usp18) specifically removes isg15 from conjugated proteins. *J Biol Chem*, 2002; 277(12): 9976-9981.
65. **Malakhova OA , Kim KI , Luo JK , Zou W , Kumar KG , Fuchs SY, . . . Zhang DE**. Ubp43 is a novel regulator of interferon signaling independent of its isg15 isopeptidase activity. *EMBO J*, 2006; 25(11): 2358-2367.
66. **Malakhova OA , Yan M , Malakhov MP , Yuan Y , Ritchie KJ , Kim KI, . . . Zhang DE**. Protein isgylation modulates the jak-stat signaling pathway. *Genes Dev*, 2003; 17(4): 455-460.
67. **Matsumiya T , & Stafforini DM**. Function and regulation of retinoic acid-inducible gene-i. *Critical Reviews in Immunology*, 2010; 30(6): 489-513.
68. **Moore CB , Bergstralh DT , Duncan JA , Lei Y , Morrison TE , Zimmermann AG, . . . Ting JPY**. Nlrx1 is a regulator of mitochondrial antiviral immunity. *Nature*, 2008; 451(7178): 573-U578.
69. **Mowen KA , Tang J , Zhu W , Schurter BT , Shuai K , Herschman HR , & David M**. Arginine methylation of stat1 modulates ifnalpha/beta-induced transcription. *Cell*, 2001; 104(5): 731-741.
70. **Munir M , & Berg M**. The multiple faces of proteinkinase r in antiviral defense. *Virulence*, 2013; 4(1): 85-89.
71. **Myers MP , Andersen JN , Cheng A , Tremblay ML , Horvath CM , Parisien JP, . . . Tonks NK**. Tyk2 and jak2 are substrates of protein-tyrosine phosphatase 1b. *J Biol Chem*, 2001; 276(51): 47771-47774.
72. **Nagahama M , Ohnishi M , Kawate Y , Matsui T , Miyake H , Yuasa K, . . . Tsuji A**. Ubxd1 is a vcp-interacting protein that is involved in er-associated degradation. *Biochem Biophys Res Commun*, 2009; 382(2): 303-308.
73. **Neel BG**. Structure and function of sh2-domain containing tyrosine phosphatases. *Semin Cell Biol*, 1993; 4(6): 419-432.
74. Ohmiya Y.). Applications of bioluminiscense , cell based assays and imaging 2019, from http://photobiology.info/Ohmiya.html

75. **Olzmann JA , Richter CM , & Kopito RR**. Spatial regulation of ubxd8 and p97/vcp controls atgl-mediated lipid droplet turnover. *Proceedings of the National Academy of Sciences of the United States of America*, 2013; 110(4): 1345-1350.
76. **Onoguchi K , Yoneyama M , & Fujita T**. Retinoic acid-inducible gene-i-like receptors. *Journal of Interferon and Cytokine Research*, 2011; 31(1): 27-31.
77. **Ozato K , Shin D-M , Chang T-H , & Morse HC, 3rd**. Trim family proteins and their emerging roles in innate immunity. *Nature reviews. Immunology*, 2008a; 8(11): 849-860.
78. **Ozato K , Shin DM , Chang TH , & Morse HC, 3rd**. Trim family proteins and their emerging roles in innate immunity. *Nat Rev Immunol*, 2008b; 8(11): 849-860.
79. **Papadopoulos C , Kirchner P , Bug M , Grum D , Koerver L , Schulze N, . . . Meyer H**. Vcp/p97 cooperates with yod1, ubxd1 and plaa to drive clearance of ruptured lysosomes by autophagy. *EMBO J*, 2017; 36(2): 135-150.
80. **Park CW , & Ryu KY**. Cellular ubiquitin pool dynamics and homeostasis. *BMB Rep*, 2014; 47(9): 475-482.
81. **Park MY , Jang HD , Lee SY , Lee KJ , & Kim E**. Fas-associated factor-1 inhibits nuclear factor-kappab (nf-kappab) activity by interfering with nuclear translocation of the rela (p65) subunit of nf-kappab. *J Biol Chem*, 2004; 279(4): 2544-2549.
82. **Paz S , Vilasco M , Werden SJ , Arguello M , Joseph-Pillai D , Zhao T, . . . Hiscott J**. A functional c-terminal traf3-binding site in mavs participates in positive and negative regulation of the ifn antiviral response. *Cell Research*, 2011; 21(6): 895-910.
83. **Peng Y , Xu R , & Zheng X**. Hscarg negatively regulates the cellular antiviral rig-i like receptor signaling pathway by inhibiting traf3 ubiquitination via recruiting otub1. *PLoS Pathog*, 2014; 10(4): e1004041.
84. **Perry ST , Buck MD , Lada SM , Schindler C , & Shresta S**. Stat2 mediates innate immunity to dengue virus in the absence of stat1 via the type i interferon receptor. *PLoS Pathog*, 2011; 7(2): e1001297.
85. **Pestka S , Krause CD , & Walter MR**. Interferons, interferon-like cytokines, and their receptors. *Immunol Rev*, 2004; 202: 8-32.
86. **Pichlmair A , Schulz O , Tan CP , Naslund TI , Liljestrom P , Weber F , & Sousa CRE**. Rig-i-mediated antiviral responses to single-stranded rna bearing 5 '-phosphates. *Science*, 2006; 314(5801): 997-1001.
87. **Pollack BP , Kotenko SV , He W , Izotova LS , Barnoski BL , & Pestka S**. The human homologue of the yeast proteins skb1 and hsl7p interacts with jak kinases and contains protein methyltransferase activity. *J Biol Chem*, 1999; 274(44): 31531-31542.
88. Promega. (2019). from https://www.promega.com/products/reporter-assays-and-transfection/reporter-assays/dual_glo-luciferase-assay-system/?catNum=E2920
89. **Raman M , Sergeev M , Garnaas M , Lydeard JR , Huttlin EL , Goessling W, . . . Harper JW**. Systematic proteomics of the vcp-ubxd adaptor network identifies a role for ubxn10 in regulating ciliogenesis. *Nat Cell Biol*, 2015; 17(10): 1356-1369.
90. **Ran FA , Hsu PD , Wright J , Agarwala V , Scott DA , & Zhang F**. Genome engineering using the crispr-cas9 system. *Nature Protocols*, 2013; 8: 2281.
91. **Rezvani K , Teng Y , Pan Y , Dani JA , Lindstrom J , Garcia Gras EA, . . . De Biasi M**. Ubxd4, a ubx-containing protein, regulates the cell surface number and stability of alpha3-containing nicotinic acetylcholine receptors. *J Neurosci*, 2009; 29(21): 6883-6896.
92. **Rijal R , Arhzaouy K , Strucksberg KH , Cross M , Hofmann A , Schroder R, . . . Eichinger L**. Mutant p97 exhibits species-specific changes of its atpase activity and compromises the ubxd9-mediated monomerisation of p97 hexamers. *Eur J Cell Biol*, 2016; 95(6-7): 195-207.

93. **Ritz D , Vuk M , Kirchner P , Bug M , Schutz S , Hayer A, . . . Meyer H**. Endolysosomal sorting of ubiquitylated caveolin-1 is regulated by vcp and ubxd1 and impaired by vcp disease mutations. *Nat Cell Biol*, 2011; 13(9): 1116-1123.
94. **Rogers RS , Horvath CM , & Matunis MJ**. Sumo modification of stat1 and its role in pias-mediated inhibition of gene activation. *J Biol Chem*, 2003; 278(32): 30091-30097.
95. **Ryu SW , Lee SJ , Park MY , Jun JI , Jung YK , & Kim E**. Fas-associated factor 1, faf1, is a member of fas death-inducing signaling complex. *J Biol Chem*, 2003; 278(26): 24003-24010.
96. **Safarik I , & Safarikova M**. Magnetic techniques for the isolation and purification of proteins and peptides. *BioMagnetic Research and Technology*, 2004; 2(1): 7.
97. **Sane S , Abdullah A , Boudreau DA , Autenried RK , Gupta BK , Wang X, . . . Rezvani K**. Ubiquitin-like (ubx)-domain-containing protein, ubxn2a, promotes cell death by interfering with the p53-mortalin interactions in colon cancer cells. *Cell Death Dis*, 2014; 5: e1118.
98. **Sanjana NE , Shalem O , & Zhang F**. Improved vectors and genome-wide libraries for crispr screening. *Nature Methods*, 2014; 11(8): 783-784.
99. **Schneider WM , Chevillotte MD , & Rice CM**. Interferon-stimulated genes: A complex web of host defenses. *Annual Review of Immunology*, 2014; 32(1): 513-545.
100. **Schroder K , Hertzog PJ , Ravasi T , & Hume DA**. Interferon-gamma: An overview of signals, mechanisms and functions. *J Leukoc Biol*, 2004; 75(2): 163-189.
101. **Schuberth C , & Buchberger A**. Ubx domain proteins: Major regulators of the aaa atpase cdc48/p97. *Cell Mol Life Sci*, 2008; 65(15): 2360-2371.
102. **Seth RB , Sun LJ , Ea CK , & Chen ZJJ**. Identification and characterization of mavs, a mitochondrial antiviral signaling protein that activates nf-kappa b and irf3. *Cell*, 2005; 122(5): 669-682.
103. **Sheppard P , Kindsvogel W , Xu W , Henderson K , Schlutsmeyer S , Whitmore TE, . . . Klucher KM**. Il-28, il-29 and their class ii cytokine receptor il-28r. *Nat Immunol*, 2003; 4(1): 63-68.
104. **Shuai K**. Modulation of stat signaling by stat-interacting proteins. *Oncogene*, 2000; 19(21): 2638-2644.
105. **Shuai K , Liao J , & Song MM**. Enhancement of antiproliferative activity of gamma interferon by the specific inhibition of tyrosine dephosphorylation of stat1. *Mol Cell Biol*, 1996; 16(9): 4932-4941.
106. **Shuai K , & Liu B**. Regulation of jak–stat signalling in the immune system. *Nature Reviews Immunology*, 2003; 3: 900.
107. **Siegal FP , Kadowaki N , Shodell M , Fitzgerald-Bocarsly PA , Shah K , Ho S, . . . Liu YJ**. The nature of the principal type 1 interferon-producing cells in human blood. *Science*, 1999; 284(5421): 1835-1837.
108. **Stark GR , Kerr IM , Williams BR , Silverman RH , & Schreiber RD**. How cells respond to interferons. *Annu Rev Biochem*, 1998; 67: 227-264.
109. **Stremlau M , Owens CM , Perron MJ , Kiessling M , Autissier P , & Sodroski J**. The cytoplasmic body component trim5alpha restricts hiv-1 infection in old world monkeys. *Nature*, 2004; 427(6977): 848-853.
110. **Suppiah V , Moldovan M , Ahlenstiel G , Berg T , Weltman M , Abate ML, . . . George J**. Il28b is associated with response to chronic hepatitis c interferon-alpha and ribavirin therapy. *Nat Genet*, 2009; 41(10): 1100-1104.
111. **Syedbasha M , & Egli A**. Interferon lambda: Modulating immunity in infectious diseases. *Frontiers in immunology*, 2017; 8: 119-119.

112. **Tissot C , & Mechti N**. Molecular cloning of a new interferon-induced factor that represses human immunodeficiency virus type 1 long terminal repeat expression. *J Biol Chem*, 1995; 270(25): 14891-14898.
113. **Trusch F , Matena A , Vuk M , Koerver L , Knaevelsrud H , Freemont PS, . . . Bayer P**. The n-terminal region of the ubiquitin regulatory x (ubx) domain-containing protein 1 (ubxd1) modulates interdomain communication within the valosin-containing protein p97. *J Biol Chem*, 2015; 290(49): 29414-29427.
114. **Uchida S , Horie R , Sato H , Kai C , & Yoneda M**. Possible role of the nipah virus v protein in the regulation of the interferon beta induction by interacting with ubx domain-containing protein1. *Scientific Reports*, 2018; 8(1): 7682.
115. **Uchiyama K , Jokitalo E , Lindman M , Jackman M , Kano F , Murata M, . . . Kondo H**. The localization and phosphorylation of p47 are important for golgi disassembly-assembly during the cell cycle. *J Cell Biol*, 2003; 161(6): 1067-1079.
116. **Uchiyama K , Totsukawa G , Puhka M , Kaneko Y , Jokitalo E , Dreveny I, . . . Kondo H**. P37 is a p97 adaptor required for golgi and er biogenesis in interphase and at the end of mitosis. *Dev Cell*, 2006; 11(6): 803-816.
117. **Valente G , Ozmen L , Novelli F , Geuna M , Palestro G , Forni G , & Garotta G**. Distribution of interferon-gamma receptor in human tissues. *Eur J Immunol*, 1992; 22(9): 2403-2412.
118. **Wack A , Terczynska-Dyla E , & Hartmann R**. Guarding the frontiers: The biology of type iii interferons. *Nat Immunol*, 2015; 16(8): 802-809.
119. **Walter MR , Windsor WT , Nagabhushan TL , Lundell DJ , Lunn CA , Zauodny PJ , & Narula SK**. Crystal structure of a complex between interferon-gamma and its soluble high-affinity receptor. *Nature*, 1995; 376(6537): 230-235.
120. **Wang P , Yang L , Cheng G , Yang G , Xu Z , You F, . . . Sutton RE**. Ubxn1 interferes with rig-i-like receptor-mediated antiviral immune response by targeting mavs. *Cell Reports*, 2013; 3(4): 1057-1070.
121. **Wang YB , Tan B , Mu R , Chang Y , Wu M , Tu HQ, . . . Li HY**. Ubiquitin-associated domain-containing ubiquitin regulatory x (ubx) protein ubxn1 is a negative regulator of nuclear factor kappab (nf-kappab) signaling. *J Biol Chem*, 2015; 290(16): 10395-10405.
122. **Wang Z , Ji J , Peng D , Ma F , Cheng G , & Qin FX**. Complex regulation pattern of irf3 activation revealed by a novel dimerization reporter system. *J Immunol*, 2016; 196(10): 4322-4330.
123. **Weith M , Seiler J , van den Boom J , Kracht M , Hulsmann J , Primorac I, . . . Meyer H**. Ubiquitin-independent disassembly by a p97 aaa-atpase complex drives pp1 holoenzyme formation. *Mol Cell*, 2018; 72(4): 766-777 e766.
124. **Wilkins C , & Gale M, Jr.** Recognition of viruses by cytoplasmic sensors. *Current Opinion in Immunology*, 2010; 22(1): 41-47.
125. **Wu-Baer F , Ludwig T , & Baer R**. The ubxn1 protein associates with autoubiquitinated forms of the brca1 tumor suppressor and inhibits its enzymatic function. *Molecular and Cellular Biology*, 2010; 30(11): 2787-2798.
126. **Xie F , Jin K , Shao L , Fan Y , Tu Y , Li Y, . . . Zhang L**. Faf1 phosphorylation by akt accumulates tgf-β type ii receptor and drives breast cancer metastasis. *Nature Communications*, 2017; 8: 15021.
127. **Xu X , Sun YL , & Hoey T**. Cooperative DNA binding and sequence-selective recognition conferred by the stat amino-terminal domain. *Science*, 1996; 273(5276): 794-797.
128. **Yang L , Wang L , Ketkar H , Ma J , Yang G , Cui S, . . . Wang P**. Ubxn3b positively regulates sting-mediated antiviral immune responses. *Nature Communications*, 2018; 9(1): 2329.

129. **Yeung HO , Kloppsteck P , Niwa H , Isaacson RL , Matthews S , Zhang X , & Freemont PS**. Insights into adaptor binding to the aaa protein p97. *Biochem Soc Trans*, 2008; 36(Pt 1): 62-67.
130. **You F , Sun H , Zhou X , Sun W , Liang S , Zhai Z , & Jiang Z**. Pcbp2 mediates degradation of the adaptor mavs via the hect ubiquitin ligase aip4. *Nature Immunology*, 2009; 10(12): 1300-U1310.
131. **Yount JS , Karssemeijer RA , & Hang HC**. S-palmitoylation and ubiquitination differentially regulate interferon-induced transmembrane protein 3 (ifitm3)-mediated resistance to influenza virus. *J Biol Chem*, 2012; 287(23): 19631-19641.
132. **Zhang JG , Farley A , Nicholson SE , Willson TA , Zugaro LM , Simpson RJ, . . . Baca M**. The conserved socs box motif in suppressors of cytokine signaling binds to elongins b and c and may couple bound proteins to proteasomal degradation. *Proc Natl Acad Sci U S A*, 1999; 96(5): 2071-2076.